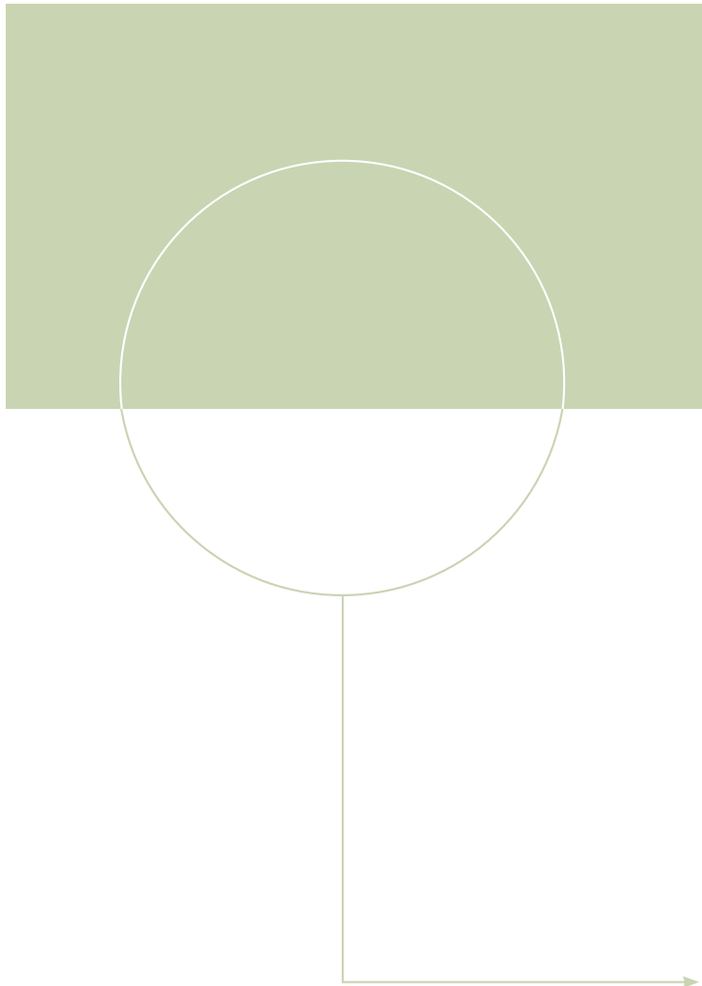

Master's thesis

2019

Karen Dimmen Opsahl

NTNU
Norwegian University of
Science and Technology
Faculty of Engineering
Department of Civil and Environmental Engineering

Karen Dimmen Opsahl

Physical modelling of debris flow countermeasure: deflection wall

Literature study and model testing in lab

June 2019

NTNU
Norwegian University of
Science and Technology

NTNU
Norwegian University of
Science and Technology

NTNU

Norwegian University of
Science and Technology

Physical modelling of debris flow countermeasure: deflection wall

Literature study and model testing in lab

Literature study and model testing in lab

Civil and Environmental Engineering
Submission date: June 2019
Supervisor: Vikas Thakur
Co-supervisor: Hervé Vicari

Norwegian University of Science and Technology
Department of Civil and Environmental Engineering

NORWEGIAN UNIVERSITY OF SCIENCE AND TECHNOLOGY
DEPARTMENT OF CIVIL AND ENVIRONMENTAL ENGINEERING

Project title: **Physical modelling of debris flow countermeasure: deflection wall** - Literature study and model testing in lab	Date: 01.06.2019 Number of pages (including appendices): 129
Author: **Karen Dimmen Opsahl** E-mail: karendo@stud.ntnu.no	Master's thesis

Degree: **Master of Science in Engineering (MSc)**
Study program: **Civil and Environmental Engineering**

Professor in charge: **Vikas Thakur**

External professional contacts/supervisors: **Hervé Vicari**

Abstract: Norway and countries with steep areas experience gravitational hazard processes due to their extreme topography, which is prone to debris flows, landslides and avalanches due to climatic or human impact. A more extreme climate is expected in the future and an increase in number of short, intense rainfall is one of the consequences. Deflection wall is an active method used to safely lead the debris flow away from settlements or infrastructure. Deflection wall is regarded as a rigid barrier. It is of great importance to learn more about the factors determining the design of such a construction in order to determine the necessary height to avoid overspill of material. Deflection walls are often curved and changes the direction of the landslide, and leads it to an area where it can deposit safely.

Eleven tests were performed in a rectangular, small-scale flume model with an inclined chute of 17,5°. The chute is 5 metres long and 30 cm wide. Two solid concentrations were examined, 50 and 60 %, as well as two deflection angles of 45 and 90°. Three reference tests without any barrier were performed to compare the effectiveness of the deflection wall. A trial test on entrainment was also performed. Main findings:

- The velocity shows jumps and drops during the flow in the chute due to the precision of the method used in Tracker. Small variations in tracking of the front gives large impact. The velocity at the deposition area is decreasing as the inclination drops to 2°. An increased water content results in larger velocity.
- Froude numbers for test 8-10 are found to be larger than what is observed in nature, and is therefore too large for Froude similarity. Test 2-7 and 11 are lower than the upper limit, and can hence be used.
- Run-up height is affected by both solid concentration and deflection angle. Run-up observed is smaller than what theory propose. The MJ model provides the most accurate predictions of run-up height for a rigid barrier, whilst the FM model gives the poorest predictions.
- Force is largest for the terminal wall, and smallest for the deflection wall. Velocity squared is correlated to force, via the hydrodynamic equation. Backsplash of debris flow material in the collision with the terminal wall reduces the force and compression of material affects the empirical factor α_3.
- Run out length is affected by the deflection angle, as a terminal wall stops the flow immediately after collision, while a deflection wall of 45° only diverts the masses to the side. Coarse levees are observed in the front and on the sides, and the degree of well-developed levees depend on the solid concentration.
- The entrainment test showed no erosion by rough visual observation.

Keywords: Debris flow, deflection wall, rigid barrier, entrainment

PREFACE

This project is a part of the course TBA4900 – Geotechnical Engineering, Master's Thesis. The Thesis accounts for 30 ECTS and is a continuation of the specialization project ''Impact force from a debris flow on a steel pillar'' conducted in the autumn semester of 2018 by the same author. The lab tests were performed in March and May 2019 at the Norwegian University of Science and Technology. The project was initiated by Professor Vikas Thakur at NTNU, with links to the Ferry Free E39-project and the Klima 2050-project.

I would like to thank my supervisors Vikas Thakur and Hervé Vicari for their help and guidance throughout this period. A special thanks to Hervé, Ashenafi Lulseged Yifru and Espen Andersen for their help in the lab.

Trondheim, 2019-06-01

Karen Dimmen Opsahl

SUMMARY AND CONCLUSIONS

Norway and countries with steep areas experience gravitational hazard processes due to their extreme topography, which is prone to debris flows, landslides and avalanches due to climatic or human impact. A more extreme climate is expected in the future and an increase in number of short, intense rainfall is one of the consequences. Deflection wall is an active method used to safely lead the debris flow away from settlements or infrastructure. Deflection wall is regarded as a rigid barrier. It is of great importance to learn more about the factors determining the design of such a construction in order to determine the necessary height to avoid overspill of material. Deflection walls are often curved and changes the direction of the landslide, and leads it to an area where it can deposit safely.

Eleven tests were performed in a rectangular, small-scale flume model with an inclined chute of 17,5°. The chute is 5 metres long and 30 cm wide. Two solid concentrations were examined, 50 and 60 %, as well as two deflection angles of 45 and 90°. Three reference tests without any barrier were performed to compare the effectiveness of the deflection wall. A trial test on entrainment was also performed. Main findings:

- The velocity shows jumps and drops during the flow in the chute due to the precision of the method used in Tracker. Small variations in tracking of the front gives large impact. The velocity at the deposition area is decreasing as the inclination drops to 2°. An increased water content results in larger velocity.
- Froude numbers for test 8-10 are found to be larger than what is observed in nature, and is therefore too large for Froude similarity. Test 2-7 and 11 are lower than the upper limit, and can hence be used.
- Run-up height is affected by both solid concentration and deflection angle. Observed run-up height is smaller than what theory propose. The MJ model provides the most accurate predictions for a rigid barrier, whilst the FM model gives the poorest predictions.
- Force is largest for the terminal wall, and smallest for the deflection wall. Velocity squared is correlated to force, via the hydrodynamic equation. Backsplash of debris flow material in the collision with the terminal wall reduces the force and compression of material affects the empirical factor α_3.
- Run out length is affected by the deflection angle, as a terminal wall stops the flow immediately after collision, while a deflection wall of 45° only diverts the masses to the

side. Coarse levees are observed in the front and on the sides, and the degree of well-developed levees depend on the solid concentration.

- The entrainment test showed no erosion by rough visual observation.

SAMANDRAG

Noreg og andre land med bratt terreng erfarer fare knytt til gravitasjonsrelaterte prosessar grunna det ekstreme terrenget som er utsett for flaumskred, skred og snøskred grunna klimatisk eller menneskeleg påverknad. Eit meir ekstremt klima er forventa i framtida, noko som vil resultere i ei auke i antal korte, intense regnskyll. Leievoll er ein aktiv metode som vert nytta til å trygt leie flaumskredet unna busetnad og infrastruktur. Leievoll blir betrakta som ei ubøyeleg barriere. Det er av stor betyding å auke kunnskapen om faktorane som ligg til grunn for utforminga av ein slik konstruksjon, slik at ein kan bestemme nødvendig vollhøgde for å unngå at massane flyt over vollen. Leievollar er ofte bøygde og endrar retninga til skredet, får så å leie det inn i eit område kor det trygt kan avsetjast.

Elleve testar vart utført i ein rektangulær, småskala modell med helling på 17,5°. Renna er 5 meter lang og 30 cm brei. To konsentrasjonar av materialet har blitt testa, 50 og 60 %, på to retningsendrande vinklar, 45 og 90°. Tre referansetestar utan barriere vart utført for å kunne samanlikne testane med barrierar med, og derav sjå effekten av bruk av leievoll. Ein prøvetest om erosjon vart også utført. Hovudfunn:

- Hastigheitsprofilane syner aukande og synkande fart om kvarandre grunna nøyaktigheita i metoden brukt i Tracker. Små variasjonar i sporinga av fronten gir store utslag. Hastigheita i avsetjingsområdet er minkande på grunn av den hellinga som no er redusert til 2°. Ei auke i vassinnhaldet resulterer i høgare hastigheit.
- Froudes tall for test 8-10 er større enn kva ein har observert i naturen, og blir vurdert som for høge til å kunne bruke det i Froude-likskapen. Test 2-7 og 11 er under den høgste verdien sett i naturen, og kan difor brukast.
- Oppskyllingshøgd er påverka av både konsentrasjonen av massen og leievinkelen. Observert oppskyllingshøgd er mindre enn kva teori føreslår. MJ-modellen gir dei mest nøyaktige anslaga for ubøyeleg barriere, mens FM-modellen gir dei dårlegaste.
- Målt kraft på plata er størst for fangvollen og minst for leievollen. Hastigheita kvadrert er forbunde med krafta via den hydrodynamiske likninga. Tilbakeslag av flaumskredmassane i kollisjon med fangvollen reduserer målt kraft og kompresjon av materiale påverkar α_3.
- Utløpslengd er påverka av leievinkelen, då ein ser at ein fangvoll stansar massane straks etter kollisjonen, medan ein leievoll leiar massane til sida. Grove levear er observert i front og på sidene, og grada av velutvikla levear er avhengig av vassinnhaldet i massane.
- Testen med erosjon av materiale i skredbana synte inga erosjon ved observasjon.

TABLE OF CONTENTS

LIST OF FIGURES

LIST OF TABLES

ABBREVIATIONS

MET - The Norwegian Meteorological Institute

NTNU - Norwegian University of Science and Technology

NVE - Norwegian Water Resources and Energy Directorate

LIST OF SYMBOLS

α = angle of inclined slope

α_2 = angle of the line which represents the run-out length

α_3 = empirical coefficient in hydrodynamic equation

β = the angle from the releasing point to the point where the inclination of the flow path reaches 20°

δ = the angle between the debris flow and the deflection wall, deflection angle

λ = scale

ρ = debris density

ρ_s = solid density

ρ_w = water density

C_s = solid concentration

C_u = coefficient of uniformity

D = destabilizing forces

d50 = 50% pass diameter in sieve analysis

d90 = 90% pass diameter in sieve analysis

F = friction

F_c = velocity independent friction

F_d = velocity dependent friction

Fo_m = force in model

Fo_p = force in prototype

Fps = frames per second

Fr = Froude number

g = gravitational constant

ΔH = superelevation

H = run-up height

H_e = energy line

H_z = height

H_p = flow height

H_k = energy height

h_0 = entry flow depth

$h_k = H_p + H_k$ = flow height + energy height

M = amount of material one should add

M_s = solid mass

M_{Tot} = total mass

M_w = mass of water

v = velocity

V_s = volume of solids

V_{Tot} = total volume

V_w = volume of water

w = natural water content

W_a = addition in water

W_m = amount of water in the material in the tank

1. INTRODUCTION

Debris flow is a gravitational hazard occurring yearly in Norway. The steep topography creates the perfect environment for this and several other types of landslides to be triggered and released towards human settlements. This risk of debris flows reaching settlements or infrastructure is something everyone want to avoid. The consequences can be fatal and lives may be lost. An increase in the amount of debris flow events are expected in the future due to a changing climate where scientists have predicted a global increase in the amount of heavy rainfall as a consequence (Hausfather, 2018). This is an unfortunate development in the light of geohazards, as water in the shape of surface runoff or additional pore pressure is one of the triggering mechanisms.

The Norwegian Meteorological Institute (MET) is responsible for monitoring the weather situation in Norway, and they prepare prognosis for the expected amount of rainfall to come in mm for each day. MET work closely with the Norwegian Water Resources and Energy Directorate, NVE, and representatives from the two parts meet every morning (NVE, n.d.) to discuss the current weather situation. Subjects like expected precipitation, soil saturation, temperature and water flow in rivers are topics to be discussed for potential regional warnings.

As a debris flow is triggered, it entrains material as it descents down the steep slope. The size of the particle of the entrained material varies from clay to stony blocks. The amount of moving mass will increase on its way if it has the capacity to entrain material, until it reaches a lower slope where the velocity decreases and the mass deposits. An increase in mass will lead to an increase in force and a debris flow imposes enormous forces on everything that is in its way. Gravitational forces and the weight makes sure of this, and an increase in water will increase the weight.

1.1 Background

Debris flow is a natural hazard that has occurred on many occasions in history and will continue to do so in the future. The climate is changing and an increase in heavy rainfall is expected. An alarming autumn was observed in Norway in 2018 after several events of heavy rainfall and storms occurred. This resulted in a large amount of precipitation which saturated the soil and put the surroundings to risk. As of mid-October, NVE published a regional warning for Western Norway, with warning level 2, see figure 1, where they requested the population to stay away from steep slopes as landslides were expected (NVE, 2018).

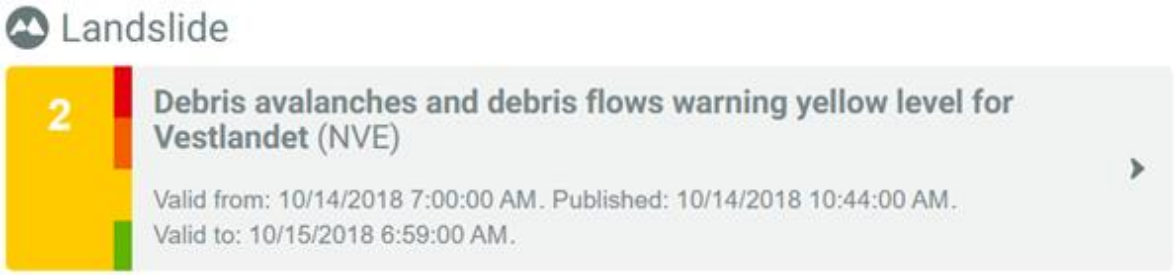

Figure 1: Regional warning for Vestlandet, October 2018 (NVE, 2018), screenshot

As debris flows are large in size and difficult to study in the field, the best approach is by performing experiments in lab, or more precisely in a flume model. This approach has become the most common way to examine debris flow at a low scale in order to understand its behaviour. The released material in these kind of tests represent snow avalanches or debris flow as these landslides often are transported in flow channels behind deflection walls and stored somewhere safe. Several studies have addressed the topic in previous years in order to predict the behaviour of debris flow and to design appropriate countermeasures. Today, it exists several types of preventative measures that either slow down the masses or lead them away from a path that would impose danger to infrastructure or settlements. One type is the deflection wall which is designed to prevent masses to spill over the top of the wall and store the masses safely away from structures that would have been destroyed if not. This type of preventative measure is common in the coastal part of Norway where slopes are steep and the frequency of landslide is high. A reason for the use of this specific countermeasure is the availability and easy access of material on site. The deflection wall is often curved to absorb the force progressively.

1.2 Objectives

The main objective of this work is to understand debris flows better, both the mechanics of the masses and how one can prevent them from destroying settlements or infrastructure, in the form of a deflection wall. To achieve this, a number of sub-objectives are defined and listed below:

1. understand the physics of the debris flow
2. understand the design principles of a deflection wall
3. examine the flow in the chute, front velocity, Froude number, flow height, run-up height, force measurements, run-out length and deposition height and pattern of a released debris flow colliding into a deflection wall
4. compare the obtained results with similar studies

1.3 Structure of the report

The next chapters in my project are as follows: Chapter 2 is a literature study of the topic debris flow. Material, debris flow types, triggering mechanisms, zones, stages, mechanics, Froude number, run-out length and impact pressure will all be described. Chapter 3 will introduce deflection wall and what parameters one need to account for when constructing this type of countermeasure. Chapter 4 will introduce the test apparatus and countermeasure set-up used for the tests, in addition to the physical modelling. All the measurement equipment will be described and the procedure for testing will be given. Chapter 5 presents the results while chapter 6 will be a discussion about my findings. Chapter 7 will propose what can be done further in the same branch of the topic of debris flow and ideas for more tests concerning entrainment. Chapter 8 is concerning a trial test about entrainment. Set-up, results and discussion for this test is all included in this chapter. Chapter 9 is listing up all the references used in this work and the Appendix is found last.

2. DEBRIS FLOW

Debris flow is a natural hazard occurring in steep terrain containing soil, which is common to find in Norway. Its topography is suitable as the slopes are covered by soil derived from the last ice age, the Weichselian glaciation. Throughout the ages, many events of this type has happened over the globe, and the Japanese expressions of this hazard are translated into ‘‘tsunami at mountain’’ and ‘‘the mountain tide’’ (Takahashi, 2014, p. 2). According to Hungr, Leroueil & Picarelli (2014), a debris flow is:

> *‘‘Very rapid to extremely rapid surging flow of saturated debris in a steep channel. Strong entrainment of material and water from the flow path’’.*

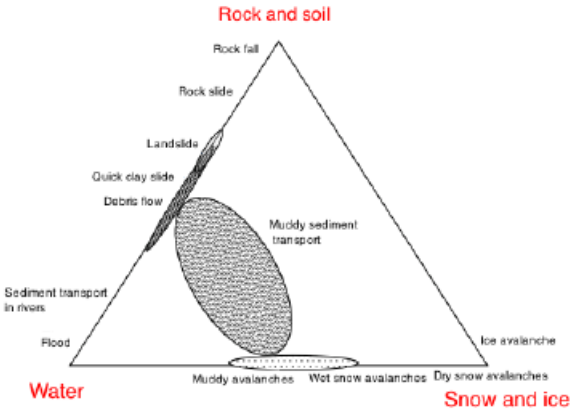

Figure 2: Classification of landslides, given the content of water, snow/ice and sediment (Statens Vegvesen, 2014), translated by Laache (2015)

Debris flow is a type of landslide containing both sediment (rock and soil) and a great amount of water, see figure 2. This makes the dynamics and behavior of the debris flow more difficult to predict, as they follow both hydrodynamic laws and granular mechanics.

2.1 Types of debris flow

Takahashi (2014) introduced a classification of debris flow types, based on the type of material and/or segregation of particle sizes:

- Stony-type debris flow is dominated by stress from grain collisions. This type erodes the bed if it has enough capacity to do so and hence increases in volume. Big boulders up to more than one meter in diameter are deposited at the sides of the flow path as levees and in the front due to inverse grading, see figure 3. The coarse front can deposit in patterns called lobes as the slope decreases (Takahashi, 2014, p. 224), see the left deposition in figure 8. The coarse material in the front is permeable and contains little water compared to the rear parts which are more liquid. The depth and velocity are maximum at the head of the flow and the debris material consists of 1-10 % fines, 30-40 % sand and 10-60 % gravels.

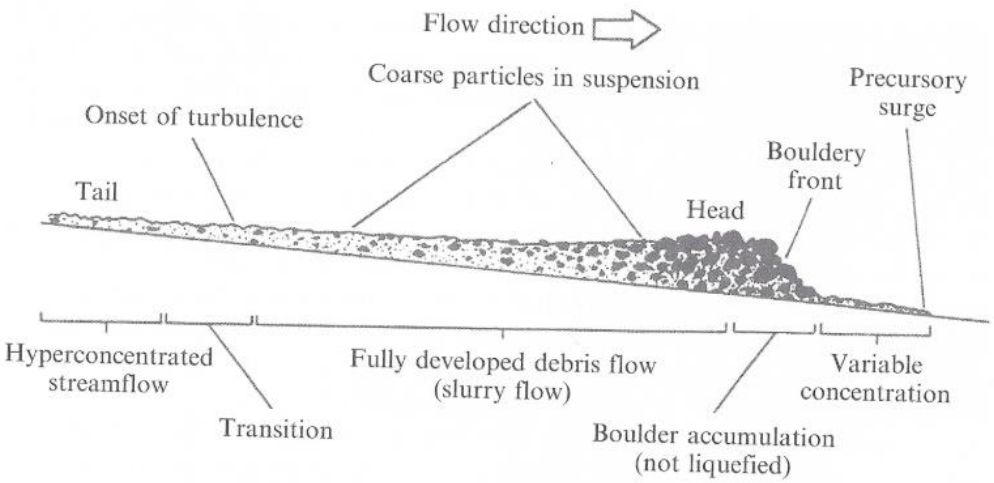

Figure 3: Particle segregation seen in profile of a stony-type debris flow (Pierson, 1986)

- Turbulent-muddy-type debris flow is characterized by the content of ash or fines in the debris material as ash is deposited as thick layers nearby an active volcano. We also see it close to glaciers where accumulation of fines occur. The turbulent-muddy-type does also carry large boulders, but these are spread out on the deposition zone. As the debris flows experienced in Norway are triggered mainly by heavy rainfall events, the turbulent-muddy-type is initiated only by slight rain as the material is easy to erode in. The term turbulent relates to the flow which has been characterized as turbulent and chaotic from the front to the end of the debris flow.

- Viscous debris flow is dominated by viscous stress. The material in the front is passing in a turbulent flow, while the following masses are flowing in a more laminar manner. The material originating from a source area are close to identical to the material which is about to deposit. As water washes away fine particles in the deposited masses, we can not compare the source material to the deposited material as they will differ. The similarity implies that the debris material does not segregate particles, and we do not see any accumulation of big boulders at the front like we do in the stony-type debris flows.

2.2 Triggering mechanisms

Triggering mechanisms of a debris flow are either due to water content in the soil or external factors. As the snow melts in the spring and heavy, rapid rainfalls are experienced in autumn, water is a large threat to life and infrastructure and can do great damage. The water will, dependent on the degree of saturation in the soil and the duration of the rainfall event, either

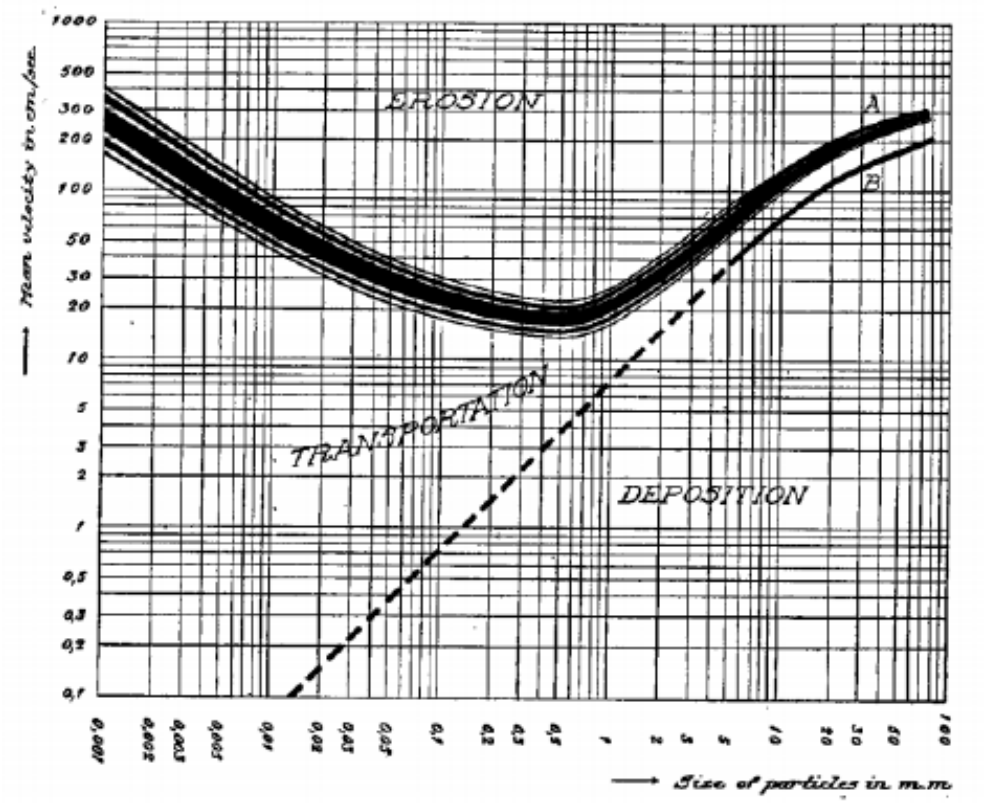

Figure 4: Hjulström's curve (Laache, 2015)

infiltrate (not fully saturated and longer rainfall event) or simply run off the surface as surface runoff. In the latter case, the water can erode in the material and create a denser material if the velocity is high enough. A visual method to see if the water will erode, deposit or transport the material is the use of Hjulström's curve, see figure 4, by examining water velocity and grain size. If the rainfall is lasting over a larger amount of time, a rise in the pore pressure is experienced and the soil is becoming saturated (NVE, 2013). The pore pressure is a key factor when a debris flow is initiated as it reduces the strength in the soil, and can be liquefied and slide out if the slope is steep enough. In a debris flow, the whole mass is being liquefied (Takahashi, 2014), see figure 5, and the material loses its strength as grains in the soil skeleton loses contact. A potential dam burst will release a great volume of water during a short amount of time and the high velocity of the water makes it erode its surroundings.

External factors such as landslides (rock fall and rock avalanches) could trigger a debris flow if it falls down on a saturated soil (rapid loading) and increase the pore pressure above a critical level (Høeg, Karlsrud & Lied, 2014, p. 83), see dotted area in figure 8. Humans can also affect the stability by excavating, impose high loads (fillings) or by changing the drainage path (tree felling or clogged culvert under a forest track) so that water finds new paths to flow.

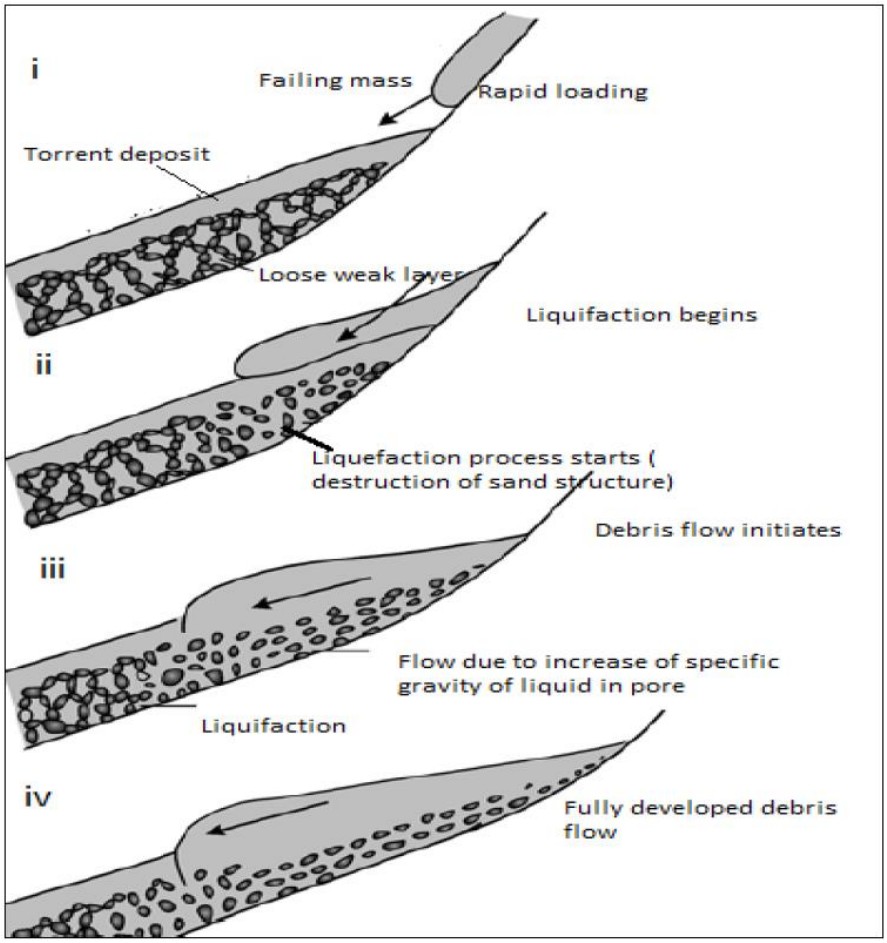

Figure 5: Liquefaction of the masses lead to a debris flow (Sassa, Kaibori & Kitera, 1985)

2.3 Mechanics of debris flow

To be able to understand how the increased pore pressure affects the strength of the material, we need to take a closer look at a soil unit in the slope.

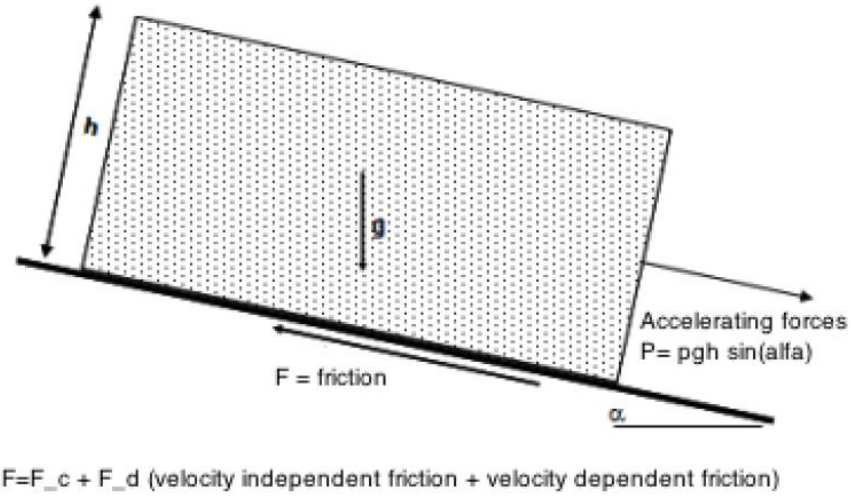

Figure 6: Illustration of stabilizing and destabilizing forces acting on a soil unit in a slope of angle α (Statens Vegvesen, 2014), translated by Laache (2015)

The soil mass itself with its density and volume is creating a downward force which will be destabilizing due to gravity:

Destabilizing forces:

$$D = \rho * g * h_0 * sin\alpha \quad (1)$$

The counterforce is due to friction from the grains. Friction usually increases as the particle size increases (Laache, 2015, p. 18). There are two components of friction, F, the friction independent of velocity, F_c, which makes it possible for a landslide to deposit at a flat area, and one friction which increases with the velocity, F_d, which makes it possible for the landslide masses to reach terminal velocity.

As stated by Newton in his second law, the mass times acceleration is equal to the difference between the driving and the stabilizing forces:

$$\Delta F = m * a = D - F = D - (F_c + F_d) \quad (2)$$

The masses will accelerate if the destabilizing force is larger than the stabilizing, and decelerate in the opposite case. An increase in pore pressure would increase the weight which implies an increase in the destabilizing forces, and hence be unfavorable for the overall stability.

2.4 Parts and stages of a debris flow

One can divide a debris flow into three parts; a source area, a transport channel and a deposition area. As the material changes from being released to entrain more material and at last deposited, this defines these three parts. The source area, or initiation zone of a debris flow, requires a steep enough slope so the masses will begin to slide as the destabilizing forces are larger than the stabilizing ones. NVE (2013) suggest an inclination angle of the source area as 25-45°, while Calligaris and Zini (2012) says that the slope can be as little as 15°, given that the soil is moist enough, the vegetation is sparse and the soil is loosely packed.

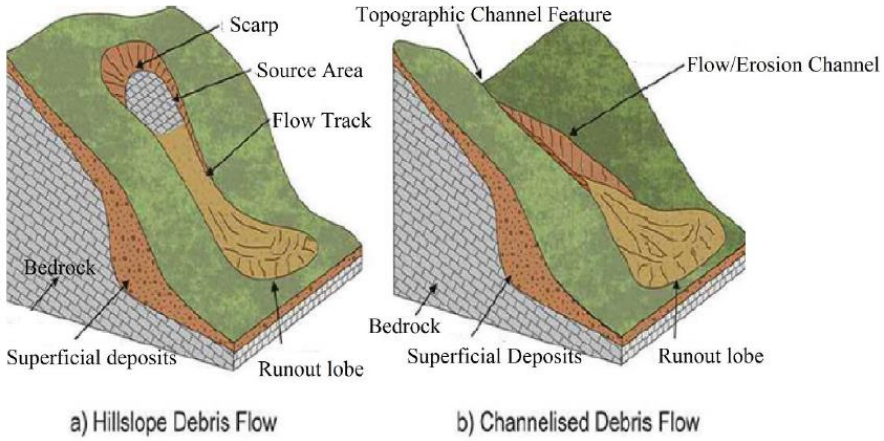

Figure 7: Illustration showing a hillslope debris flow and a channelized debris flow (Nettleton et al., 2005)

A debris flow can follow either hillslopes or gullies/drainage channels (channelized debris flow), see figure 7, and entrain both sediment and water on its way if it contains too small mass of sediment, which increases the volume. The angle of the transport channel can be less than the inclination in the source area due to the volume and force from the sliding mass, and is given to lie between 20-30° (Høeg, Karlsrud & Lied, 2014, p. 81). Materials are deposited on the side of the channel as levees if the mass of sediment is too large so that there is no capacity to erode (Rosy, 2017, p. 19). These can achieve a height of several metres and extend tens of

metres along the channel (VanDine, 1996, p. 9). The channel makes the mass maintain a constant thickness and larger blocks at the bottom will be relocated to the surface of the flow (inverse grading, see figure 3)(NVE, 2013) if the debris flow is either of the stony or the viscous type. A study on viscous debris flows conducted by Chinese scientists confirmed this as the upper sensors on a pillar in the chute encountered more coarse material than the lower sensors (Cui, Zeng & Lei, 2015, p. 1652). The density of debris flow vary between 1800-2300 kg/m^3 (Christiansen, 2013, p. 3) and this type of landslide can achieve a velocity of 5-10 m/s. As the slide exits the channel, it increases in width and starts to decrease in speed as the inclination is reduced. The angle of which the masses will deposit depends on the topography, type of debris flow and volume, but is typically less than 15-20° (Høeg, Karlsrud & Lied, 2014, p. 81) and often just a few degrees. If the debris flow follows a channel, it ends up at an old debris fan consisting of old landslides/debris flows. Human settlements are often placed on these fans and are in great danger of being hit. The boulder materials are deposited first, while the fine particles are deposited further down alongside with water. The amount of water gives this type of natural hazard an enormous range in area.

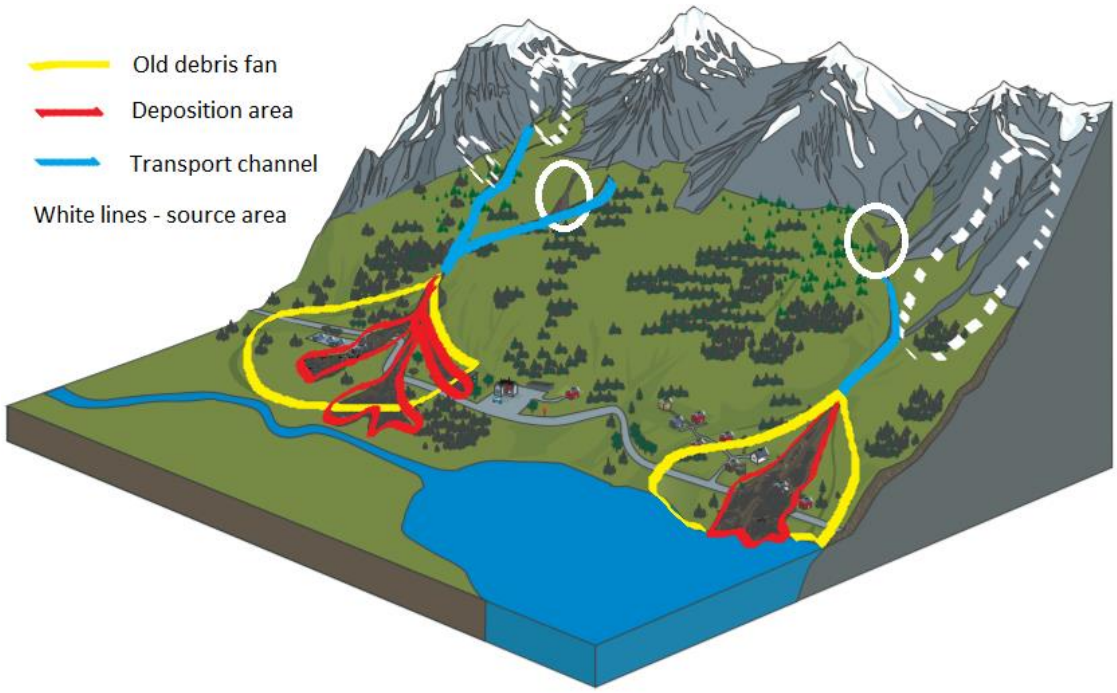

Figure 8: The three parts of a debris flow; source area, transport channel and deposition area (NVE, 2013, coloured by Opsahl)

The first of five stages of a slide is the initiation. Rapidly, it enters the next stages, which are transport to the channel, storage of material in the channel, entrainment of bed and deposition on debris fan.

2.5 Froude number

Flow is characterized by three states of flow: subcritical, critical and supercritical. Subcritical flow is dominated by gravitation and supercritical by inertial forces (Christiansen, 2013, p. 8). The transition from subcritical to supercritical is found from the Froude number (Fr):

$$Fr = \frac{v}{\sqrt{gh}} = \frac{kinetic\ force}{gravitational\ force} \quad (3)$$

where v represents velocity, g the gravitational constant and h the flow depth.

Froude number is Fr =1 for critical flow while it is Fr >1 for supercritical and Fr <1 for subcritical (Sæterbø, Syvertsen & Tesaker, 1998, p. 75). Under follows a table over reviewed papers in the working process of this thesis, where comparison of flume model, aim, material type, Froude number, velocity and flow depth is done. The table gives information about other studies which has performed similar flume experiments. The studies have examined different aspects of a debris flow. Some specializes on run-up height against the barrier or the forces from a debris flow, while others do testing on different types of barriers, such as baffles, deflection walls and dual-barriers.

Table 1: Other flume experiments

Paper	Flume experiment	Aim of test	Material type	Froude number	Velocity	Flow depth
Christiansen, 2013	5 m channel, two inclinations; 13,8° and 23,0°	Run-up on deflection wall with different inclination and deflection angles	d50 = 1,2 mm, d90 = 2,7mm	Do not have any information regarding the flow height, impossible to calculate Fr	1,44-2,76 m/s	
Choi et al., 2014	5 m rectangular channel, inclination 26°	varying parameters of baffles		0,5-6	1,5-3,25 m/s	
Cui et al., 2015	3 m channel, three inclinations: 10°, 13° & 15°	impact forces from debris flow	d50=2,7 mm	0,6-10,8	2,36-5,20 m/s	62-112 mm
Au-Yeung, 2015	5 m channel, inclined from 0-50°	Run-up on a rigid barrier	Diameter: 0,3-0,6 mm	1,0-14,0	0,15-5 m/s	2,5-31,5 mm
Iverson, George and Logan, 2016	90 m long flume, inclination 31°	Debris flow run-up on vertical barriers		3,0-9,0	Approximately 15 m/s	0,1-0,4 m
Ng et al., 2018	5 m rectangular channel, inclination 26°	Flow interaction with dual-barrier systems	Diameter (max) = 0,6 mm	2,5-4-5	Max 2,7 m/s	
Opsahl, 2019	5 m rectangular channel, inclination 17,5°	Run-up against vertical deflection walls	d50=1,4 mm	4,67-9,75	1,78-4,86 m/s	23,43-31,11 mm

2.6 Run-out length

Run-out length is defined as the outer boundary of the deposited masses. As slurry separates from the more firm masses and continues further than the rest due to the high mobility, the run-out length is limited to those masses which can damage the considered infrastructure or settlements (Norem & Sandersen, 2012, p. 38). International practice defines the run-out length by the outer boundary of deposits of a certain thickness and would therefore not include the thin deposits of fine grains. Two types of models are used in calculation of run-out length; dynamic and topographic models. The dynamic models assume that one know the profile of the flow path, important physical quantities and the properties of the landslide. Topographic models only contain information about the flow path and none parameters are determined by judgement. One example of a topographic model is the α-β-method developed by NGI. α_2 is the angle from the releasing point to the point of the front of the deposited masses, and β is the angle from the releasing point to the point where the inclination of the flow path reaches 20°, see figure 9. α_2 is expressed by the angle β. The deceleration of the masses starts at about this angle, and the masses do not erode any more. Examined landslides in Norway have a varying β-value of 23-30°. The best fit for the angle α_2 is set as:

$$\alpha_2 = 0{,}96\beta - 4° \tag{4}$$

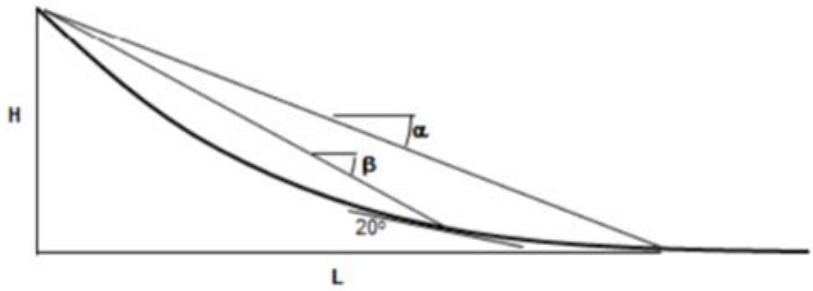

Figure 9: α-β-method (Norem & Sandersen, 2012, p. 41)

A small inaccuracy in the β will give large effect on the calculation of the run-out length. An alternative has therefore been proposed, see figure 10. This method is based on the same 20°-line as before, but now includes an energy line. This is inclined between 11,3° (0,2) and 16,7° (0,3), and makes us able to predict the run-out length. The small inclination coincide with smaller events or very coarse material in the debris flow, while a steeper inclination of the energy line represent large events or events with a large amount of fines (Christiansen, 2013, p. 17).

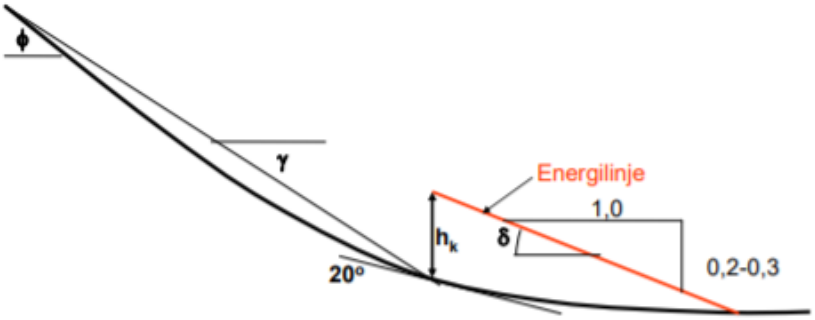

Figure 10: Calculation of run-out length by energy line (Norem & Sandersen, 2012, p. 41)

The energy in a debris flow is given by Bernoulli's equation:

$$H_e = H_z + H_p + H_k \tag{5}$$

where H_z = z, the height above sea level

$H_p = h_0$, the entry flow height

$H_k = v^2/2g$, the energy height

A debris flow can achieve velocities of about 5-10 m/s, and 15 m/s in very large events. h_k, is given by flow height and $v^2/2g$, which is the energy height. These two contributions are added and back-calculation shows that the inclination of the energy line varies between 0,2-0,3.

For infrastructure like roads and railways, an average of these two methods are applied and used for calculating run-out length. Settlements are planned using the longest run-out length calculated by either the energy line-method or by equation 4 where the angle α_2 is reduced by 3° (Norem & Sandersen, 2012, p. 42).

2.7 Impact pressure

The impact from a debris flow can be separated into two components; impact from slurry and impact from grains. The slurry consists of a fluid mixed with fine particles such as clay and silt. The transport of coarse material and boulders in the debris flow creates the largest impact forces, as the boulders generate the largest impact force and the coarse material the second largest (He, Liu & Li, 2016).

The testing we did in the lab does not separate forces generated by slurry and grains. The impact processes of a stony-type debris flow can be divided into three stages:

- The head is producing the peak loading pressure and is flowing stable or slightly turbulent, see figure 11a. The stage starts from the first measurement at the pillar until a maximum has been reached.
- The body is decreasing in depth from the back of the head and back towards the tail, and provides a more steady pressure against the pillar. The weak turbulence found in the flowing mass makes one say that it is a steady laminar flow.
- The tail is characterized by a lower velocity and a thin flow thickness, see figure 11b.

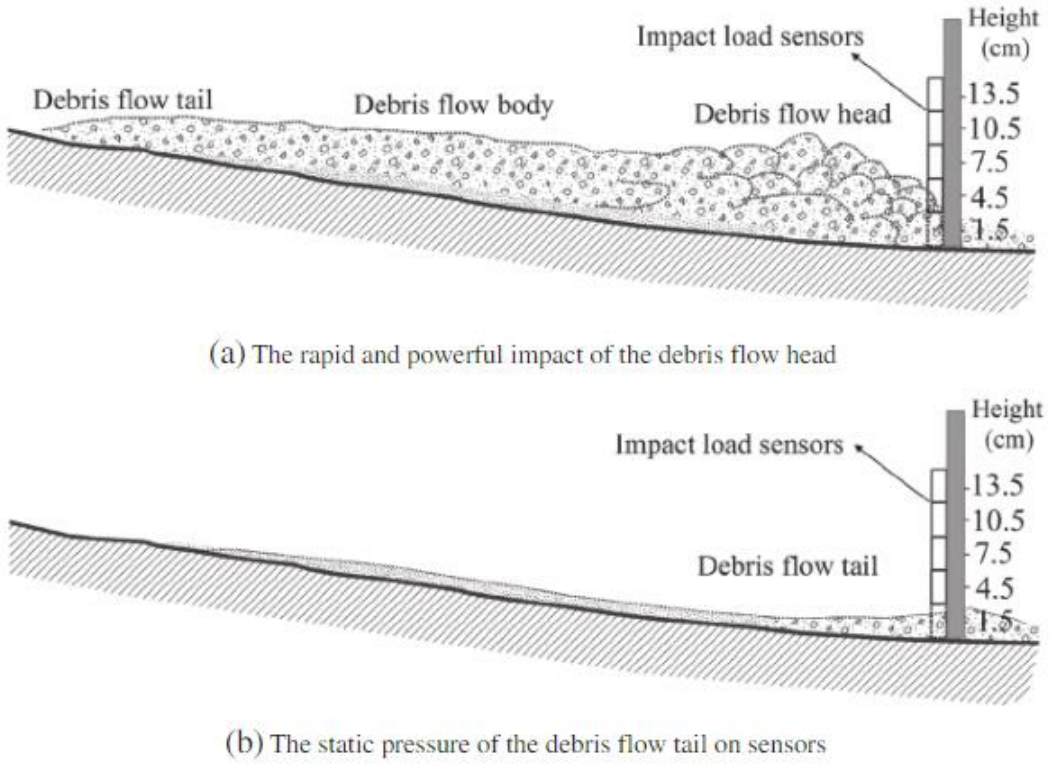

Figure 11: Two of three stages of the impact processes from a stony-type debris flow (Cui, Zeng & Lei, 2015)

Debris flows damage its surroundings through deposition, entrainment and direct impact, with the latter being the most damaging factor concerning structural damage (He, Liu & Li, 2016). Theoretical equations to calculate the force impact of a debris flow are roughly containing the same parameters, but some differences occur. The equations used to calculate the impact forces on a rigid barrier are related to the pressure being considered as hydrostatical or kinematic flow height (Rosy, 2017, p. 31). These considerations results in three different types of models,

namely hydrostatic, hydrodynamic and mixed models. Hydrostatic and -dynamic models will be examined here.

The hydrodynamic equation is as follows:

$$P_{hd} = \alpha_3 * \rho * v^2 \quad (6)$$

where ρ is the bulk density, v is the velocity and α_3 is an empirical factor. See table 2 for values of α_3 found in literature.

Table 2: Values of α_3 found in literature (Cui, Zeng & Lei, 2015, p. 1651)

Source	Empirical coefficient, α_3
Mizuyama (1979)	1,00
Hungr et al. (1984)	1,50
Armanini (1997)	0,45-2,2
Watanabe and Ikeya (1981)	2,00
Zhang (1993)	3,0-5,0
Opsahl (2019)	0,04-0,19
Opsahl (2018)	0,84-1,42

Bulk density is the density of the debris flow, and is calculated as:

$$\rho = \rho_s * \frac{C_s}{100} + \rho_w * \left(1 - \frac{C_s}{100}\right) \quad (7)$$

where ρ_s is the soil density, Cs is the solid concentration by volume and ρ_w is the water density.

The hydrostatical equation is:

$$P_{hs} = k * \rho * g * h_0 \quad (8)$$

The parameter ρ is representing bulk density, while g and h_0 represents gravity and maximum entry flow height, respectively. k is an empirical factor in the range of 2,5-11 (Lichtenhahn; Armanini; Scotton and Deganutti; all cited in Vagnon and Segalini, 2016).

3. DEFLECTION AND TERMINAL WALL

Preventative measures for reducing the threat on human life or infrastructure can be separated into two groups: passive and active methods (VanDine, 1996, p. 3). Passive methods are not about controlling the event, but to reduce the potential damages by avoiding the exposed area, apply land use regulations, inform and educate the people or establish warning systems. Active methods are controlling the hazard by designing protective measures to reduce or eliminate the hazard.

The goal of debris flow control structures is to protect buildings and infrastructure located on the debris fan, in addition to stream crossing (VanDine, 1996, p. 4). This is done by leading the debris across the fan to an area where it can deposit, while controlling the velocity. The main purpose in protection of settlements and infrastructure is to control the coarse-grained debris movement as this can destroy buildings just by its force. The fine-grained sediments pose a threat as it mixes with water and can bury houses (Hungr et al. cited in VanDine, 1996, p. 4).

Most preventative measures are constructed in the discharge area as this is close located to the infrastructure we want to secure, and is in addition easily accessed for construction machines (Norem & Sandersen, 2012, p. 77) in both construction and maintenance phases. Choosing the appropriate preventative measure is dependent on the type, volume and consequence of the debris flow, character of the debris fan, resources and equipment for design and construction and good access for maintenance of the structure (Christiansen, 2013, p.18; Norem & Sandersen, 2012, p. 82; VanDine, 1996, p. 20). The different types of preventative measures can be used either alone or together with one another. Deflection wall is regarded as a rigid barrier.

3.1 Deflection wall

Deflection wall, also called deflection berm, is considered as an active method (VanDine, 1996, p. 4). This structure leads the debris flow towards an area where it can safely deposit. Deflection walls either lead the masses towards an area where the masses deposits or towards bridges, above tunnels or above avalanche superstructures (Norem & Sandersen, 2012, p. 77).

The terrain the deflection wall is built on has to be steep enough in order to prevent the masses from depositing in the flow path or along the deflection wall. If the front stops, the rear parts can climb above the masses and tip over the deflection wall and impose damage to human settlements or infrastructure according to Brateng (cited in Christiansen, 2013).

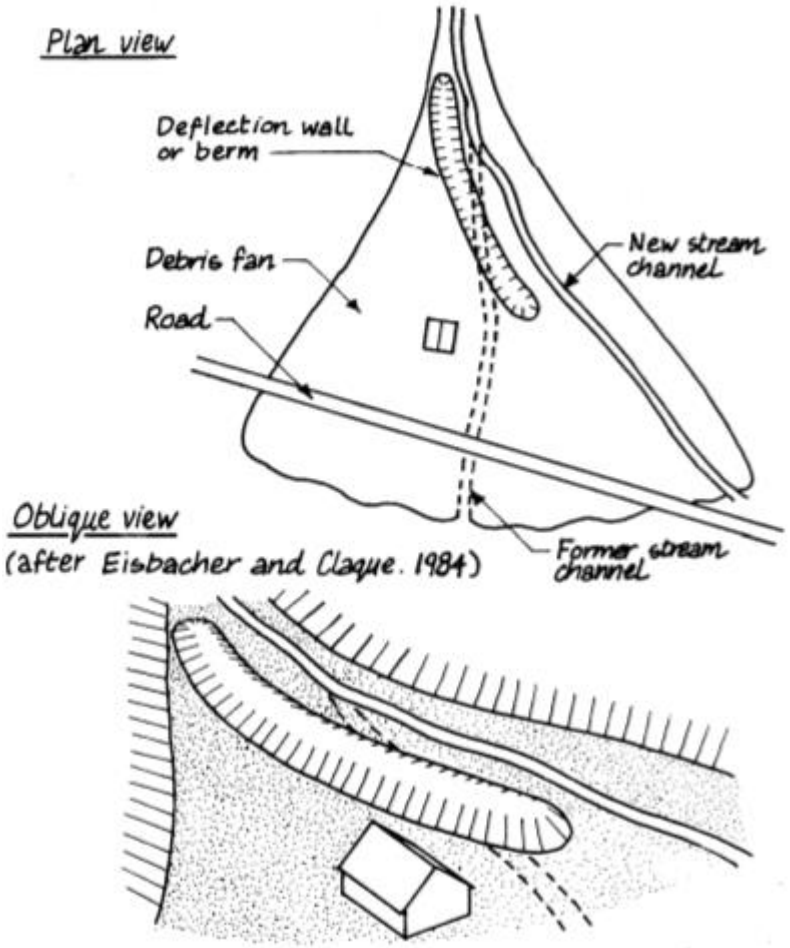

Figure 12: Plan and oblique view of deflection wall or berm (VanDine, 1996, p. 27)

If a deflection structure is combined with other active methods, for example check dams, the deflection wall is constructed as the last element to reduce remaining risk. Access for machines is of great importance as they maintain and empty the channel after an event, and fix any erosion

damage along the deflection wall. The process of cleaning the flow path is done in order to maintain a high effective height of the deflection wall (Christiansen, 2013, p. 20).

Deflection structures are constructed of concrete, reinforced concrete, boulder revetments, gabions, earth or other materials (Huebl & Fiebiger, 2005, p. 477). Material found close to the location is preferred as this saves both time and money. One example is reinforced soil of granular material. By the use of geogrids, this allows soil to be built steep and is easily adjusted to the terrain (Christiansen, 2013, p. 21).

Figure 13: Deflection wall along E39, Flåskjer, Ørsta

Dimensioning of the wall should be done by considering the pressure from the front of the debris flow in addition to the shock from the large boulders (Hungr, Morgan & Kellerhals, 1984, p. 674). After the front hits the barrier at the initial collision, the masses stops and forms an inert mass which protects the structure from further loading.

In order for a deflection wall to provide optimal security, one should think especially about location, design and dimensions (Norem & Sandersen, 2012, p. 77). Important parameters are listed under and explained closer in the following pages:

- Angle between the debris flow and the deflection wall and any change of direction of the deflection wall
- Inclination on the flow path side of the deflection wall
- Height of the deflection wall
- Design of the flow path
- Drainage of the deposition area
- Erosion protection of the area

Angle between the direction of the debris flow and the deflection wall:

The angle between the debris flow and the deflection wall, named δ, should not exceed a critical value in order for the deflection wall to function optimally (Norem & Sandersen, 2012, p. 78). The recommended value of δ should not exceed 10-20°, but δ up to 30° have accomplished satisfactory results in the past. The angle should not be too large due to the low strength in debris flow due to its high content of water.

A change in the direction of the deflection wall is seen when it is constructed to secure roads or railways, see figure 14. The deflection wall is then deflected much more than 20-30° in order to make the deflection wall parallel to the infrastructure. The change in direction has to happen gradually, but if the angle is large at some point, one need to construct the height of the deflection wall to be large enough to avoid overspill. The debris flow masses are led into depressions or excavated areas close to the infrastructure.

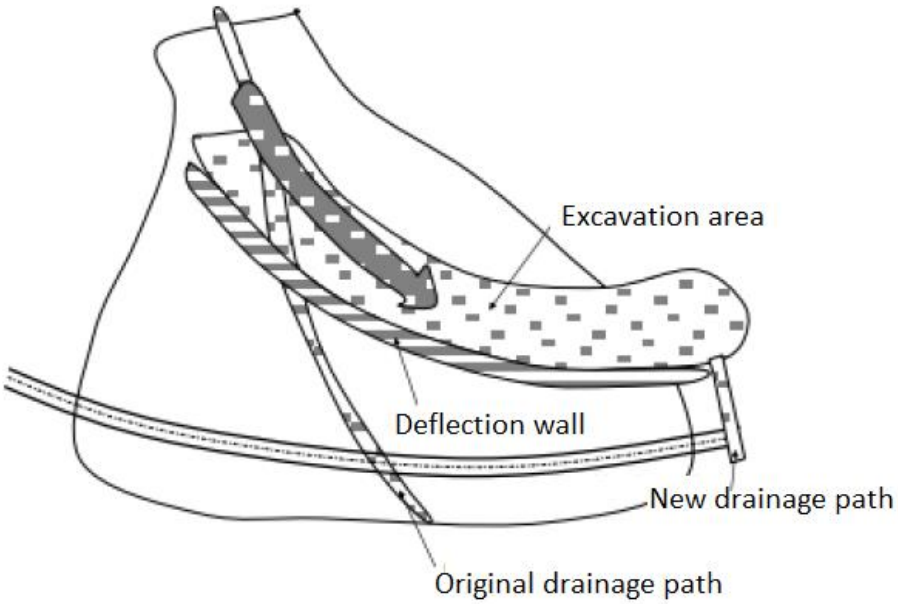

Figure 14: Deflection wall to secure road (Norem & Sandersen, 2012, p. 77)

Inclination on the flow path side of the deflection wall:

The steeper inclination of the deflection wall is giving a larger effect. The steeper angle, the larger is the effective height, which is favourable (Norem & Sandersen, 2012, p. 78). This is experienced from both models and real life. A steep wall can be constructed by the use of reinforced soil in geogrids (Christiansen, 2013, p. 24).

A deflection wall with height 5,0 m is built on a terrain with constant inclination of 11°. Two different inclinations of the deflection wall is examined, 1:1,5 (33,7°) and 3:1 (71,6°), see figure 15. In the first example where the inclination is 33,7°, the effective height, which is height from toe to apex in the direction of the debris flow (Norem & Sandersen, 2012, p. 80), is reduced from 5,0 to 1,4 m. The low inclination makes it easy for debris flow material to flow over the barrier. The deflection wall with an inclination of 71,6° reduces the effective height only from 5,0 to 4,0 m and is more efficient in transporting the flowing masses to its deposition area.

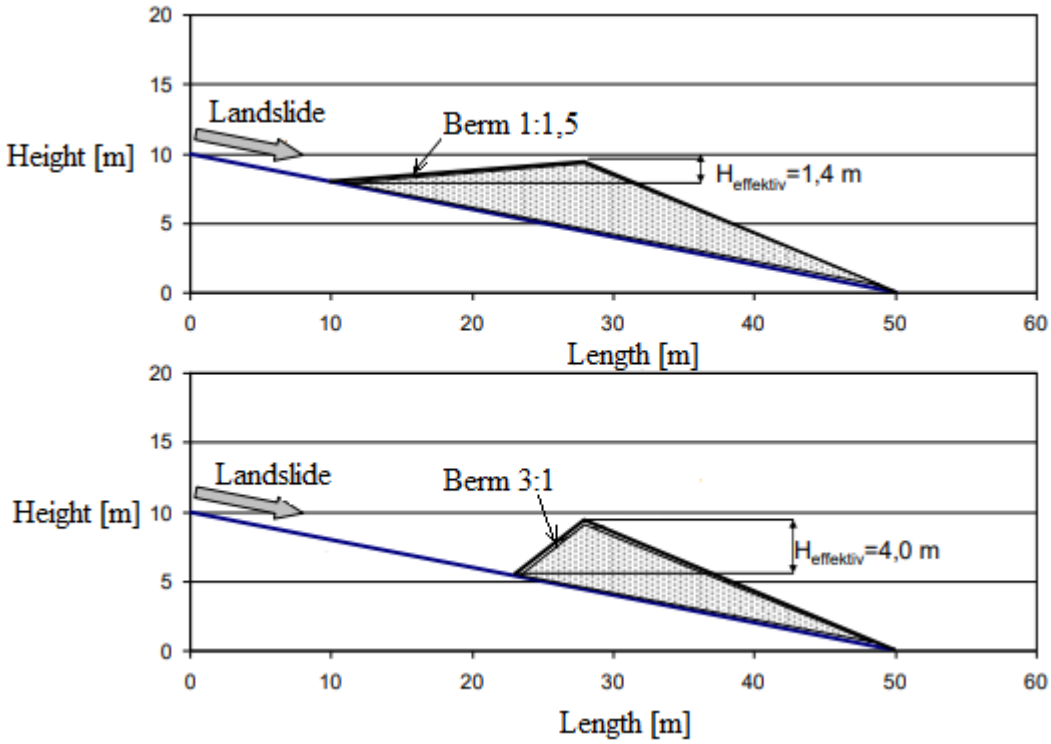

Figure 15: Cross section of terrain and deflection wall (Norem & Sandersen, 2012)

An important aspect with steep inclination is the possibility that it generates a shockwave which is sent backwards, see figure 16, and slows down the velocity of the debris flow (Christiansen, 2013, p. 25). Lack of literature makes this important to study in the future for optimization of deflection walls.

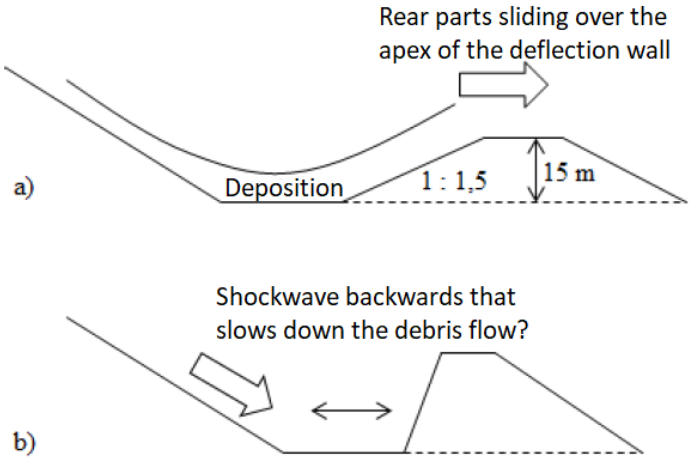

Figure 16: a) The low inclination permits the avalanche to exceed the apex of the 15 m high deflection wall. b) Possible shockwave pushed backwards at a large inclination (Christiansen, 2013, p. 26)

Height of the deflection wall:

The height of the deflection wall needs to be sufficient to avoid overspill of debris flow material, especially where the angle between the direction of the debris flow and deflection wall is large. The effective height is affected by the velocity, width, size, flow height and flow properties of the debris flow, in addition to the angle between the direction of the debris flow and the deflection angle (Norem & Sandersen, 2012, p. 80).

A change in direction of the debris flow will make the debris flow go higher on the deflection wall than if no change in direction is applied. This is due to the velocity of the debris flow and is called the superelevation, ΔH, and is calculated as:

$$\Delta H = \frac{(v*sin\delta)^2}{2*g} \quad (9)$$

where v is the velocity at the front, δ is the angle between the direction of the debris flow and deflection wall and g is set as 9,81 m/s^2 in Norway. The height of the deflection wall needs to be higher than the entry flow height of the debris flow, h_0, and the superelevation, ΔH. The run-up is calculated as below, and is named the energy principle approach:

$$H = h_0 + \Delta H \quad (10)$$

Debris flow has a velocity between 5 and 10 m/s, and calculation gives us a ΔH for both the deflection angles (δ); 45° and 90°. When δ is set as 90°, the deflection wall is defined as a terminal wall. ΔH is calculated as 1,27-5,10 m for the terminal wall, while it is reduced to 0,64-2,55 m for 45°. The larger δ, the higher effective height is needed to avoid overspill of debris flow masses. Flow height is usually between 1-2 m and larger than 3 m for extremely large debris flows (Christiansen, 2013, p. 27). This approach is one of two recommended methods by the GEO Report 270 from 2012 (Au-Yeung, 2015, p.14) in estimation of run-up height on a rigid barrier.

The other recommended method is the Momentum Jump (MJ) Model, a more complex model which includes conservation of mass and momentum (Hákonardóttir et al, 2003; Jóhannesson et al., 2009).

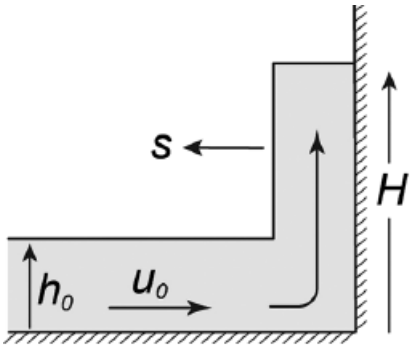

Figure 17: Momentum Jump Model, s represents the speed of a shock which goes backwards (Iverson, George & Logan, 2016, p. 2334)

According to Iverson, George & Logan (2016), this approach is of great relevance for the tests with the wall oriented normal to the chute and flow path. A change of density from upstream to downstream is included in the formula, but as this was not measured in this thesis, we assume the ratio $\rho_f/\rho=1$.The equation for calculation of the run-up height by this model is:

$$\frac{H}{\frac{v^2}{g}} = \frac{2}{\kappa} * \left(\frac{H/h_0}{\left(\frac{H}{h_0}\right)^2 - 1} \right) - \frac{1}{Fr^2} \quad (11)$$

where H is run-up, v is velocity, g is gravitational constant, κ is pressure coefficient, h_0 is entry flow height and Fr is Froude number.

A third model, the Frictionless Finite Mass (FM) Model, has been examined. This model considers a finite mass and its mechanical energy balance. Potential, kinetic and total energy are found in the body's centre of mass, and during run-up against a vertical barrier, the total energy is converted into potential energy. Equation for run-up height:

$$\frac{H}{\frac{v^2}{g}} = 1 + \frac{1}{Fr^2} \quad (12)$$

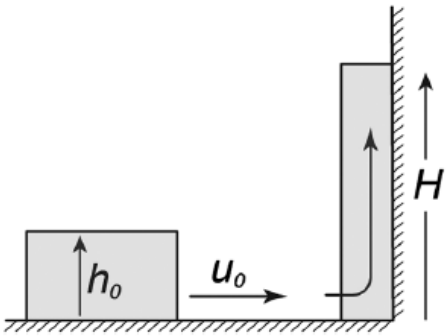

Figure 18: Frictionless Finite Mass model (Iverson, George and Logan, 2016, p. 2334)

For the deflection wall to be able to lead the debris flow masses along the wall and to its intended location, the deflection angle should be less than the 15-20° and not above 20-25°. An effective height of 4-5 m is then usually sufficient (Norem & Sandersen, 2012, p. 81). If a large amount of fines are present in the debris flow material, the angle of the critical angle should be reduced as the flow properties are improved (Christiansen, 2013, p. 28).

Brateng (cited in Christiansen, 2013) performed tests in lab regarding snow avalanches. His results revealed that the curved deflection wall was high enough for the front of the avalanche, but due to the change of direction, the masses lost velocity and increased in height. The masses in front which were slowed down decreased the effective height of the deflection wall and the rear parts of the avalanche were lifted above the front and spilled over the barrier.

Design of the flow path:

Deflection berms are often constructed of excavated masses (Norem & Sandersen, 2012, p. 81) at the location. By excavating and hence lowering the flow path, one increases the effective height of the berm and increases the space in the flow path, which both are favourable in avoiding overspill of debris flow masses. The berm itself has a steep inclination on the side which is hit by the landslide, while the other side has a low inclination to distribute the forces from the debris flow better (Christiansen, 2013, p. 29). The inclination of the excavation floor has a low inclination pointing away from the berm in order to prevent erosion in the toe of the berm and reduce the pressure of the landslide on the deflection structure (Norem & Sandersen, 2012, p. 81), see figure 19.

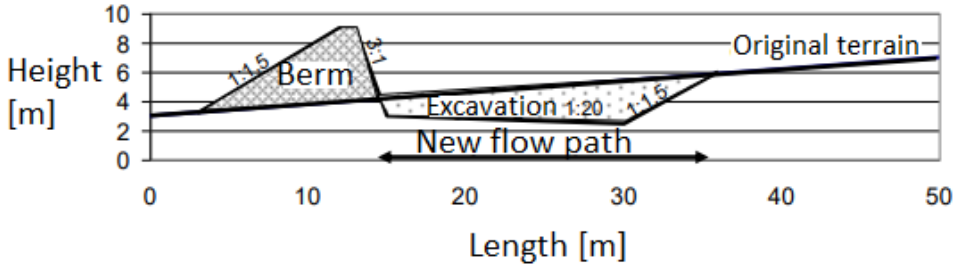

Figure 19: Cross section of excavated area (Norem & Sandersen, 2012, p. 81)

In order to prevent the berm from stopping the debris flow in an unfavourable spot, the path must be wide enough and the inclination of the apex should be even over the whole structure to maintain a constant effective height (Norem & Sandersen, 2012, p. 81). Curved berms are experiencing overspill where the angle δ is larger than 30-40° or at the end of the berm. This implies that the effective height must be increased in the zone where the angle is larger than 30-40° and the basin where the masses are stored must be large enough. The deposition basin is in addition located below the level of which the road/railway is located on to prevent it from flowing out on the infrastructure (Norem & Sandersen, 2012, p. 82), see figure 20.

Drainage of the deposition area:

Construction of a deflection wall changes the path of drainage. The change of direction leads the water somewhere else, see figure 14, and one need to drain this area properly. The new drainage path is preferably situated some distance away from the foot of the wall to prevent erosion of the structure and is safely connected to other drainage systems (Norem & Sandersen, 2012, p. 82). If the old drainage path is wanted preserved, a culvert can be built through the deflection wall, but as this will be clogged between events, an alternative drainage path must be established additionally.

Figure 20: Culvert through a deflection wall along E39, Flåskjer, Ørsta

Erosion protection of the area:

Shear stresses from the flowing masses are of considerable size and demand a need for protection against erosion, especially if the structure is constructed of soil. Erosion protection is needed both at the side which is hit by the landslide and in the newly established flow path, see figure 21. The most exposed area is by the toe of the deflection wall. The deflection wall must be designed to cope with shear stresses up to 10 kPa, which is generated by a landslide

with a flow height of 3 m, a terrain inclination of 10° and a debris density of 2 000 kg/m^3 (Norem & Sandersen, 2012, p. 83).

Figure 21: Erosion protection in Hallinggrovi, Norway (Høydal & Kronholm, 2013, p. 48)

3.2 Terminal wall

Terminal wall is designed in the same way as a deflection wall, but the angle which the debris flow hits the barrier at, is 90°. The same demands apply for this structure as for deflection structures regarding maintenance, drainage and erosion protection (Norem, 2011, p. 91).

Figure 22: Terminal wall in Norway (Norem, 2011, p. 90)

The area where the material is deposited has to be large enough, and the volume of the debris flow is hence of great importance. This storage area is possible to determine for snow avalanches, and is calculated by drawing a line with inclination 5° from the apex to the terrain. For debris flow which has better flow properties, this inclination should be 0-5° (Christiansen, 2013, p.30).

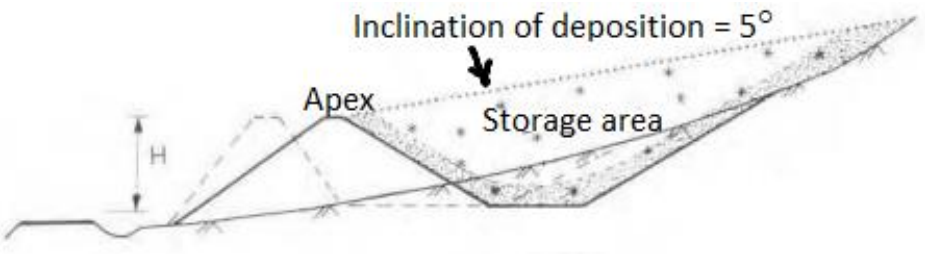

Figure 23: Cross section of a terminal wall hit by a snow avalanche (Norem, 2011, p. 89)

This structure is most efficient when the velocity of the landslide masses is moderate and the structure is hence optimally placed in the outer parts of the discharge area (Norem, 2011, p. 90).

Figure 24 Terminal wall along Rv. 70, Hjørundfjorden, Ørsta

4. MODEL SET-UP

To represent a debris flow as realistic as possible in lab, a flume model was made in the winter of 2018. It is located in the Hydraulics Lab at the Norwegian University of Science and Technology (NTNU) and is an improvement of the old model from 2009. This was a smaller model with a different system of releasing the debris flow. The improved model consists of different parts which all represents characteristic zones of a debris flow.

4.1 Test apparatus and cameras

The releasing tank in the model is set to behave as the source area of a real debris flow. It has the shape of a cylinder with a diameter of 0,4 m, see figure 25, and weighs approximately 225 kg alone. It is filled with debris flow material and water from the top and contains a rotating mechanism which mixes the material with water to a debris flow mixture. The material is released from the tank by removing the bottom which is done from a computer. The old model from 2009 used a different releasing tank where one encountered the problem of material staying inside the box after opening it. This problem is avoided by using the improved releasing tank.

Figure 25: Releasing tank (Vicari, 2018)

The material is released into the chute as a fully developed debris flow. This is not the case in nature, where a debris flow develop during initiation (Le et al., 2016, p. 1240). As the material is released, it follows a chute at an inclination of 17,5°. The chute represents the transport channel where one of the two side walls is transparent. This makes it possible to observe the flow of material from the side, and the transparency provides light into the channel which is favorable for improving the light conditions for the GoPro-cameras. Flow height sensors are placed at three locations right above the chute, see figure 28, in order to measure the flow height of the flowing material. The chute has a total length of 6 m but as the releasing tank is lifted up to the chute, it is not placed at the far end, but some distance away from it. The distance between the cylinder and the end of the chute is 5 m.

The flat and wide area at the end of the model represents the deposition area, also called the run-out zone, see figure 27. The inclination of this part is as low as 2° and gives the material a chance to deposit as velocity decreases in this part of the model. The distance between the white markings in the run-out zone is 20 cm.

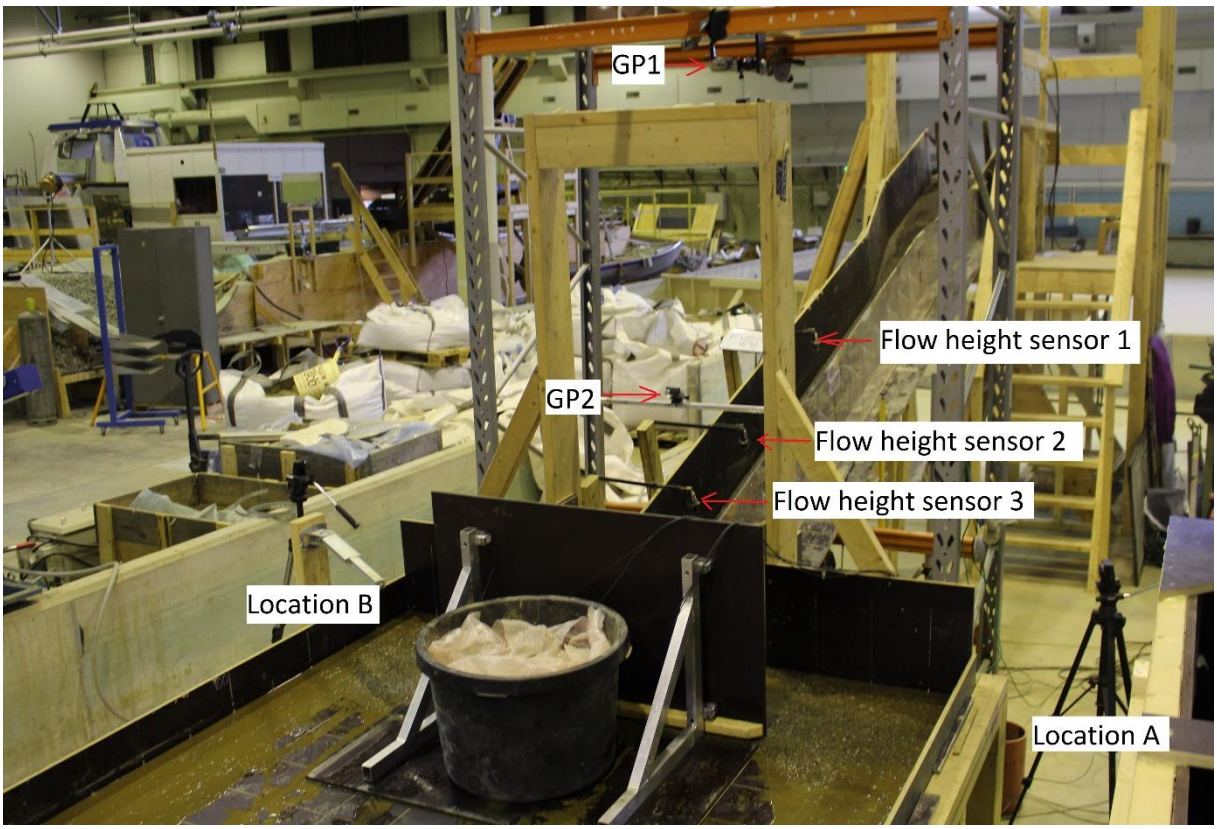

Figure 26: Geometry of the model

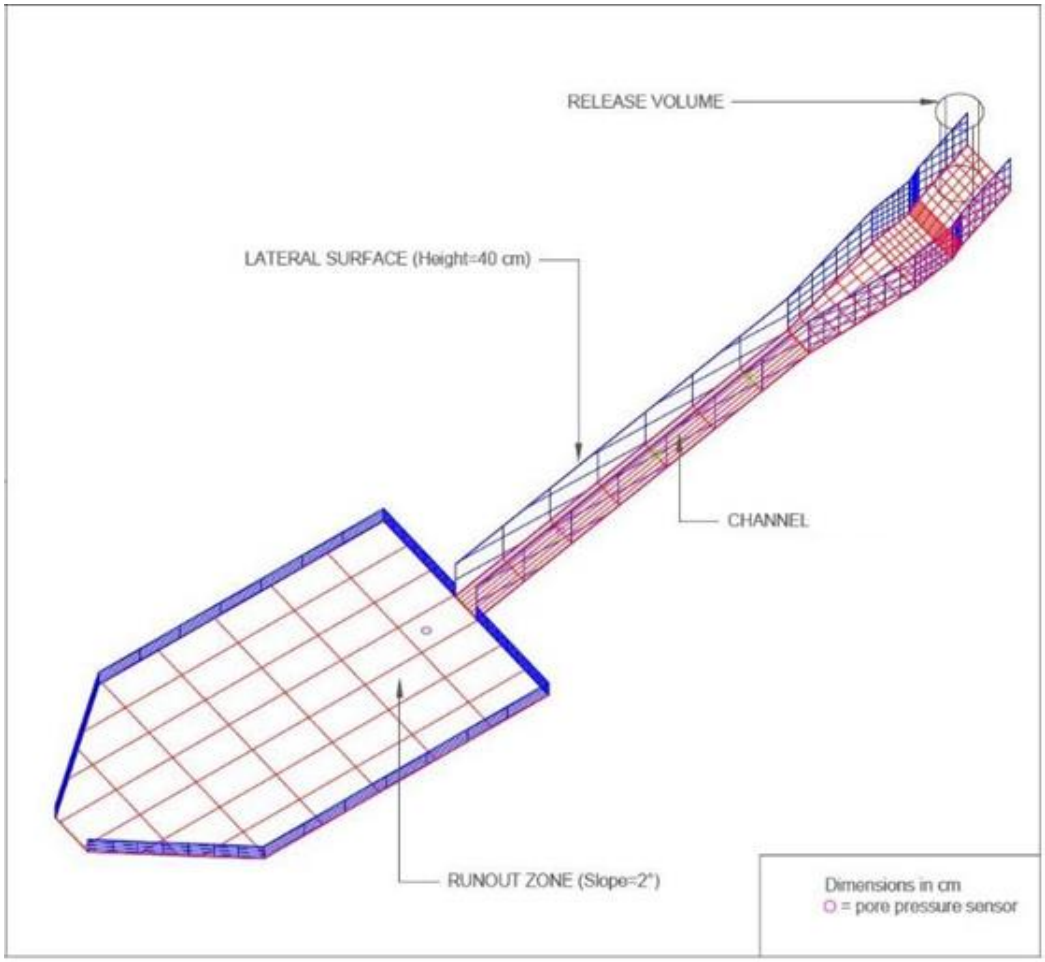

Figure 27: Geometry of the model and definition of coordinate system (Vicari, 2018)

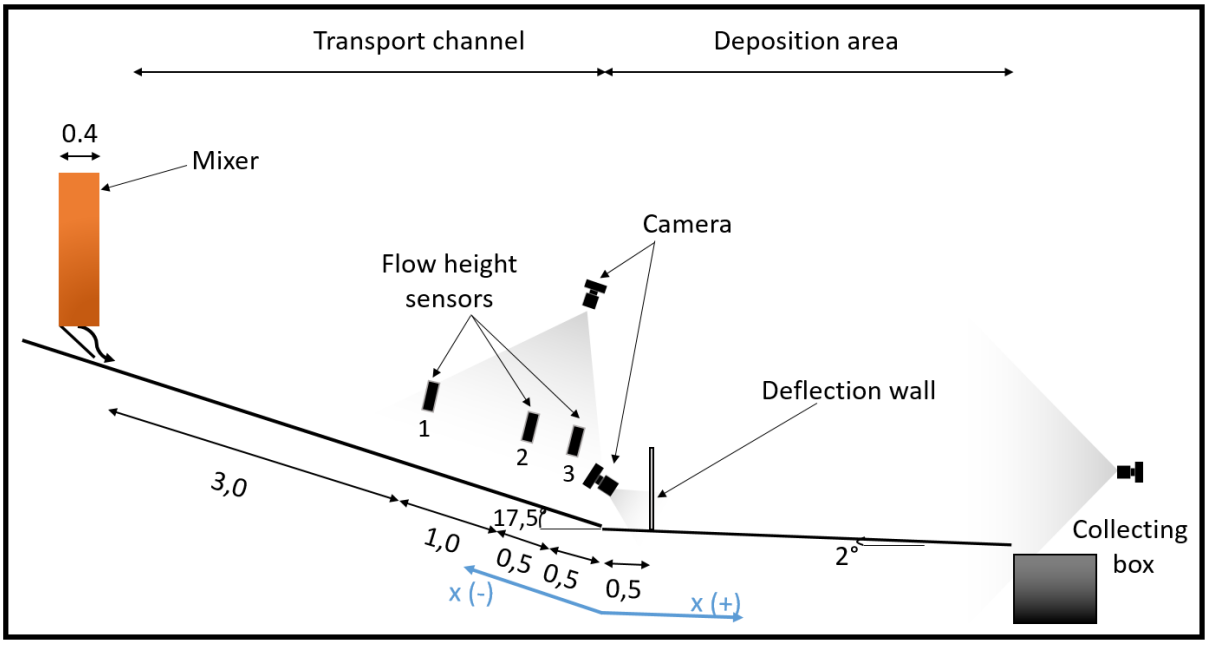

Figure 28: Overview of the model, here for the terminal wall (modified from Vicari, 2018)

4.2 Debris flow material

The samples are made of material from a local quarry not far from Trondheim. The material was weighed and dried previous to the tests in order to determine its natural water content. The solid concentrations we wanted to use were 50 and 60 %. The material used was the same as the material used in Opsahl (2018). The material had since then dried significantly during the autumn and winter, and a water content of the soil was calculated as slightly under 1 %. This was so low that a water content of 0 % has been used.

The water content was further used to calculate the amount of water we need to add to obtain our wanted solid concentrations of 50 and 60 % a and total volume of 25 L. Equations used to obtain the water amount and how much material to fill the tank with are as follows:

The solid mass, M_s, is calculated as: $M_s = V_s * \rho_s$

Volume of solids: $V_s = V_{Total} * \frac{C_s}{100}$

Volume of water is equal to the mass of water: $V_w = M_w = V_{Total} - V_s$

The total mass is: $M_{Total} = M_s + M_w$

Amount of material filled in the releasing tank: $M = M_s * \left(1 + \frac{w}{100}\right)$

Amount of water in the material in the tank: $W_m = M - M_s$

Water needed to obtain wanted concentration: $W_a = V_w - W_m$

Table 3: Calculation of how much water one should add to get the right solid concentration

Solid concentration, C_s	***Total volume, V_{Tot}***	***Solid mass, M_s***	***Solids volume, V_s***	***Water volume, V_w***	***Water mass, M_w***	***Total mass, M_{Tot}***	***Total material to fill in the tank, M***	***Water in the scoop, W_m***	***Addition in water, W_a***
[%]	*[L]*	*[kg]*	*[L]*	*[L]*	*[kg]*	*[kg]*	*[kg]*	*[kg]*	*[kg]*
60	25	41,3	15	10	10	51	41,25	0	10
50	25	34,4	12,5	12,5	12,5	47	34,38	0	12,5

The tank was filled with debris flow material by a shovel and weighed on a rough weight with no decimals. Water was added by filling a bucket with a water hose in the lab and poured onto the tank.

The material was taken to a laboratory where the grain size distribution (GSD) was determined for two samples. GSD is shown in figure 29. The grain size distribution showed a medium graded material as the coefficient of uniformity, Cu, was determined as:

$$C_{u,1} = \frac{d_{60}}{d_{10}} = \frac{1{,}80}{0{,}28} = 6{,}42$$

$$C_{u,2} = \frac{d_{60}}{d_{10}} = \frac{1{,}60}{0{,}31} = 5{,}16$$

Seen from figure 29, the percentage of sand in sample 1 is barely exceeding 60 %, but is enough for the material to be characterized as a sand (Statens Vegvesen, 2005). The content of gravel is about 37 %, which is high enough to name the soil by an adjective. The material will hence be characterized as a gravely sand. The second sample is also characterized as a gravely sand. d50 is equal to 1,45 mm in the first sample, and 1,3 in the second.

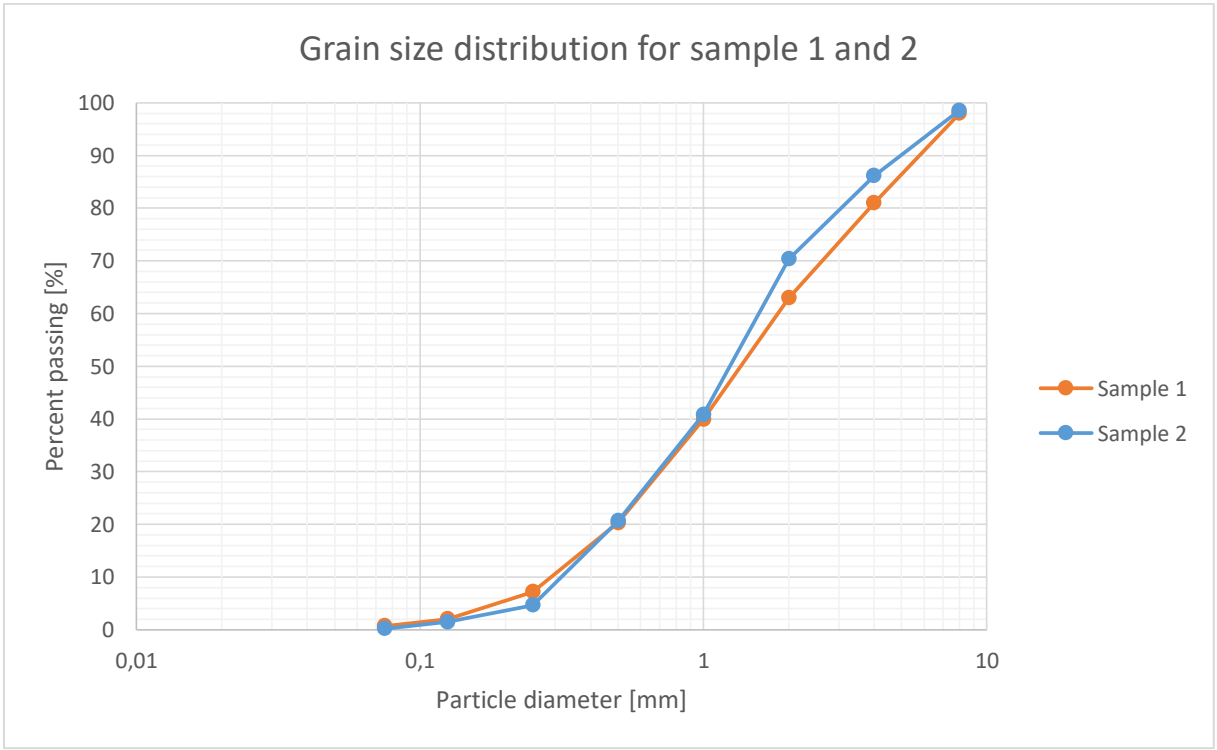

Figure 29: Grain size distribution curve for sample 1 and 2

The grain size density was found in the specialization project as 2,753 g/cm^3. It was done in lab by a pycnometer using grains smaller than 4 mm in diameter. The same number has been used in this master's thesis.

4.3 Deflection wall

The deflection wall was constructed in February by technicians in the Geotechnical department of NTNU. It is constructed of a 11 mm thick plate with white lines for each 5 cm in the vertical direction. The plate is connected to two rows of force sensors in order to measure the force from the debris flow. The wall is supported by a horizontal plate and a frame, in addition to a bucket of sand which is placed on top of the horizontal plate to prevent the structure to slide due to its relative light weight, see figure 26.The height of the wall is 70 cm and it is 120 cm long.

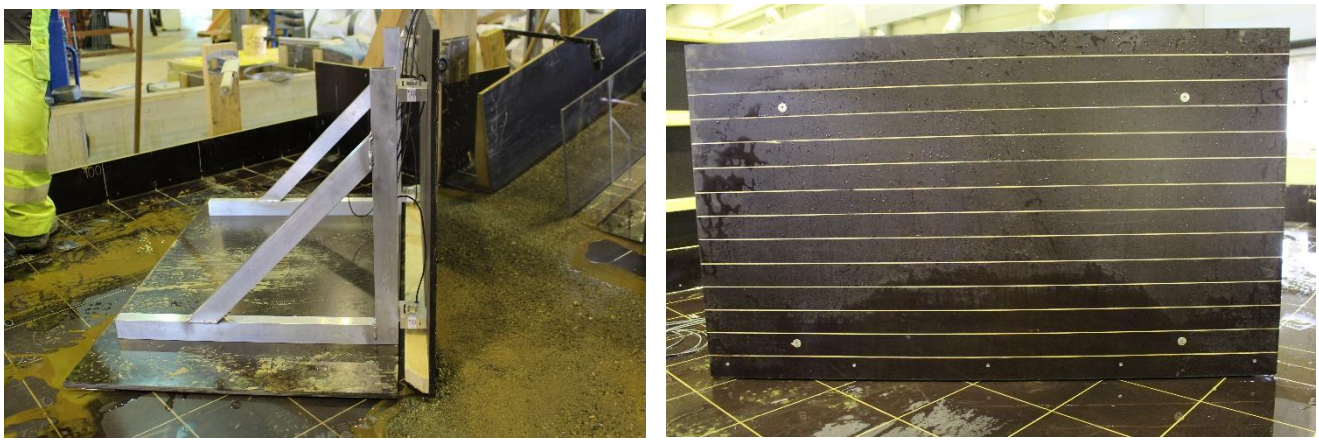

Figure 30: Deflection wall seen from the side and the front

The wall is located at the deposition area of the model, but not fixed to the floor in order to make it possible to change to the deflection angle easily. In addition, two small metal plates were placed under the horizontal plate of the wall to avoid friction between the wall and the floor.

White dots in the grid markings on the floor are marked to place the wall in the correct angle in relation to the direction of the debris flow. The inclination angle of the wall has not been examined in this project.

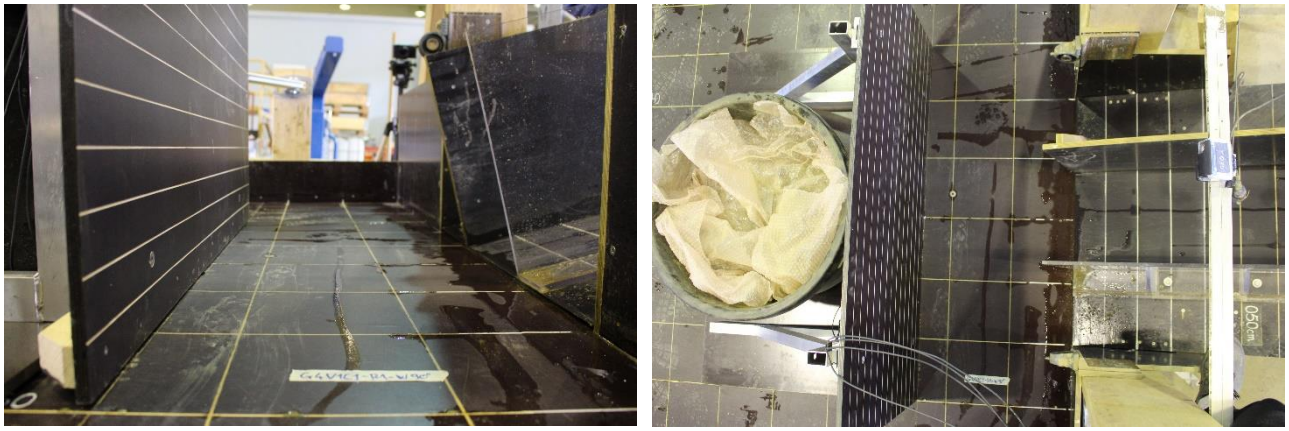

Figure 31: Terminal wall seen from the side and above

The wall is placed in the middle of the deposition area, so the distance to the two columns of sensors are the same. The wall is placed 49,5 cm from the end of the chute. Total force is obtained by adding the measurements from the four sensors.

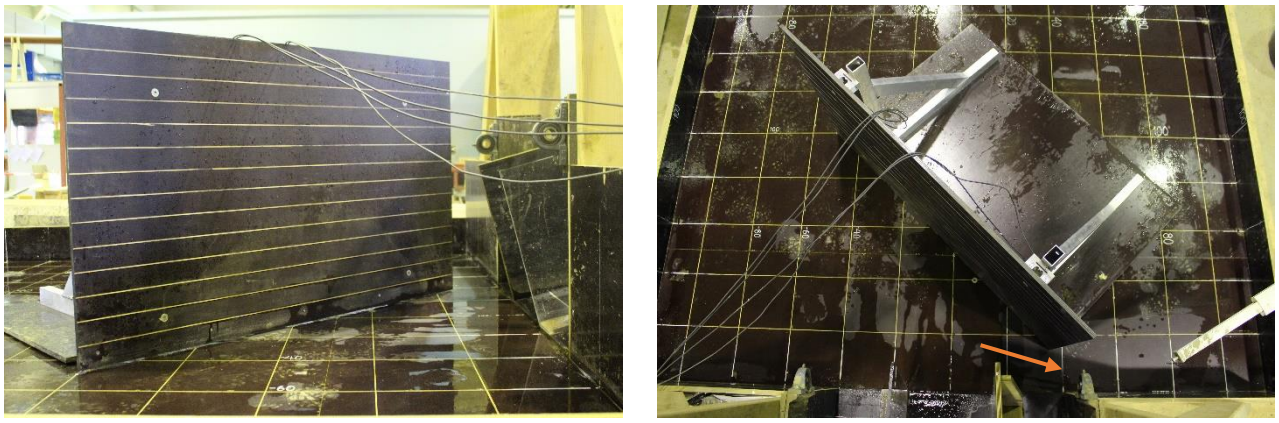

Figure 32: Deflection wall with angle 45°. Arrow marking the path we do not want material to flow

The wall is placed at a position to prevent material from going around the wall and to the right, see orange arrow in figure 32. The distance between the two columns of sensors is 80 cm, and at this angle, located in such a way that the two columns of sensors are located approximately 30 (sensors B and C) and 50 cm (sensors A and D) from the centreline. The coordinates of the end of the plate is marked on figure 33. F_A correspond to the force from sensor A, F_B to sensor B, etc.

The maximum force is found by adding the four forces in the plate, just as for the terminal wall. This is the orthogonal force which is compared to the terminal wall, while the force in the direction of the chute (F) is found by multiplying with cosine (45), see figure 33.

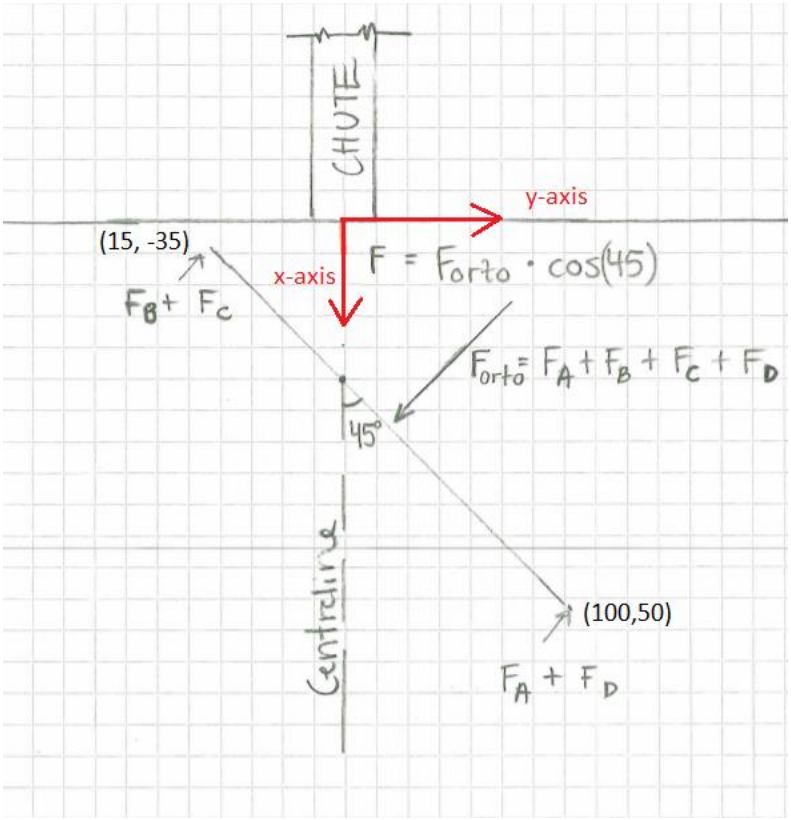

Figure 33: Forces acting on a deflection wall with a deflection angle of 45°

4.4 Physical modelling

The difficulty in examining natural events makes us dependent on the opportunity to examine small-scale events and link these. Froude number is a way to correlate a prototype to a model. As described in Crowe et al. (2009, p. 259), similitude is a method to predict the performance in a prototype done from model observations. This similitude involves the Froude number, and we can predict the performance of a real debris flow, which will be the prototype, from the tests performed on the model in lab. The indexes m and p denotes model and prototype, respectively.

The two types of similitude are geometric and dynamic. Geometric similitude suggest that the geometry of the model is exactly the same as the prototype, only smaller, see figure 34. This implies a scale, for example 1:10 or 1:20. If geometric similitude is satisfied, then:

$$\frac{l_m}{l_p} = \frac{w_m}{w_p} = \frac{c_m}{c_p} = \frac{1}{R} = L_r \tag{13}$$

where l, w and c are dimensions associated with model and prototype.

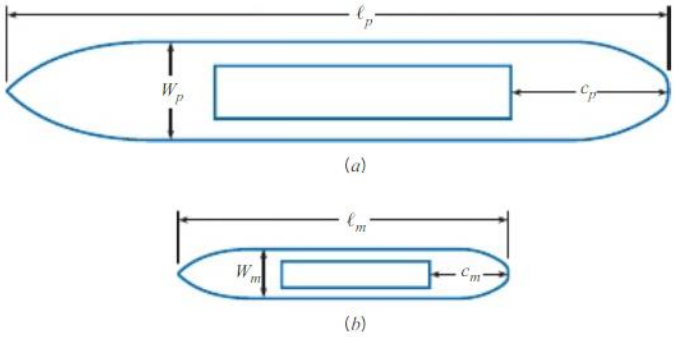

Figure 34: Dimensions in (a) prototype (b) model (Crowe et al., 2009, p. 260)

Dynamic similitude means that forces from the masses in the model and in the prototype are in the same ratio (Fo_m / Fo_p = constant). Forces acting on fluid elements will yield the same flow patterns due to dynamic similarity. Crowe et al. (2009, p. 261) derived equation 14 from the force of gravity on both model and prototype:

$$\frac{v_m}{\sqrt{gh_{0,m}}} = \frac{v_p}{\sqrt{gh_{0,p}}} \text{ or } Fr_m = Fr_p \quad (14)$$

which means that the Froude number in the model is equal to that in the prototype.

This similitude in Froude number has made the scientific community accept the values from small scale tests to be applicable for real events (Vagnon & Segalini, 2016, p. 1692). Froude number found from several studies, see table 1, reveal high Froude numbers, while natural events usually are below 3, see table 4. The values in table 4 are found in Hübl et al. (2009).

Table 4: Froude number in nature

Torrent	Froude number
Rio Reventado	0,5
Hunshui Gully	1,9
Bullock Creek	1,26
Pine Creek	7,56
Wrightwood Canyon (1969)	0,95
Wrightwood Canyon (1941)	0,87
Lesser Almantinka	0,84
Nojiri River	2,71

The model used in lab is not representing a specific debris flow, but is characterized as a principle model which represents a typical debris flow (Laache, 2016, p. 38). The model tries to aim at a 1:20 scale, as this is a large model practical to use and a smaller scale could impose scale effects (Hiller & Jenssen, 2009, p. 2).

$$\lambda = \frac{model}{nature} = \frac{1}{20} \tag{15}$$

The equality of Froude numbers in prototype and model enables us to predict the magnitude of velocity and flow height in natural events:

$$Fr_{model} = Fr_{nature} \tag{16}$$

$$\frac{v_{model}}{\sqrt{gh_{0,model}}} = \frac{v_{nature}}{\sqrt{gh_{0,nature}}} \tag{17}$$

Rewriting the expressions gives us:

$$\frac{h_{0,nature}}{h_{0,model}} = \frac{{v_{nature}}^2}{{v_{model}}^2} \tag{18}$$

And we have the relation between model and nature for velocity and flow height.

$$v_{model} = v_{nature} * \sqrt{\lambda} \tag{19}$$

$$h_{model} = h_{nature} * \lambda \tag{20}$$

The velocity of a natural debris flow is found in the range of 5-10 m/s, which would in lab be seen as 1,12 and 2,24 m/s, respectively. The flow height, which is usually around 1 m in real events, and up to 3 m in large ones, are in the flume model 5 cm.

4.5 Experimental plan and data processing

Table 5: Experimental plan

Type of countermeasure	Number of repetitions	Name of test	Registered parameters	Test performed
No wall	3	G4V1C1-R1	· velocity	March 11th
		G4V1C1-R2	· flow height	
			· run-out length	
			· deposition shape	
Deflection wall	2	G4V1C1-R1-W45	· velocity	March 11th
(δ= 45°)		G4V1C1-R2-W45	· flow height	
			· run-up height	
			· shape of splash	
			· force	
			· run-out length	
			· deposition shape	
Terminal wall	6	G4V1C1-R1-W90,	· velocity	March 11th,
(δ= 90°)		G4V1C1-R2-W90,	· flow height	22nd and
		G4V1C1-R3-W90,	· run-up height	29th
		G4V1C3-R1-W90,	· shape of splash	
		G4V1C3-R2-W90	· force	
		G4V1C3-R3-W90	· run-out length	
			· deposition shape	
Entrainment	1	Entrainment	· erosion	May 15th

The name of the tests are described by letters and numbers. G represents the material type, V the volume and C the concentration. G4 is the material type used in this thesis. V1 is 25 L, C1 is 60 %, and C3 is 50 %. R is the number of repetition and W represents the angle between the direction of the debris flow and deflection wall.

Three whiteboards are updated before each test, showing the test name and providing information about the number of repetition. The three sensors were placed at x= -200 cm, x= -100 cm and x= -50 cm, see figure 28 and 35.

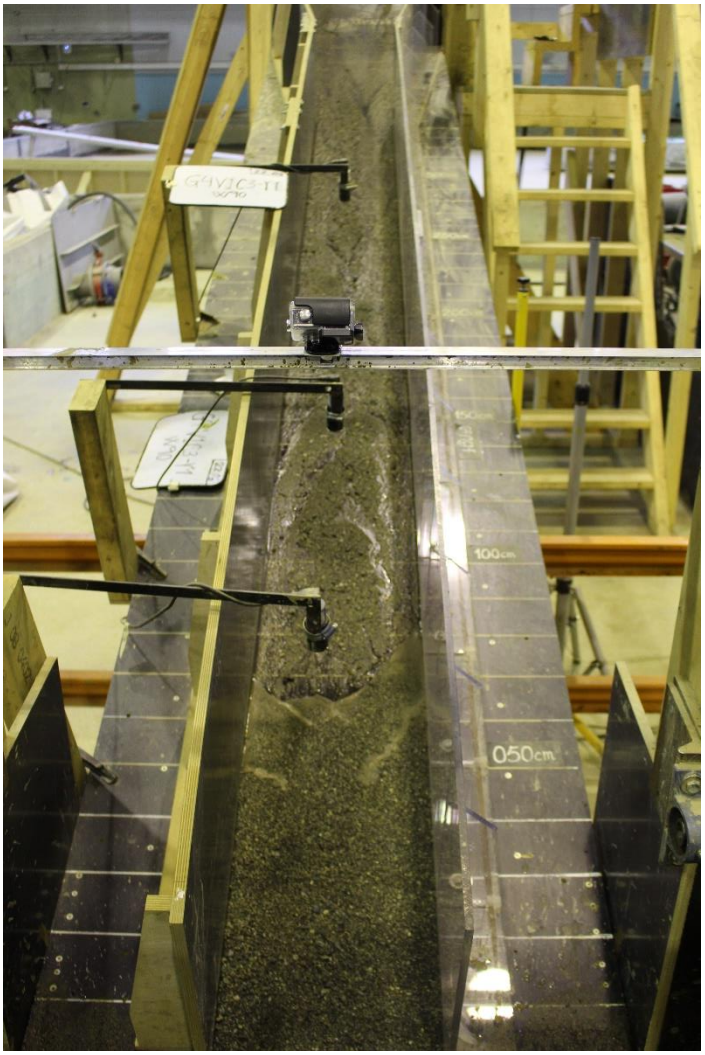

Figure 35: GoPro camera and flow height sensors

Table 6: Equipment

Equipment	Name	Comment
GoPro Hero 4	GP1 and GP2	Fps of 120 and a resolution of 1080p. Tracks the flow front and makes us able to find the velocity of the front. Placed at two different locations, one at the top of the model, and one looking down at the deflection wall from an angled position, see figure 26.
High speed-camera (Canon)	SIDE	Video camera with a fps of 1000. High frame rate setting. Located at the side of the model, it films the material exiting the chute and colliding into the deflection wall in slow motion, visualizing the run-up when it collides. Placed on a stand at location A, see figure 26.
Camera (Canon)	Front and side 2	Fps of 1000. The camera is placed behind the collection box in the tests without any deflection wall. It is located as close as location A as possible when examining the deflection angle of 45°, while on the opposite side at location B, see figure 26, for the terminal wall. Backup if the high-speed camera did not capture the splash.
Ultrasonic sensor	Flow height sensor 1-3	Three flow height sensors registers the height of the moving flow front. Sampling frequency of 50 and 100 Hz. Entrainment test: 1000 Hz

The sampling frequency was increased from 50 to 100 in test 9,10 and 11, as more readings provide a more accurate development of the flow. The resulting plot was more detailed but no other difference was present.

Velocity was calculated by two different methods. The first calculates the velocities at three locations in the chute, at x= -200, x= -100 and x= -50 cm. This is done in Tracker where a 20 cm long calibration stick is placed 10 cm before and 10 after the locations, see blue line in figure 36. The velocity is found by tracking a point mass along the front of the flow, and the average is calculated and presented as the velocity at that location. The point mass is marked at the flow front for each frame and will therefore represent the velocity of the flow front. The calibration stick and purple coordinate system is moved to next location when finished.

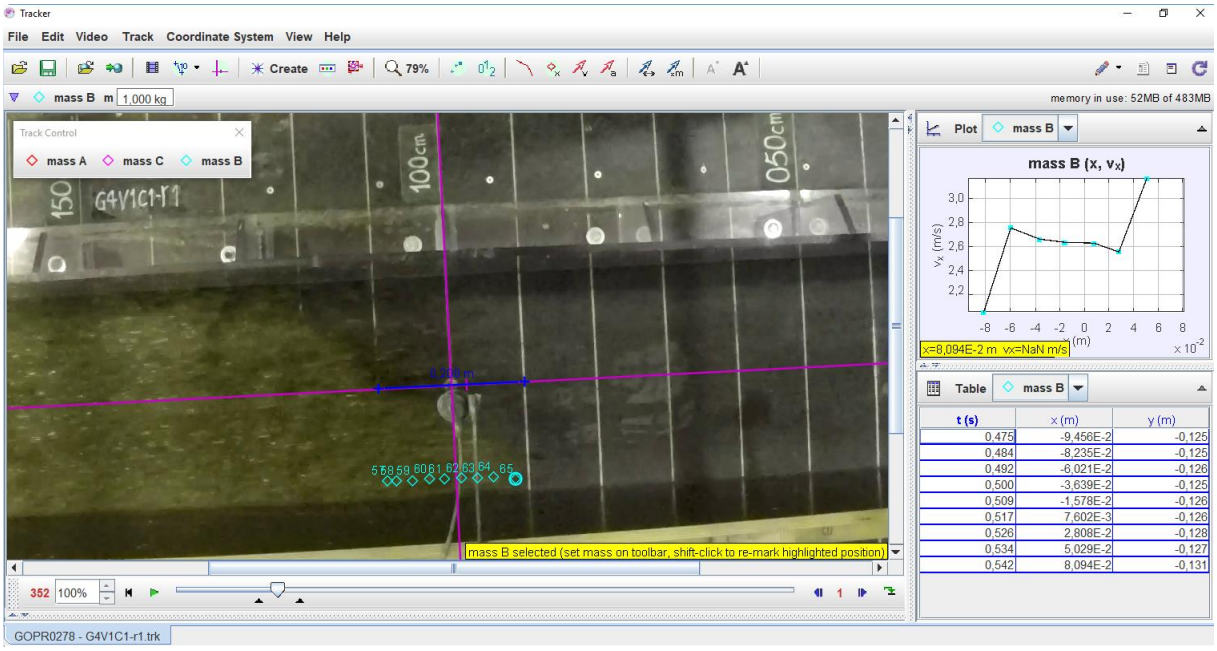

Figure 36: Tracking of point mass to determine the front velocity in test nr. 1

The second method draws us a graph of how the velocity changes along the lower part of the chute (x= -200 cm to x= 0 cm) and during the first part of the deposition area. The camera is placed far down in the chute and has therefore no recording of the velocity at the start of the chute (x= -500 cm) until x= -200 cm. The velocity is found by using filters in Tracker which makes the distance between the white lines equal. For the chute, the fisheye-filter with a field of view angle of 63° avoids radial distortion, while for the deposition area, a perspective filter is needed in addition to the fisheye. The flow front is manually tracked as before with the step size set as 2.

4.5.1 Procedure of testing

All days in lab were efficient as we were two or three persons present. Each test took about 30 minutes to perform, and the procedure of testing is as follows:

1. Prepared the debris material by filling the tank with the desired amount of material and water
2. The crane lifted the ‘‘debris flow’’ up to the top of the model
3. Pushed ‘‘Start Mixer’’ which mixed the material with water
4. Updated the whiteboards accordingly
5. Prepared LabView
6. Cameras turned on and recording
7. In LabView: Pushed ‘‘Set all zero’’ for the flow height and force sensors
8. Pushed ‘’Start test’’, saved the data and pulled out the actuator
9. Stopped the movie-recordings
10. Took photos of the resulting debris flow
11. Cleaned the model and releasing tank before conducting new test

The model is cleaned after each test and all the material is collected in a box at the far end of the model. The used material is thrown away and not re-used because of the outwash of fine particles and the high water content added from the cleaning. As the water from the cleaning process is swept into the collection box, one loses control of the concentration as one has no quantity of the water being added and hence how much material to add to get the correct solid concentration.

5. RESULTS

The results from the eleven performed tests are presented in this chapter. Measured parameters in lab were flow height, front velocity, run-up height, deposition height, force and run-out length. This resulted in six subchapters which presents the results of the mentioned parameters, in addition to the Froude number. This chapter includes mainly results and a brief discussion which will be extended in the sixth chapter.

5.1 Flow

The material released from the tank is well mixed by the built-in mechanism, and there is no sign of any freezing masses which has been a problem in previous Master Theses where mixing was not standardized. Each test is unique for the eleven tests.

In some tests, the premier part of the debris flow is at the right side along the whole flume, while in other tests, this changes location completely in a matter of seconds, see figure 37. This is due to fast flowing material in the left part of the chute, seen from the top of the model. The front is in every of these tests first at the right side, but is at the opposite side towards the end of the chute.

Large particles that separates from the debris flow masses are observed in front of the debris flow front in test 1 and 7. These particles are called up on towards the middle of the chute seen in GoPro 1, about x=-120 cm.

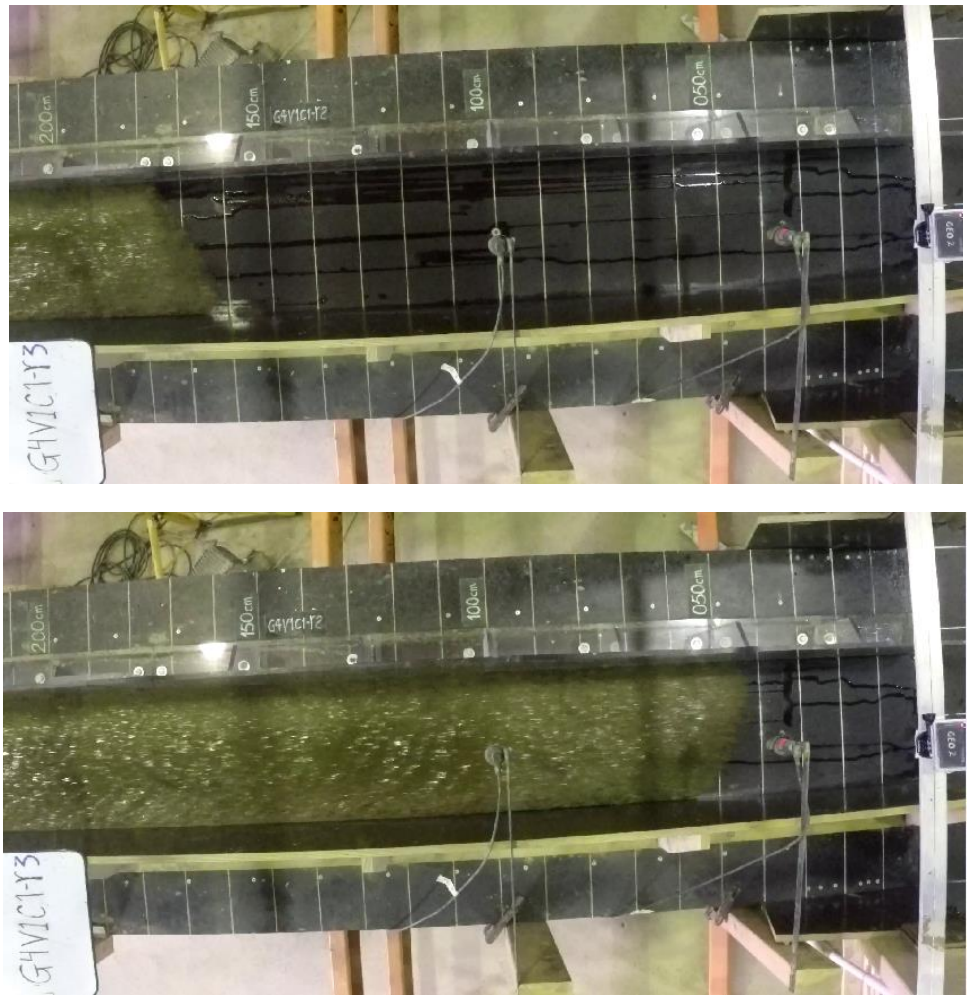

Figure 37: Change of flow front in test 3

Collision against the terminal wall results in a upstream-propagating shock against the wall, and as material from behind continue to collide into the wall, the masses are shunted to the sides and a backsplash is created, see figure 38. This falls down on the incoming masses and creates a chaotic movement where some of the material is thrown back towards the chute. As the supply of material ends, the grains in the material deposits and water and fine particles runs out of the mix. This slurry is collected in the box at the end of the model.

The deflection wall with a deflection angle of 45° is characterized by a lower run-up height compared to the terminal wall. After the collision, the material moves along the wall before it drops and creates a new front which expands mainly in the y-direction. As the supply of material ends, the material deposits and fine material mixed with water runs out of the masses.

Figure 38: Upper left: Collision into the plate, middle: lateral shunting to the side of the plate, upper right: backsplash. Lower left: Backsplash mixes with incoming material and creates a chaotic movement, lower right: deposition height (screenshot of test nr. 4 from Tracker).

Figure 39: Upper left: Collision into the deflection wall, middle and upper left: upward splash and movement along the wall. Lower left: creation of a new front, lower right: height after the event (screenshot of test nr. 6 from Tracker).

5.2 Front velocity

The velocity of all the eleven tests was found by tracking the flow front at three locations, and is presented in table 7.

Table 7: Velocity

Test nr.	Name of the test	Deflection angle	Solid concentration	Velocity at x= -200 cm	Velocity at x= -100 cm	Velocity at x= -50 cm
		[°]	*[%]*	*[m/s]*	*[m/s]*	*[m/s]*
1	G4V1C1-R1	0	60	2,8	2,64	2,88
2	G4V1C1-R2	0	60	2,69	2,57	2,56
3	G4V1C1-R3	0	60	2,62	2,43	2,63
4	G4V1C1-R1-W90	90	60	2,77	2,27	2,22
5	G4V1C1-R2-W90	90	60	2,82	2,34	2,43
6	G4V1C1-R1-W45	45	60	2,4	2,3	2,5
7	G4V1C1-R2-W45	45	60	2,91	2,56	2,23
11	G4V1C1-R3-W90	90	60	2,57	2,34	2,67
8	G4V1C3-R1-W90	90	50	3,28	3,19	3,85
9	G4V1C3-R2-W90	90	50	4,11	3	3,74
10	G4V1C3-R3-W90	90	50	4,27	3,96	3,09

Velocity is then found by a second method to see if they give somewhat the same, see chapter 4.5 for explanation. Figure 40 illustrates the likeness of the two methods over the distance from x= -200 cm to about x= 90 cm, where the end of the velocity plot is where the debris flow exits the view of the camera. The rest of these plots are found in Appendix A.

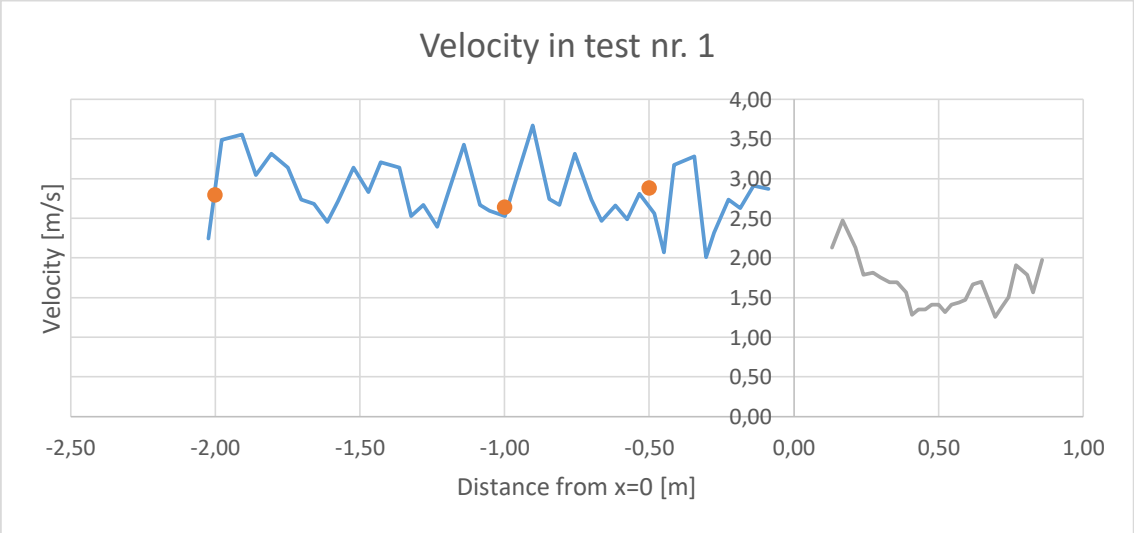

Figure 40: Change of velocity (x=-200 to x=88 cm) and point velocities

5.3 Froude number

Froude numbers (Fr) were found at the three locations where the ultrasonic sensors registered flow heights. The maximum flow height was selected from the ultrasonic sensor recordings and noted. The velocity is the second parameter in the equation, and was found by the first method described in chapter 4.5.

Table 8: Froude number at three locations in the chute

Test nr.	Name of the test	Deflection angle	Solid concentration	Froude number at x= -200 cm	Froude number at x= -100 cm	Froude number at x= -50 cm
		[°]	*[%]*	*[-]*	*[-]*	*[-]*
1	G4V1C1-R1	0	60	-	-	-
2	G4V1C1-R2	0	60	5,19	5,75	6,16
3	G4V1C1-R3	0	60	4,74	4,75	5,21
4	G4V1C1-R1-W90	90	60	5,32	4,80	5,01
5	G4V1C1-R2-W90	90	60	5,84	5,11	5,58
6	G4V1C1-R1-W45	45	60	4,89	4,67	5,25
7	G4V1C1-R2-W45	45	60	5,65	5,65	5,03
11	G4V1C1-R3-W90	90	60	4,86	4,96	5,72
8	G4V1C3-R1-W90	90	50	6,42	6,85	9,41
9	G4V1C3-R2-W90	90	50	8,34	6,81	9,75
10	G4V1C3-R3-W90	90	50	8,91	8,03	8,30

Figure 41 shows a correlation between the Froude number and the run-up height for the two different types of deflection angles. An increase in Froude number implies an increased run-up height.

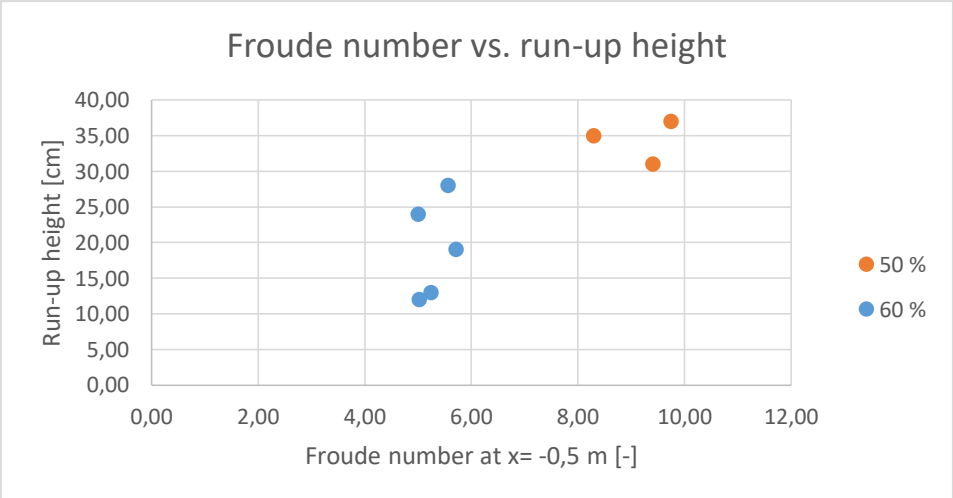

Figure 41: The correlation between Froude number and run-up height

Figure 42 illustrates the change of Froude number along the lower part of the chute. All values are implying a supercritical flow as all the values of Fr is greater than 1. The lines between the three positions are not representing the Froude number as this is unknown, but are drawn to easier show the associated dots.

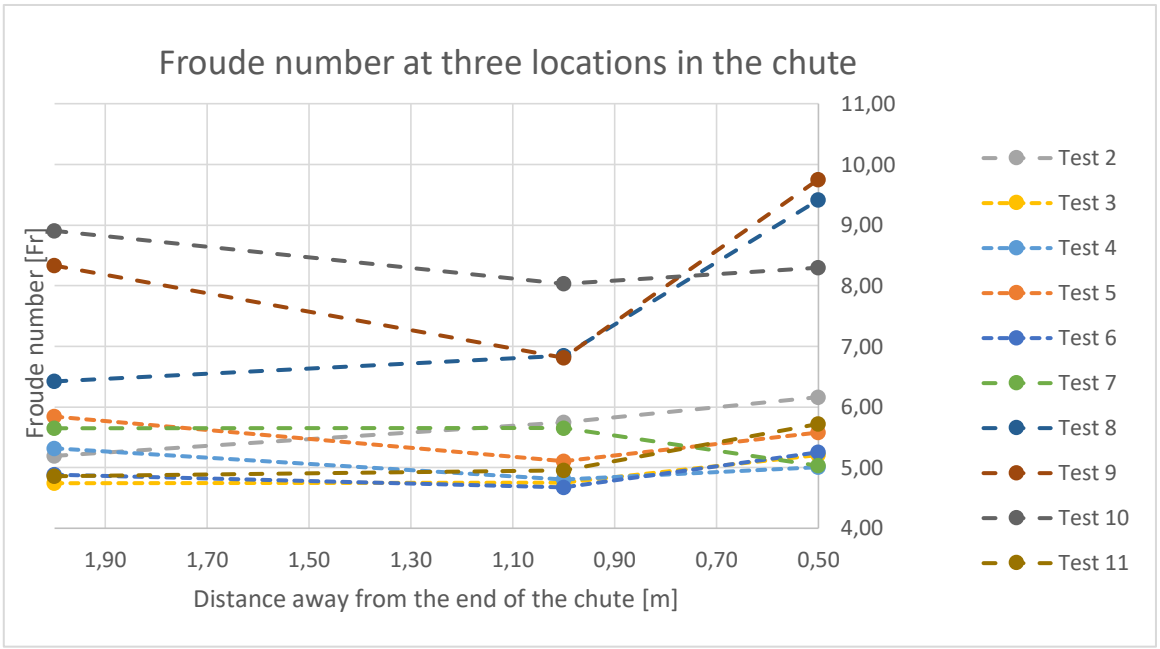

Figure 42: Change of Froude number along the chute

5.4 Flow height and run-up height

The development of flow height for ten tests is presented in Appendix B. The first test lacked flow height measurements. The flow is first measured at sensor 1, before it is registered at sensor 2 and later 3. This is due to the distance between the sensors. The peak represents the head of the flow. The accumulation seen towards the end in figure 43 for sensor 3 is due to the deposited masses which prevents material from exiting the chute.

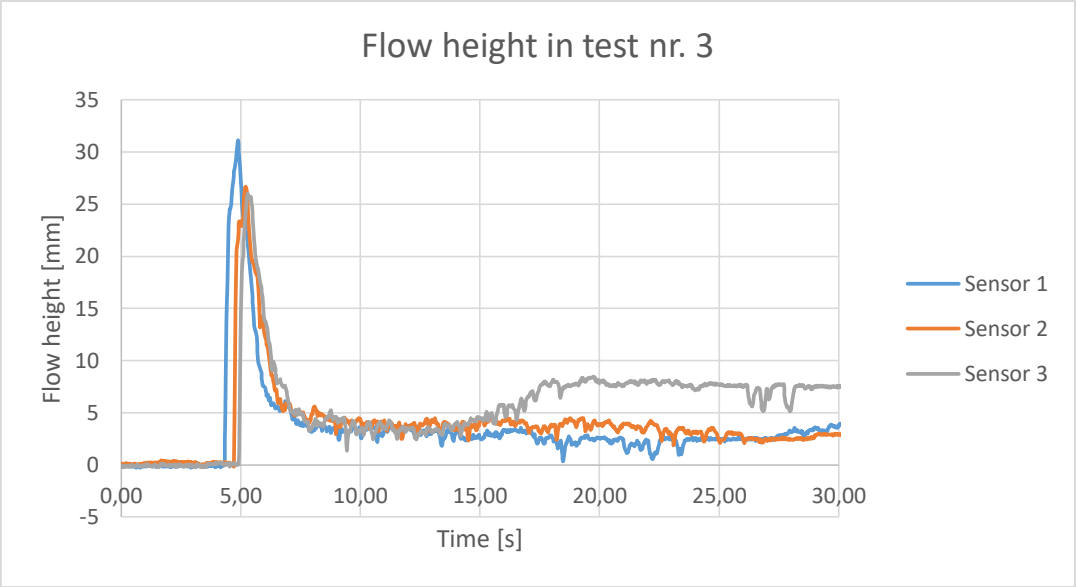

Figure 43: Flow height in the flume for test nr. 3

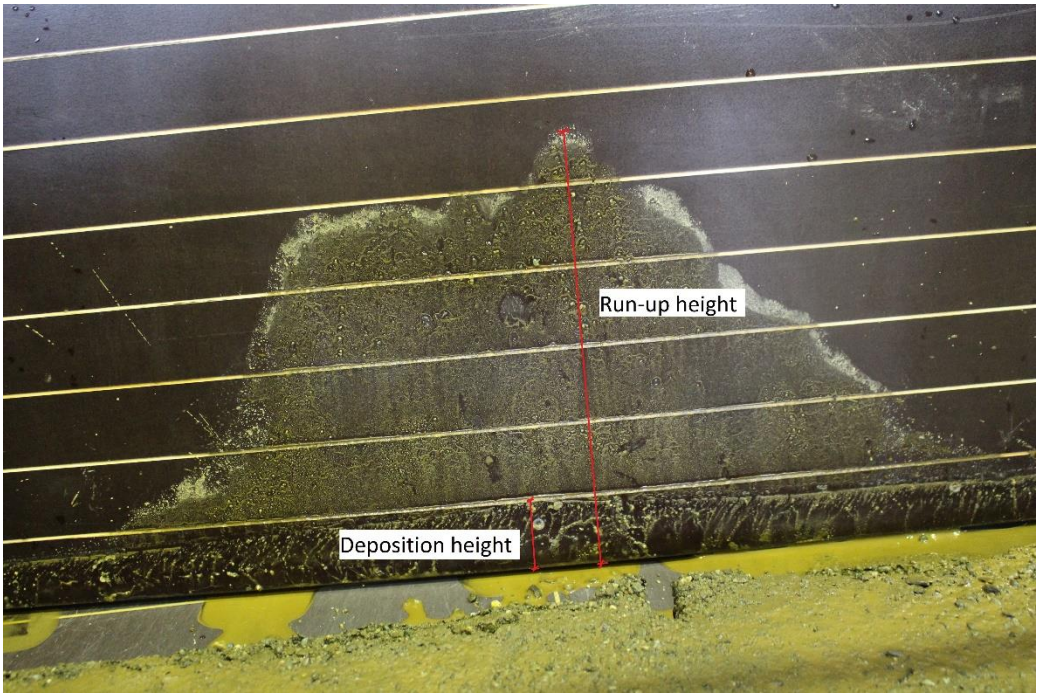

Figure 44: Illustrations of deposition height and run-up height

The run-up height is the highest point the debris flow reaches on the wall as a result of the upstream-propagating shock, see figure 44. Table 9 presents the run-up height and the deposition height measured in lab, in addition to the theoretical run-up height given by the energy principle approach, equation 10. This number is higher than measured in lab, so the right columns shows the percentage of overestimation.

Table 9: Run-up heights

Name of the test	Deflection angle	C_s	Flow height at sensor 3, h_0	Deposition height, H_{final}	Run-up height, H	Theoretical run-up height, equation 3.2	Overestimation
	[°]	*[%]*	*[cm]*	*[cm]*	*[cm]*	*[cm]*	*[%]*
G4V1C1-R1-W90	90	60	2,001	5,00	24,00	27,12	13,00
G4V1C1-R2-W90	90	60	1,936	5,00	28,00	32,03	14,40
G4V1C1-R1-W45	45	60	2,309	3,00	13,00	34,16	162,80
G4V1C1-R2-W45	45	60	2,003	3,00	12,00	27,35	127,91
G4V1C1-R3-W90	90	60	2,221	5,00	19,00	38,56	102,93
G4V1C3-R1-W90	90	50	1,705	3,50	31,00	77,25	149,20
G4V1C3-R2-W90	90	50	1,499	4,70	37,00	72,79	96,73
G4V1C3-R3-W90	90	50	1,413	3,50	35,00	50,08	43,08

Run-up height is also affected by the velocity in the chute, as seen in figure 45. The higher velocity, the higher splash and run-up height. A reduction in the solid concentration from 0,6 to 0,5 gives higher velocities which results in larger run-up heights. The two lowest measurement of the run-up height is for the deflection wall of 45°, so if two trend lines were drawn for the two deflection angles, the two lines would be increasing. The plot hence reveals the close relationship run-up height has with deflection angle, which needs to be studied.

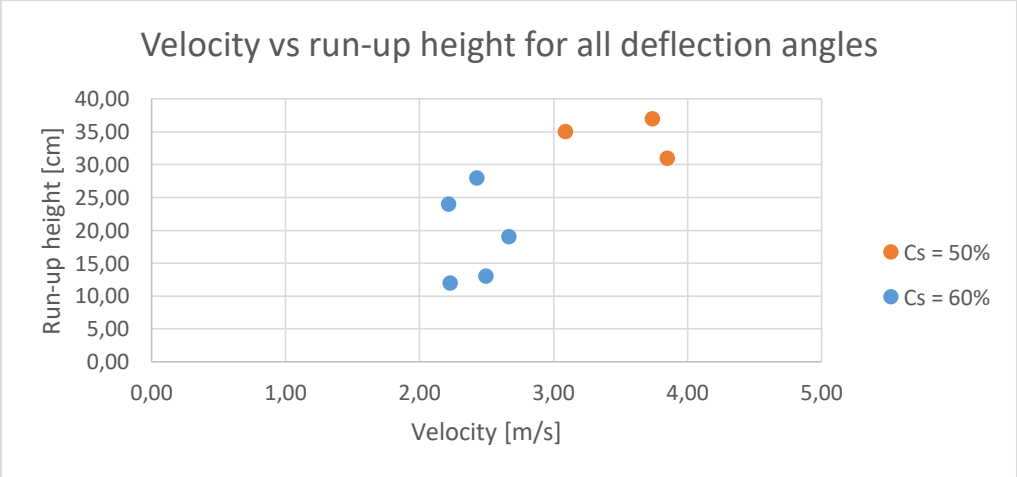

Figure 45: Velocity plotted against run-up height

The effect of the deflection angle is demonstrated in figure 46, where an increase in the deflection angle increases the registered run-up height.

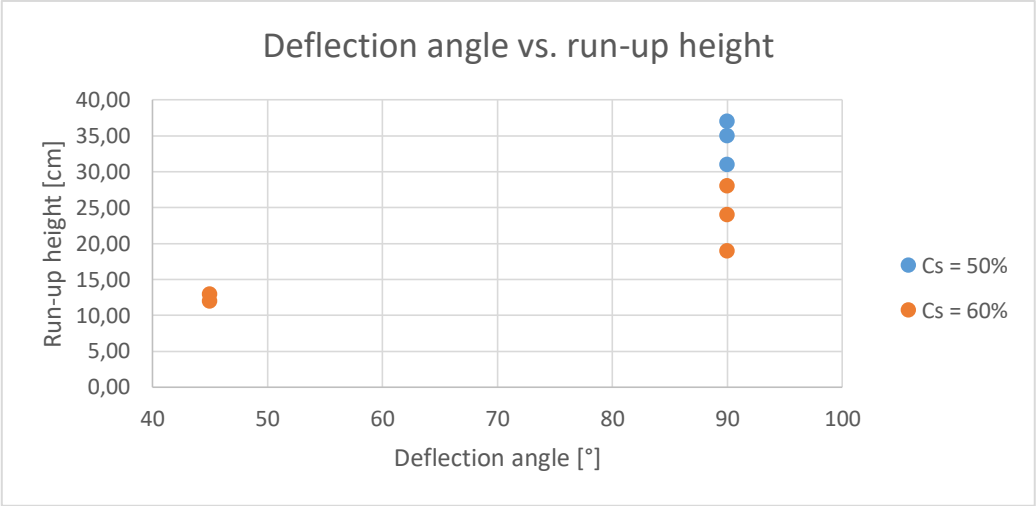

Figure 46: Deflection angle plotted against run-up height

5.5 Force measurement

Maximum force is calculated as the maximum of the sum from force sensors 1-4, see figure 47 and 48. Force plots for all tests are found in Appendix C. The maximum force is highest for the terminal wall. For the terminal wall, the force is positive in the two lower sensors, while it is negative in the two upper. This also the case for the wall with a deflection angle of 45°. The force is observed to last longer for the deflected wall compared to the terminal where the collision happens abrupt.

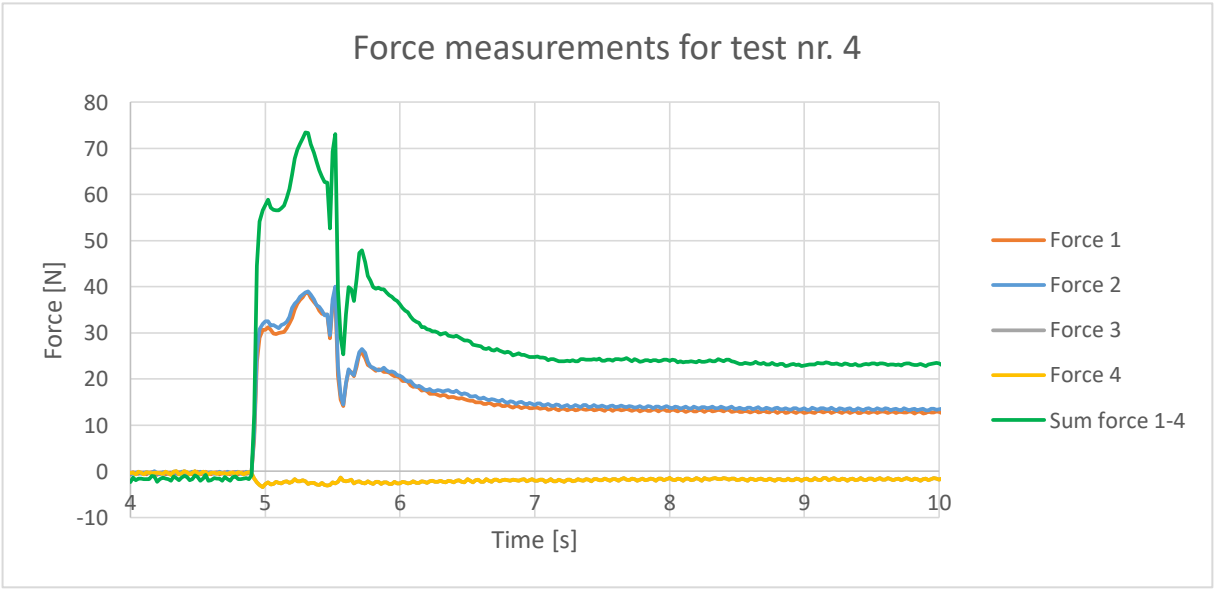

Figure 47: Force measurements for test nr. 4

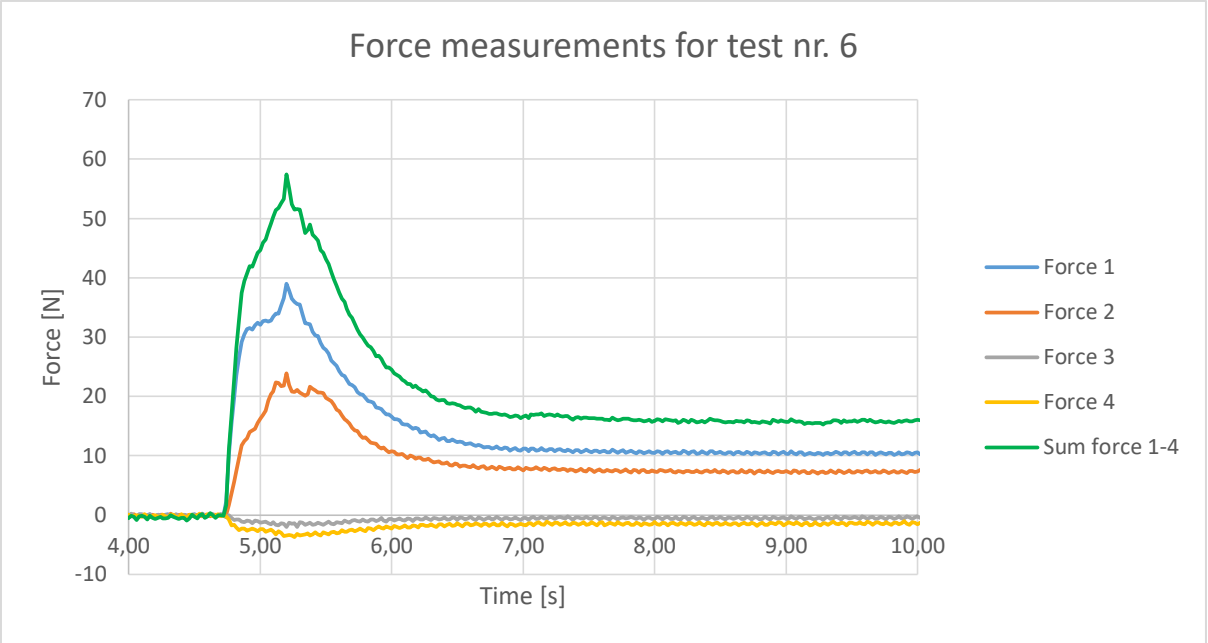

Figure 48: Force measurements for test nr. 6

Table 10: Force measurements

Test nr.	Name of the test	Deflection angle	Solid concentration	F (orthogonal)	P(max)	α_3	k
		[°]	*[%]*	*[N]*	*[Pa]*	*[-]*	*[-]*
4	G4V1C1-R1-W90	90	60	73,47	1356,54	0,134	3,37
5	G4V1C1-R2-W90	90	60	92,21	2341,84	0,193	6,01
6	G4V1C1-R1-W45	45	60	57,42	922,91	0,072	1,99
7	G4V1C1-R2-W45	45	60	51,52	652,15	0,064	1,62
11	G4V1C1-R3-W90	90	60	80,55	1435,83	0,098	3,21
8	G4V1C3-R1-W90	90	50	87,95	1809,67	0,065	5,77
9	G4V1C3-R2-W90	90	50	97,79	1101,86	0,042	4,00
10	G4V1C3-R3-W90	90	50	81,82	765,96	0,043	2,95

Figure 49 presents a plot of the velocity squared vs. measured force for the terminal wall. These parameters are plotted in the same plot due to the hydrodynamic equation, which says that the force is equal to the empirical parameter α_3 multiplied with the density and velocity squared. The average value of α_3 for the six tests with the terminal wall is 0,1.

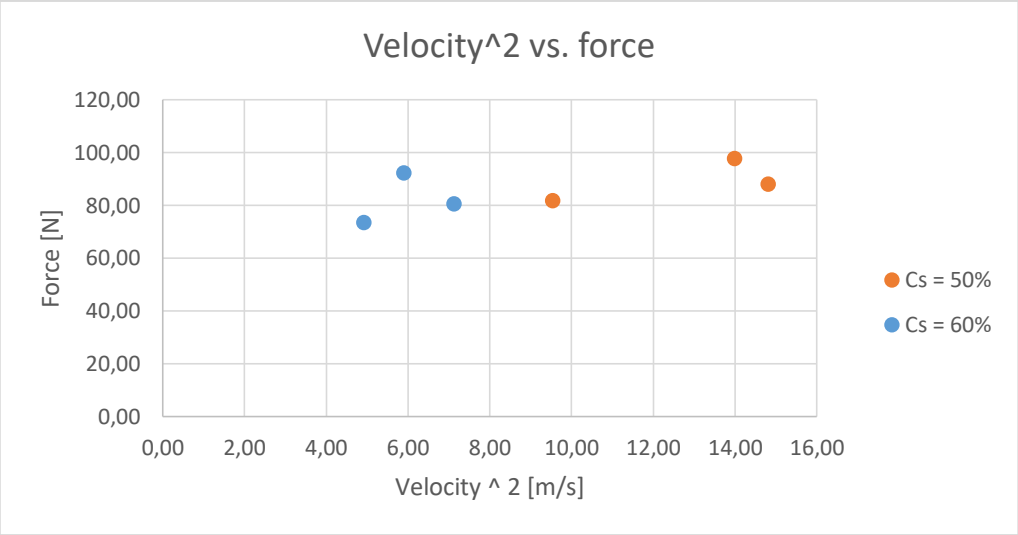

Figure 49: Velocity squared vs. force for the terminal wall

Figure 50 shows the correlation between the measured force and the deflection angle of the wall. As one increase the deflection angle, an increase in the measured force is registered. The solid concentration of 50 % gave a higher force than the 60 %.

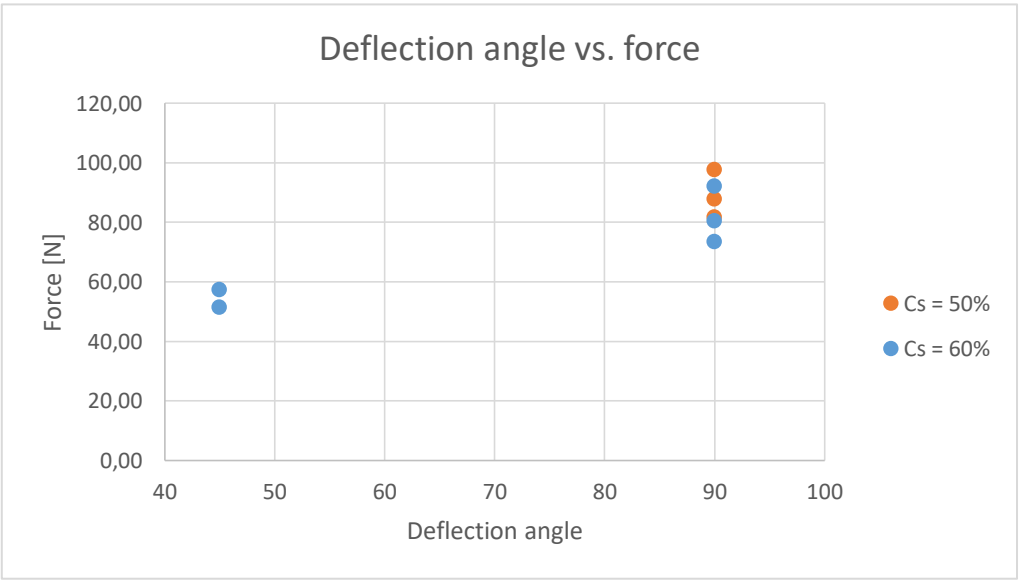

Figure 50: Deflection angle vs. force

5.6 Run-out length

The run-out length was registered for each debris flow event and noted. The length is measured from the start of the deposition area, x=0 cm.

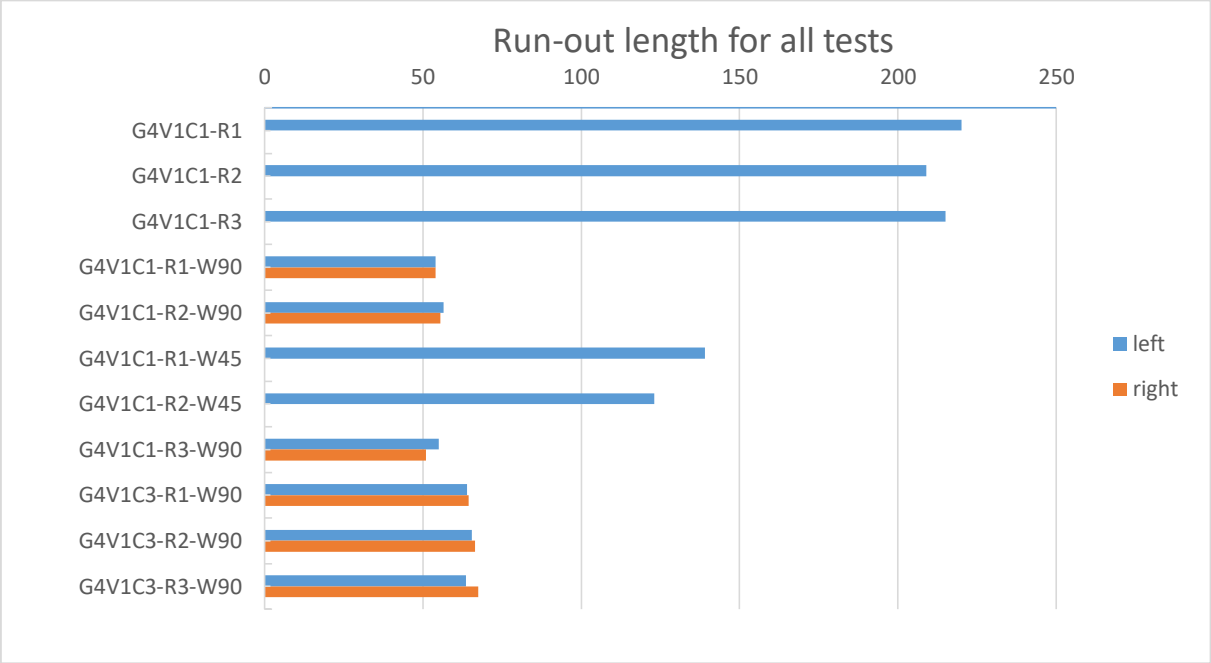

Figure 51: Plot presenting the run-out length for three reference tests and with two different deflection angles

The three upper run-out lengths marked in figure 51 are there as reference and shows how far the slides can reach if no preventative measure is present. These reference lengths are ranging from 2,09-2,20 metres and are close in run-out length. The deflection wall with a deflection angle of 45° is diverting the material to one side and reduces the run-out lengths, which are in the range of 1,23-1,39 m. The terminal wall is placed 49,5 cm from the end of chute, and with run-out lengths in the range of 51-67,5 cm, depending on the solid concentration of the debris material, which illustrates the effectiveness of this type. The material stops after only a few cm and is wide in its deposition shape as this barrier distributes masses to both sides of the wall. These are denoted left and right and is coinciding to the left and right ends of the plate, seen from above, see figure 52.

A table of all the run-out lengths and pictures of all the deposition patterns are found in Appendix D.

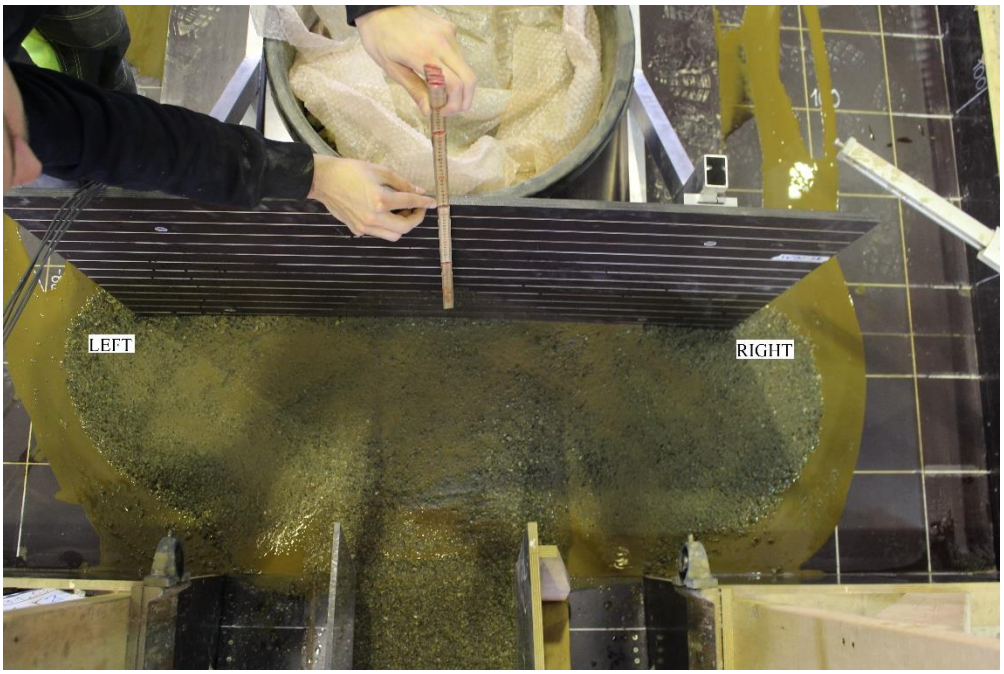

Figure 52: Deposition pattern of test nr. 5 and defining the left and right side of the run-out lengths

6. FURTHER DISCUSSION

This chapter will discuss the results in light of the objectives defined in Chapter 1.2. Discussion will be about the flow, front velocity and force measurements, in addition to flow height, run-up height, Froude number, run-out length, deposition height and pattern.

6.1 Flow

Flow in the chute (x= -200 to x= 0 cm) is characterized by a moving front which is either located in the centre of the chute, or at the right side. The flowing masses are flowing as a continuous mass, and no part moves slower due to bad mixing before the release. Presence of frozen masses are hence absent in all the eleven performed tests due to the improved releasing tank.

The front change shape as a result of the walls in the chute. Material is led via the walls with a high velocity, and is in one test sent from the wall and into the centre of the chute where it gain high velocity and catches up with the front towards the end of the chute. This can create a large wave-looking surge, and is observed in test nr. 4 and 5, see figure 53.

Figure 53: Wave-looking surge from test nr. 4

This ‘‘wave’’ is not seen in every test, but the foremost part of the front is moved from right to left due to material coming from behind at the left side of the chute, seen in test nr. 3, 4, 5, 6, 7 and 11, see figure 37. The foremost part of the front can also be constantly at the right side of the chute, which is observed in test 1, 2, 8, 9 and 10.

The shape of the front is curved, and the water content seems to be constant within the mass, except for test 1 and 7 where some dry particles travels in front of the foremost part of the debris flow. The material is called up on as the masses gain speed. The front in test nr. 1 seems to be called up on around x=-120 cm and travel as one mass, but in GP2 one can observe that the coarse particles once more is moving in front of the front before it is called up on. This is not the case for test 7.

At the material exits the chute, the behaviour of the flow becomes dependent of the deflection angle of the barrier placed on the deposition area. In collision with the terminal wall, the material is sent upwards in an upstream-propagating shock. Material is shunted laterally and a backsplash is generated. After the backsplash has reached its maximum height, the material recedes downslope and sends small portions of debris flow material into the chute at great velocity. The terminal wall diverts the material to the two sides of the wall, with allegedly the same amount of material on each side. For the deflection wall, the material is not sent back in direction of the chute, but lifted up against the wall and diverted to the side as seen in figure 39. The material recedes down while it slides along the wall and mixes with material traveling on the left side of the chute. This creates a front which is spreading in the y-direction.

The backsplash created from the collision with the terminal wall generates more material being sent back in comparison with the deflection wall which only diverts the material. This is due to the fact that a larger deflection angle is more abrupt and disturb the masses. This shortens the time of the collision, which is longer for a deflection wall due to the low deflection angle.

6.2 Front velocity

The front velocity for all the eleven tests are different, and the change of velocity along the chute and deposition area are unique for each test, see Appendix A. The lack of data between approximately x=-5 cm and x= 15 cm is due to the missing picture as GP1 misses the last part

of the chute as the beam where GP2 is covering a part of this view, and GP2 is inclined and miss the first part of the deposition area.

The front velocity is affected by the shape of the front which is changing along the flume model. This changing location in the transversal direction makes the velocity differ at different points in the front which makes the method imprecise. Difficult lighting conditions in the chute will also affect the tracking of the front as it may deviate.

The velocity in a real debris flow is between 5-10 m/s, and increasing with the size of the debris flow. Scaling used in the model is set as 1:20 which gives a velocity of 1,12-2,24 m/s in model, see chapter 4.4. In the tests, the maximum velocity in the chute was found in a test with C_s= 0,5 as 4,86 m/s (test 8). The minimum velocity in the chute was found as 1,78 m/s and was found from a test with C_s= 0,6. In nature, this correspond to 7,96 and 21,73 m/s, respectively. The latter is larger than what the velocity of a great debris flow can achieve, as these can be in the range of 15 m/s. An explanation for the high velocity in the flume experiments is the smooth bed surface. The fact that the velocity is exceeding the upper limit makes it too high for Froude similarity, and hence, we are not able to link it to natural debris flows. Vicari (2018) claims that the obtained values however are representative for a thin mass that moves fast.

Velocity is registered to increase as the solid concentration decreases, which would increase the water content. The effect of this reduction is seen in table 7, and one can clearly see the jump in front velocity compared to the eight other tests with a higher C_s. By averaging the velocity in the test for 50 % and 60 % at the three locations, an increase of 44, 39 and 42 % is registered by this reduction in C_s. The explanation for this reduction is the increased water content which improves the flow conditions (Iverson, 1997, p. 248; Christiansen, 2013, p. 3). More water in the mixture increases the flow mobility and reduces the friction between particles (Rosy, 2017, p.77) which will increase velocity.

Figure 40 and the ten other plots in Appendix A shows good interaction between the velocities found by the use of fisheye-filter and by averaging the velocity at the same location at three places in the chute. Figure 40 does also illustrate the importance of plotting the velocity along a part of the chute, as three points excludes the trend. Seen in test nr. 1, the point velocities at x= -200, x= -100 cm and x= -50 cm gives the impression that the velocity is increasing towards the end, as the velocity at x= -50 cm is higher than at x= -100 cm. The velocity towards the end of the chute is however lower than the point velocity would imply, and this is important to include.

‘‘The flow velocity of highly transient and surge like debris flows are difficult to estimate regardless of the instrument or method used’’ (Choi, 2014, p. 543). Finding velocity manually in Tracker is affected by errors, as one wrong marking has a great effect and can give us a different value of the velocity. Therefore, it is important to be consequent about tracking the front, and place the point correctly at the edge of the front for each frame. The plots in Appendix A show jumps and drops, both along the chute and after the transition to the deposition area. This can be a result of the tracking of the front in Tracker. Small variations in marking of the front of the flow gives a large impact on the resulting velocity.

Seen in figure 40, the velocity in test nr. 1 is decreasing before it again increases. Seen in Tracker, this is because of coarse particles which travels first in the debris flow are called up on when velocity is at its lowest, and gains velocity after it mixes. The two last reference tests show a decreasing trend from x= 15 to x= 85 cm, which is logical as the low inclination angle should deposit the debris flow. No coarse particles are seen in the front in these tests and hence, no material will come from behind at a great speed.

For the two tests with the 45° deflection wall, the velocity is (by average) reduced by 56 % in the collision with the deflection wall, as energy is lost as heat and transformed into potential energy. The trend at the beginning of the deposition area is negative, and a great drop is seen after the collision with the deflected wall.

The terminal wall stops the debris flow faster than the 45° deflection wall. The velocity was not analyzed after the collision into this type of wall as the velocity was visually determined to be extremely low as the material deposited almost instantly. This coincides with Christiansen (2013) as her study concluded with an increasing loss in energy as the deflection angle was increased.

6.3 Froude number

The Froude number (Fr) is the parameter that enables us to link results from the model to the prototype. Froude number has been found at three locations in the chute, and is found to vary between 4,67 and 9,75. These are high values due to high velocities and low flow heights. The range of Froude number characterizes the flow as supercritical, which is an assumption for run-up dynamics as it creates backwater effects. If the obstacle had been hit by a subcritical flow,

then run-up would be determined by the accumulation of mass located behind the obstacle (Iverson, George & Logan, 2016, p. 2335).

The increase in water content for test 8-10 resulted in a larger velocity for the three tests. This is very easily seen in figure 41 and 42 as these points are a lot higher than the solid concentration of 60 %.

Froude number has been examined in several studies previous to this thesis, due to the Froude similarity. In the paper by Iverson, George & Logan from 2016, the Froude values are found to range from 3-9 during an experiment, which is quite similar to the range of Froude number calculated in this thesis. Table 1 in chapter 2.5 presents different papers and their range of Froude numbers, and table 4 presents Froude number for natural events. Three of the values for Froude in this thesis are larger than the largest seen in nature (Pine Creek, Fr= 7,56). The Froude values for C_s=0,5 are exceeding the limit, and are hence not valid for Froude similarity.

Figure 41 represents the Froude number plotted against the run-up height for the vertical deflection wall. Two trend lines drawn through the six upper (terminal wall) and two lower points (deflection wall) shows an increasing trend as one increase the Froude number. The two parameters are hence said to be correlated.

Figure 42 illustrates the development of Froude from x= -200 cm, x= -100 cm and until x= -50 cm, hence at three locations in the chute. The development show two possible outcomes, the first showing increasing Froude number from the first to the last sensor and the second showing a decrease from the first sensor to the second, then an increase at the last sensors. Four of the tests shows an increasing trend over the three sensors, five of the tests showed first a decrease and then an increase, and one test showed no change in Fr from the first to the second sensor but a decrease was measured at the last sensor.

Naaim et al. (2010) investigated an avalanche in the French Alps, where Froude number and volume of avalanche material were found to be the two most relevant descriptors of interaction between avalanches and obstacles. Another study that investigated the Froude number in relation to obstacles in the flow path, is Choi et al. (2014). This study investigated baffles in a chute as a preventative measure against debris flow. Froude height was calculated in the flow just as the material entered rows of baffles and as time passed. It was observed that a decrease in Froude number was registered after the debris flow material entered the area with baffles, and the flow changed from being super- to subcritical. For implementation in relation to

deflection walls, baffles could be established in the transport zone and change the flow form super- to subcritical. This would reduce the run-up height and reduce the height of the deflection wall. The cost of baffles compared to a higher deflection wall would be higher, so the cheapest method would be by building a higher deflection wall which is hit by a supercritical flow.

6.4 Flow height and run-up height

The movement of the head in the chute is well illustrated in Appendix B. The graphs illustrates the peak which represents the front, and how it decreases from one sensor to the next. This is due to elongation of the debris flow due to the flow front's steepness (Jakob & Hungr, cited in Vicari, 2018, p. 61). The max flow height at displacement sensor 1 is not at the same time as the peak at displacement sensor 2 or 3, as the debris flow material needs time to move between the sensors.

By looking at the development of the flow heights in the different displacement sensors in figure 43, we identify that the front is thicker compared to the body and tail of the slide, which coincide with theory in chapter 2.7.

The peak flow height for the ten tests were in the range of 23,43-31,11 mm at x= -200 cm, which in nature correspond to 0,47-0,62 m. This is a bit less than registered debris flows, which normally are around 1 m in height, and 3 m for very large events. This is accordance with Vicari's (2018) results, as his heights also were smaller than expected, which again is relatable to a thinner flow, as the high velocity also implied. It is observed that the concentration also affects this aspect of a debris flow, as a more dense mixture transports more material, and hence will be thicker. More water in the mixture reduces the number of particles transported at the time (Rosy, 2017, p .79), and hence, the three tests with the reduced solid concentration were the ones with thinnest flow and lowest peak flow.

Towards the end of all the ten graphs, the flow height increases in sensor 3, and only here. This is a consequence of incoming material, which is prevented from exiting the chute due to deposited masses at the deposition area. Material is hence accumulated in the chute and the flow height increases, see figure 54.

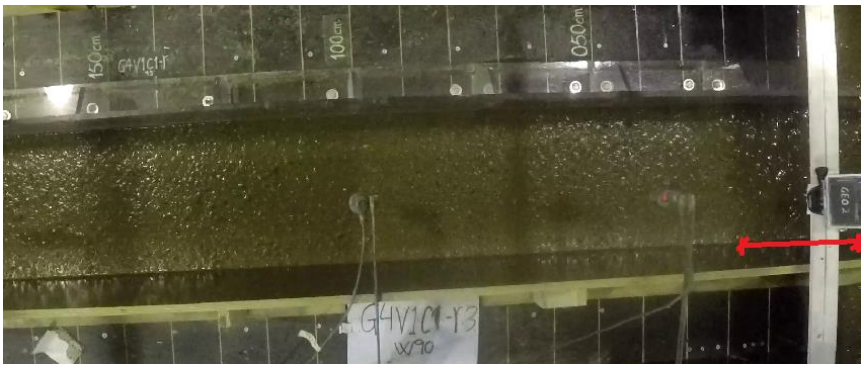

Figure 54: Accumulation of debris flow material in the chute in test nr. 11

Debris flows transform potential into kinetic energy from initiation to deposition (Takahashi, 2014, p. 8). As the debris flow collides into an obstacle on its way and is lifted, it is transformed into potential energy. The ability to predict the height of the run-up is strongly influenced by the run-up dynamics which is a complex process. This process of run-up against an obstacle involves deceleration of flow and redirection of mass (Iverson, George & Logan, 2016). The terminal wall where the obstacle is oriented normal to the flow path, is dominated by rapid development of a shock, or jump in flow height, as the material collides into the obstacle linked to the flow front's abrupt deceleration. The velocity is correlated to the run-up height, see figure 45 as an increase in velocity results in a larger run-up height. This is the trend for both the deflection angles.

The magnitude of the run-up showed a clear correlation to the deflection angle. The terminal wall has a higher run-up height compared to the deflection wall. This is due to a larger change of direction as the deflection wall only diverts the masses and hence, this run-up height will be affected by it. The terminal wall had an average run-up height of 23,67 and 34,33 cm for C_s = 0,6 and 0,5, respectively. The deflection wall measured an average of only 12,5 cm. According to Le et al. (2016), this correlation between deflection angle and run-up height coincide with work done in previous projects by Mears, Hungr et al. and Hungr and McClung (all cited in Le et al., 2016, p. 1242). Christiansen (2013) also reports this correlation in her master's thesis.

In order for the infrastructure or settlement to be safe from destruction due to overtopping, the run-up height has to be lower than the effective height of the deflection wall. The three average values of the superelevation are in nature in the magnitude of 4,73 m and 6,87 m for the two concentrations hitting the terminal wall, and 2,50 m for the deflected wall. In chapter 3.1, page 24, the values of the theoretical run-up height were proposed to be in the range of 1,64-3,55 m

for the 45° deflected wall, and from 2,27 to 6,10 m for the terminal wall. This is when assuming a flow height of 1 m. The 45° deflected wall is within the limit, while the terminal wall is within the boundaries for the denser concentration, but not for C_s = 0,5, which exceeds the upper boundary by 0,77 m.

Christiansen (2013) performed similar tests with deflection angles of 20, 40 and 90° for a fully saturated material. For the 40° deflected wall, the three tests gave a run-up height of 12, 14 and 16 cm. Compared to the 45° deflected wall in this thesis, this is coinciding as it measured 12 and 13 cm. The terminal wall in Christiansen (2013) registered run-up heights with magnitude 18, 23 and 48 cm, which in this study ranged from 19-37 cm. The necessity to have a small gap (approximately 5 mm) between the plate and the deposition area in order for no friction between plate and bed, affected the run-up height for the debris flows with a solid concentration of 50%. This is a more liquid and less dense mass, and hence, some of the material went straight under the wall, and did not contribute to the run-up height. Still, it was this concentration that gave the highest run-up heights for all the performed tests, as the velocity in these tests were found to be greatest.

Terminal wall as a barrier will divert material to the sides after the collision. Material goes up and to the sides as more incoming material hits the wall. This is called lateral shunting (Iverson, George and Logan, p. 2345) and distributes symmetrically around the centerline in the model for the dense material with C_s = 0,6. The other concentration shows three different patterns on the wall due to the upstream-propagating shock. The first test with this C_s shows an incoming flow located a bit to the right of the centerline (a), which also is seen from the pattern on the wall where the max run-up height is located a bit to the right of the centerline (b), see figure 55. For the second test, the maximum run-up height is seen as two peaks on each side of the centerline, and for the third, the run-up height is located to the left of the centerline, opposite of the first test with this concentration.

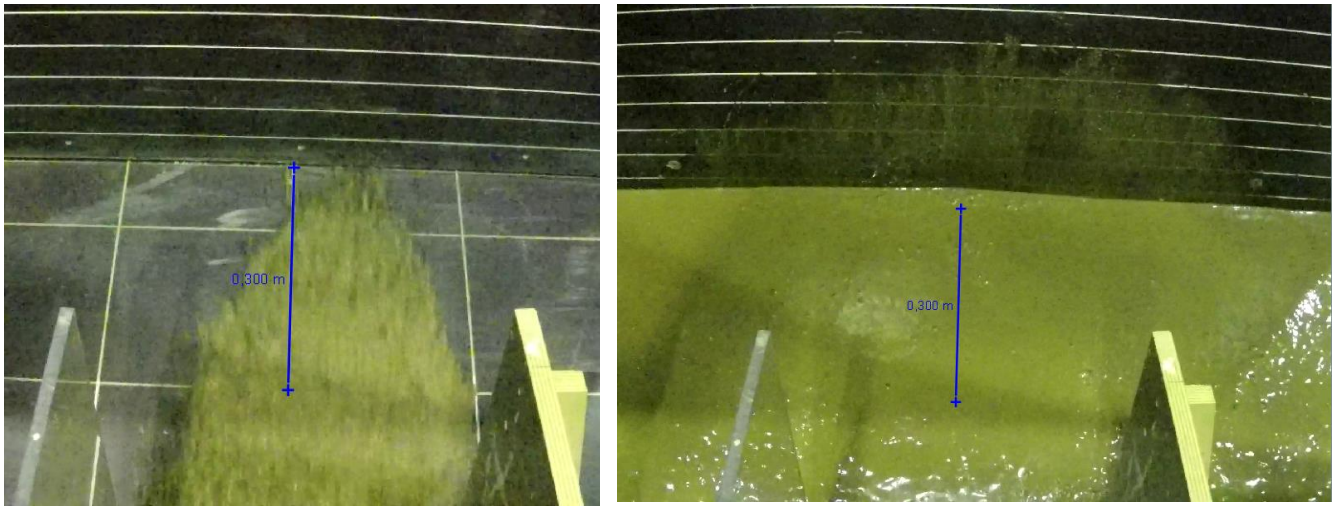

(a) (b)

Figure 55: Incoming flow and markings on wall after upstream-propagating shock

The theoretical values of run-up height calculated by equation 10, overestimates the measured values by 69,9 % for the terminal wall, and 145,4 % for the deflection wall. For the two concentrations, the C_s of 0,6 is closest to the measured run-up height.

The Momentum Jump Method has been used to present normalized run-up heights found in lab and plot it against the Froude number, see figure 56 and 57. This was done for the terminal wall only. Density before and after collision are set as equal as no available measurement can tell us otherwise. A back-calculation done for the six tests found κ, which represents the pressure coefficient, to be equal to 0,48 (equation 11). Plotting the obtained values from lab (dots) and lines with different values of κ, one can see that the results from lab fit well to the model. κ represents the ratio of longitudinal to vertical normal stress, and the value 0,48 implies that the deformation happens in a compressional mode (Iverson, George & Logan, 2016, p. 2336). According to Iverson, George and Logan (2016), an increase in Froude number would increase the normalized run-up height (H/h_0), but decrease ($H/(v_0^2/g)$). This is verified by the results seen in the figures below. Iverson, George and Logan (2016) proposed four models in their paper, but concluded that this model predicts the closest run-up height compared to results from lab. This is in accordance with the relevance this model plays for barriers oriented normal to the direction of the flowing masses.

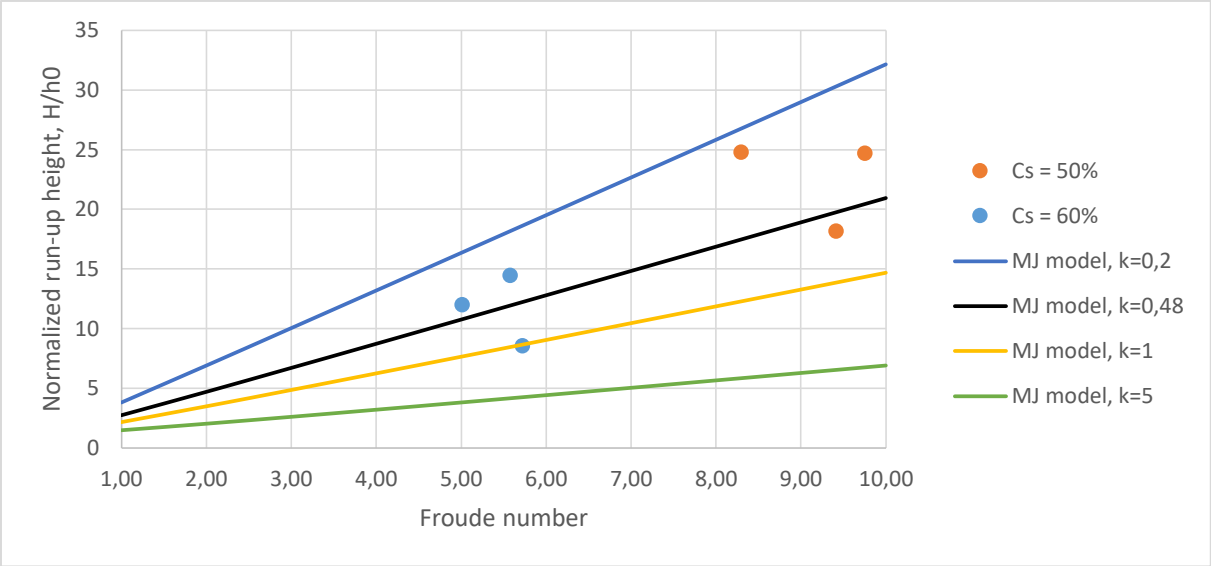

Figure 56: Normalized run-up height, H/h_0, vs. Froude number for terminal wall by the MJ model

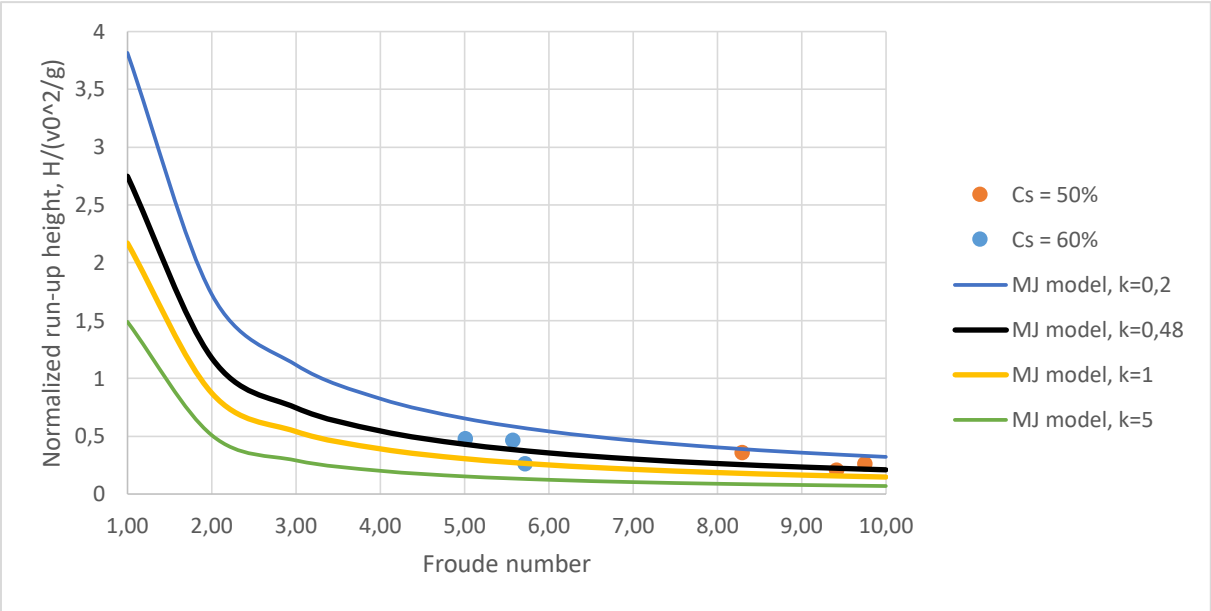

Figure 57: Normalized run-up height, $H/v_0^2/g$, vs. Froude number for terminal wall by the MJ model

The Frictionless Finite Mass Model predicts higher run-up heights than experienced in lab. The gap between the predicted and observed heights is large, and compared to the MJ model, the FM model gives the poorest predictions. Iverson, George and Logan (2016) also concluded with this, justifying it by flawed assumptions.

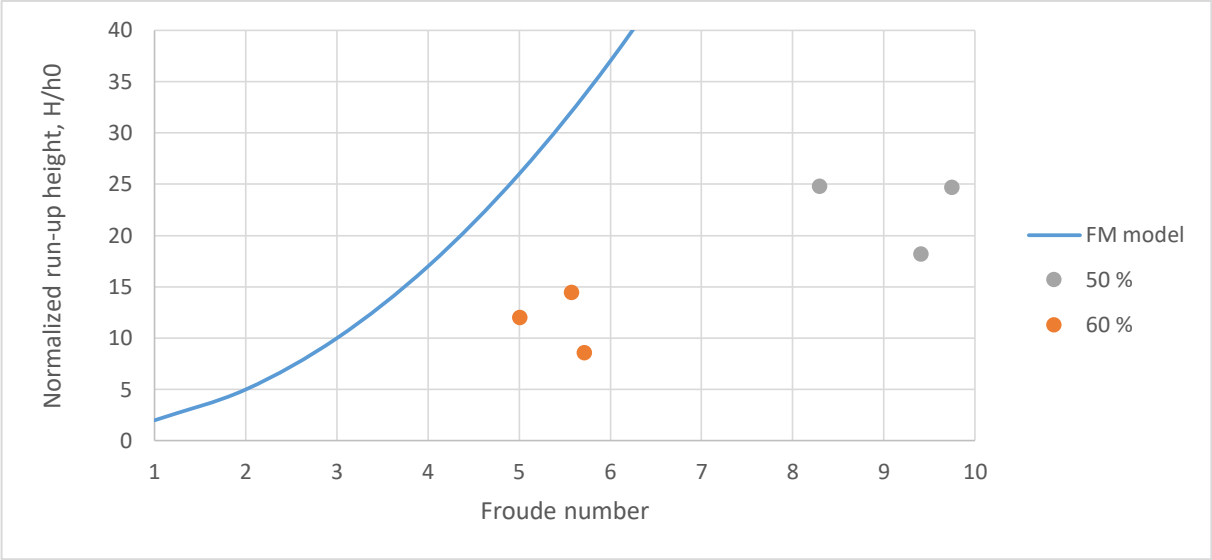

Figure 58: Normalized run-up height, H/h_0, vs. Froude number for terminal wall by the FM model

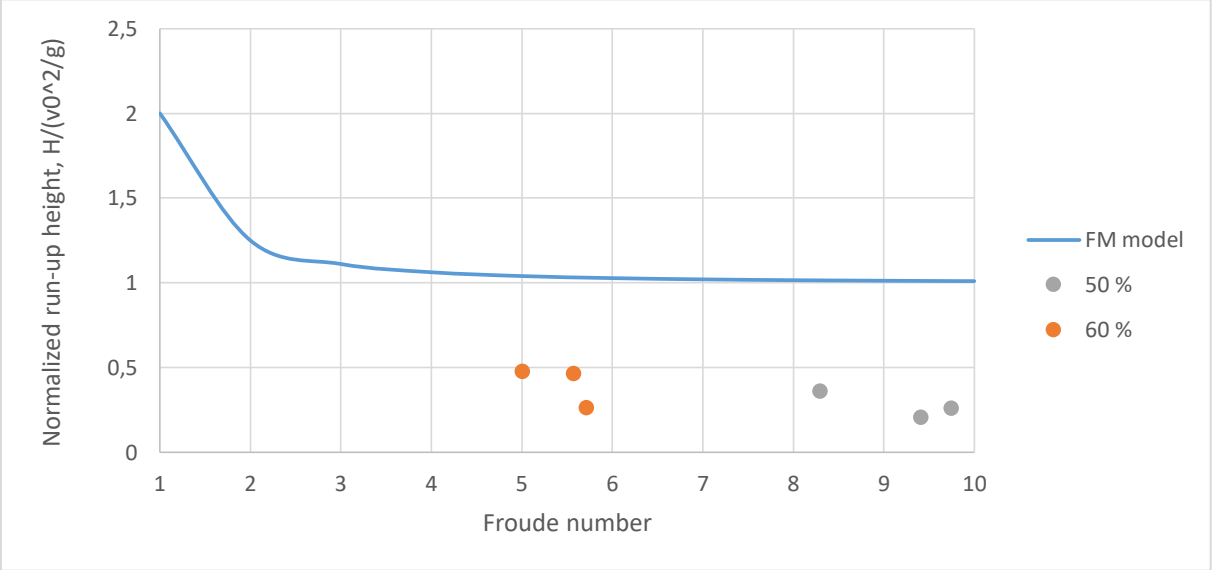

Figure 59: Normalized run-up height, $H/v_0^2/g$, vs. Froude number for terminal wall by the FM model

The terminal wall creates backsplash in all the tests. For C_s = 0,6, the height of the backsplash is equal or less to the run-up height, while it is significantly higher for C_s = 0,5. The run-up height in the three tests with this latter concentration were 31, 37 and 35 cm, and the backsplash reached 45, 43 and 44 cm, respectively, seen from the high frame rate-video on the side of the model, see figure 60. The height of the backsplash is not a problem when examining a vertical wall as the material goes back and away from the wall, but must be taken into account if the wall is inclined, as an inclined wall commonly increases run-up height (Iverson, George & Logan, 2016, p. 2333).

Figure 60: Backsplash from tests 8-10. Left: test 8. Middle: test 9. Right: test 10.

6.5 Force measurement

The graphs in Appendix C are presenting the force measurements and the shapes of the graphs are clearly affected by the angle of the deflection wall. The wall with a deflection angle of 90° is showing peak values before a clear drop in force, see figure 47. The peak forces for the terminal wall is in the range of 73,47- 97,79 N. The drop happens 5,58 seconds into the first test examining the terminal wall. The drop is seen to be due to the first portion of backsplash which recedes and meets the incoming material from the chute. This reduces the mass which is hitting the wall for a short period of time before it once more is colliding into the wall with strength. This is seen in the graph as the first peak after the large drop and is reduced due to the backsplash which reduces the amount of material hitting the wall. The force stabilizes gradually as the deposition height in front of the wall reaches its max, and the amount of mass behind the wall is constant and not increasing, as the deposited masses prevent further mass from exiting the chute.

The debris flows with C_s = 50% shows a more complex force graph as the maximum is not the first peak, but the second. The second peak is due to a high run-up which imposes large forces on the wall. This mixture is less dense and flows faster than the 60 %, which is denser and flows slower. The measured forces are slightly higher than for the C_s = 60% as the kinetic energy is smaller for the denser flow. A potential trend line in figure 49 implies a correlation between force and velocity squared for the terminal wall.

The deflection walls located 45° to the direction of the flow path shows one peak force, see figure 48. The peaks are in a range of 51,52-57,42 N and hence smaller compared to the terminal wall. The correlation between the force and deflection wall is presented in figure 50, where an increase in deflection angle increases the force measurement. The peak is due to run-up against the deflection wall and the width of the masses colliding into the wall. High values for the force are lasting over a longer period of time for this kind of barrier as it is diverting material to the side. This gentle leading of material gives a force plot with no drop, as no material is thrown backwards. The force stabilizes as the material recedes down from the wall and material is led via the wall and leaves a deposition height. The deposited masses are spread in x- and y-directions.

The two equations in chapter 2.7 are the hydrodynamic and hydrostatic equations for pressure. According to Hübl et al. (2009), force from a flow with high magnitude of Fr (as we experience in this study) is best calculated by the hydrodynamic equation. This equation includes the empirical coefficient α_3, which in this study is back-calculated and found to range from 0,04 and 0,19. This is less than what literature proposes, which is 0,4-5 (Scheidl et al., cited in Vicari, 2018). The gap between the obtained and proposed values may be due to the mechanism of impact. The terminal wall is stopping the flow significantly and modifying its behaviour. During the impact, the flow is internally deforming which absorb energy, therefore a lower pressure is transmitted to the wall which gives a lower α_3.

The hydrostatic equation is said to fit best for flows with low values of Froude numbers (less than 1). This equation includes the empirical coefficient k which is found to vary between 2,5 and 11 (Lichtenhahn; Armanini; Scotton and Deganutti; all cited in Vagnon and Segalini, 2016). k in this study is found to range from 1,62-6,01, which is within the limit.

As the empirical factor differ from location to location (Cui, Zeng & Lei, 2015, p. 1653), an improvement was made to the hydrodynamic model by introducing the Froude number. The results from many studies are presented in figure 61, and based on the trend line, our values seem to be below the trend line.

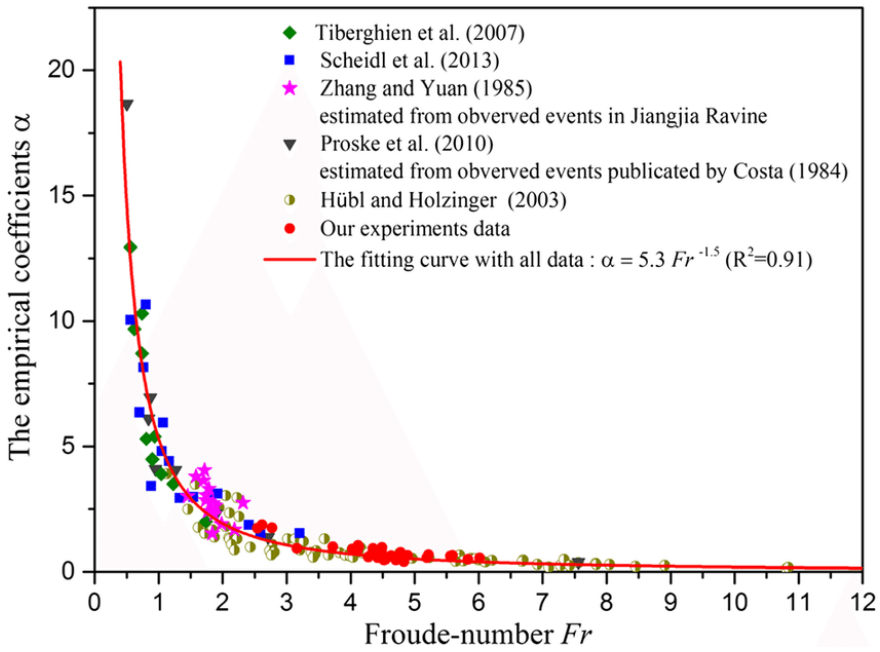

Figure 61: Relationship between Froude number and empirical coefficient α_3 (Cui, Zeng & Lei, 2015)

The specialization project conducted by Opsahl in the autumn of 2018 examined pressure on a thinner structure. The released debris flow hits a plate and tilts it, which will generate a force. Three steel plates with three widths, 25, 50 and 75 mm were attached to a pillar in the middle of the chute and the average pressures of eight tests for the three different widths were 18,41 kPa, 13,81 kPa and 14,91 kPa, respectively. The middle plate experienced a lower pressure compared to the two other. α_3 and k were found to be in the range of 0,84 -1,42 and 20,89 - 66,16, respectively. The values obtained for α_3 falls within the proposed limit of (Scheidl et al., cited in Vicari, 2018) as the pillar transfer the force completely as the flow behaviour is not modified due to the small dimensions of the pillar. k is larger than proposed (Lichtenhahn; Armanini; Scotton and Deganutti; all cited in Vagnon and Segalini, 2016). Froude number was not examined in this project, so no relation will be drawn between α_3 and Froude number for the specialization project.

The pressure at the deflection wall is in the range of 0,65-2,34 kPa, due to the larger contact area the force is acting on. The lowest pressures are measured for the 45° deflection wall. The wall needs to withstand the force from the slide, and the pressure it imposes on the structure. The aimed scale of 1:20 implies that the pressure in nature would be of the size 13,04 – 46,84 kPa, and natural debris flows are found to impose a dynamic pressure in the range of 10-5000

kPa (Huang, Yang & Lai, 2007, p. 1). The obtained pressures in this study falls within this range.

6.6 Run-out length, deposition height and pattern

Run-out length

Run-out length is limited to the masses that damage the considered infrastructure or settlements (Norem & Sandersen, 2012, p. 38), and does not include the water mixed with fine material which can travel longer distances due to its high mobility. The three reference tests illustrated the run-out length when no preventative measure was in use, and reached lengths in the range of 209-220 cm from the start of the deposition area.

The terminal wall is placed 49,5 cm from the start of the deposition area, and the run-out lengths for the debris flows hitting this barrier is greatly affected by the deflection angle. These run-out lengths are only a few centimeters on each side of the plate due to the masses being distributed to two sides. The distance from the plate to the front of the deposited debris flow is in the range of 1,5-7 cm for C_s = 0,6, and 14-18 cm for C_s = 0,5. The short run-out length for this type of barrier is due to the large deflection angle and wide plate which stops the debris flow close to completely. The deflection angle is normal to the flow direction and makes the masses create a backsplash. A lot of the energy is then lost as the kinetic energy has been transformed to potential, and as it hits the ground level, the energy is smaller than on top of the chute.

The difference in run-out length for the two examined concentrations is due to the water content in the mixture. According to Rosy (2017, p. 77) is the intergranular space between grains filled with water which both reduces the friction between particles and increases the fluidity of the debris flow. A higher water content will therefore reduce the friction at the flume bed which will create a longer run-out distance. It was observed that boulders were spread out beyond the front of the deposited masses at the lower solid concentration, compared to none for the Cs = 0,6 which formed a defined boundary for the deposited masses. The spreading of boulders made it more challenging to determine the run-out length accurately. Another effect of differing solid concentrations is the difference in kinetic energy. The more water, the higher kinetic energy is present, as discussed in chapter 6.2. According to Takahashi (cited in Rosy, 2017, p.78), one

way to reduce this kinetic energy, is by imposing friction between the debris flow material and the bed, which here is very smooth. The higher difference in kinetic energy, the longer run-out distance is needed. The increase in run-out length as one decrease the solid concentration is verified by Vicari (2018).

The angle of deflection is seen to have a clear effect on the run-out length, as the range for a terminal wall is in the range of 1,5-18 cm, while the 45° deflected wall has a run-out length of 123-139 cm, minus the distance from the end of the chute and until the point where the material meets the plate. This is at x= 0,49 and x= 0,44 m for test 6 and 7, respectively. The shape of the front affects the location of this point as it is changing and the foremost parts can be concentrated to one of the sides. Compared to the three reference tests, the terminal wall shows a reduction of 93,7 % in run-out length, while the deflection wall shows a reduction of 38,9 %. The terminal wall is clearly stopping the debris flow most efficiently. In terms of energy, the loss due to the collision with the deflection wall is smaller compared to the terminal wall. The higher amount of kinetic energy in the masses requires more energy to be dissipated before the masses will deposit and the velocity will be reduced to zero. Velocity is lost via friction against the bed and flow along the wall.

All the material in the cylinder are contributing to the run-out length, as all the material except some material staying inside the cylinder. This amount is negligible. The tests showed a large degree of repeatability of the run-out length.

Deposition height

The height of the deposited masses in front or along the wall was measured straight after the events, but not for the three reference tests. The average deposition height for the deflection wall was 3 cm, for the terminal wall with C_s = 0,6 it was 5,0 cm, and the terminal wall with C_s = 0,5 it was measured as 3,9 cm, see table 9. The difference in deposition height for the two concentrations against the terminal wall, is due to the water concentration which widens the deposit and spreads the masses more. The deflected wall has a lower deposition height due to the longer run-out length which makes the deposited layer of masses thinner than for the terminal wall. This trend of an increasing deposition height as one increase the deflection angle is verified by Christiansen (2013), who also registered this increase.

Deposition pattern

Observations in the lab identified accumulation of coarse particles in the flow front and on the sides (levees) in all tests, and the water content is high in the parts behind the front. The observations makes us characterize the conducted debris flow tests as stony types where inverse grading lift boulders to the top of the flow, see Appendix D.2. Water and fine particles are seen to run further than the debris flow in each of the pictures in Appendix D. This indicate that the levees are not well developed as water is able to escape the deposited masses (Vicari, 2018, p. 66).

The shape of the three reference tests are consistent, as it is elongated due to poorly developed levees which prevent lateral expansion. Two of the three reference tests have the maximum run-out length at the centerline of the deposition area, while the third test forms two small lobes on each side of the front, see Appendix D. 2. The amount of water exiting the deposited masses are less in the third test compared to the two first. We can hence say that the third test has developed more solid levees than the two others.

The shape of the deposited masses are affected by the deflection angle. As a 45° deflection wall only diverts the masses in one direction, this will give a different shape compared to the barrier where the slide is stopped completely. The shape is the same for the two tests with the deflected wall, and the front was observed to be coarse, just like a stony type debris flow. The wall at the side of the deposition area stops the expansion in y-direction, which could have given a wider deposit. Water is exiting the masses, and some is entrapped behind the masses. Some water is also accumulated between the impermeable plate and the material. This is at the middle of the plate and towards the two sensors farthest away from the chute.

The shape of the deposits in front of the terminal wall have the shape of an rectangle for the concentration of C_s=0,6. For the C_s =0,5, the enhanced mobility increases run-out and spreads the masses over a wider area, and as this concentration makes it difficult for levees to be fully developed and as a results, the front is not easy to determine. The increasing width of the deposits of a lower solid concentration coincide with what Rosy (2017) registered.

7. CONCLUSIONS AND RECOMMENDATIONS

7.1 Conclusions

Eleven tests have been performed in a flume model to examine the effect of a deflection wall as a preventative measure against debris flow. The understanding of debris flow mechanisms was done in a literature study and the relation between experiments and natural events seen in nature are via Froude number. The examined parameters in lab were front velocity, force measurements, flow height in chute, run-up height against deflection wall and run-out length. One trial test was additionally performed to investigate entrainment.

The volume was constant for each of the eleven tests and two different concentrations were examined. The deflection wall was tested for two deflection angles, 45° and 90° and three reference tests were examined to compare the results to.

Results obtained from the study showed that the velocity increased by 42 % by reducing the solid concentration from 60 to 50 %. The increased water content which fills the void and the intergranular friction decreases between the particles, which gives a higher mobility for this concentration. The velocity plots showed jumps and drops which can be explained by small variations in tracking the front of the flow.

Froude number is found to be in the range of 4,67-9,75, which characterizes the flow as supercritical. This is larger than observed in nature, as this is ranging from 0,5-7,56 (Hübl et al., 2009). Hence, the obtained Froude numbers under this upper limit are valid for Froude similarity, while the ones above, which is for the C_s=0,5, is not valid.

Force is seen to peak and then drop suddenly for the abrupt change of flow direction as a terminal wall is creating a backsplash in the direction of the chute. When the backsplash reaches

the level of which the incoming material is sliding on, it mixes, and a drop in the force plot is seen. The force is never reaching the same magnitude as the first peak. The 45° deflected wall is not seeing this drop due to the small deflection angle. Material still runs up against the wall, but not as high as for the other wall, and diverts to the side.

Peak flow height is measured at the first sensor. The last sensor registers an increase towards the end due to the prevention of material exiting the chute after deposition. The theoretical run-up height calculated by equation 10 gave higher numbers than experienced in lab. The MJ model presented the best estimate of the run-up height, compared to the FM model which gave the poorest estimation.

In relation to which deflection angle we should use to avoid overspill of a typical deflection wall of 4-5 m, which is the typical height of this kind of barrier in Norway, a 45° deflection wall is best. The run-up height is significantly lower compared to the terminal wall, due to the redirection of the masses instead of a large backsplash. The terminal wall is stopping the debris flow faster, but this angle requires a higher height of the wall which is more expensive. Max run-up height in this thesis would imply a wall of 7,40 m for the C_s of 50 %.

Run-out length is affected by the deflection angle. The wall stops the debris flow immediately after collision, while a deflection wall of 45° only diverts the masses. The amount of kinetic energy is hence a lot more where the deflection wall is used due to the low deflection angle. The width of the deposits in front of the terminal wall is dependent on the water content in the mixture. The more water, the wider and hence thinner deposit.

7.2 Recommendations for further work

As the equipment used to measure flow height, velocity, etc. are showing good results, this is not a focus area for further research. The only thing that could have improved the model was a material on the flume bed, which would impose friction between the bed and the material. The velocity would then have been reduced and possibly fallen within realistic range in order to be compared to a natural debris flow.

One ultrasonic sensor should be present at the deposition area to calculate Froude number in this part of the model, to see if it has decreased compared to the magnitude in the chute.

To further examine vertical walls as a protective measure against debris flows, one should test more deflection angles of the wall. A deflection wall of 60° would have been interesting to see what effect it has on the run-up height.

By reducing the inclination of the slope, smaller values of Fr could be achieved and compared to the graph where the normalized run-up height was plotted against the Froude number.

The trial test on entrainment did not show any visual erosion. The upcoming master's thesis next spring on this topic can focus on concentration of the material in the entrainment space. Several concentrations can be examined and see how it affects the quantity of eroded material. The parameters examined can be run-out length, see how much material was entrained, change of velocity, Froude number, etc. The slope should be more inclined to increase the erosion.

8. TRIAL TEST – ENTRAINMENT

The experiment with entrainment was executed in the same model as previous. The force on the wall not the goal for this test, but to see the erosion of masses, and hence the wall was removed and not a part of this test. The chute is still inclined 17,5° and the released debris flow masses had a solid concentration of 60%. The same amount of material and water was used as for the tests with the deflection wall. The masses in the entrainment area could not be as liquid as this, as it would only slide out of the space due to gravity. Material and water was mixed together manually by a shovel, and obtained a water content of 16 %.

The flow height sensors are placed at x=-200 cm, x=-70 cm and x=-50 cm and the sampling frequency was 1000 Hz. Velocity was calculated at these three locations, in addition to tracking the whole front. Froude number was found at x=-200. Red spray was applied on the top layer to be able to see how entrainment in the chute happened, seen from the side camera.

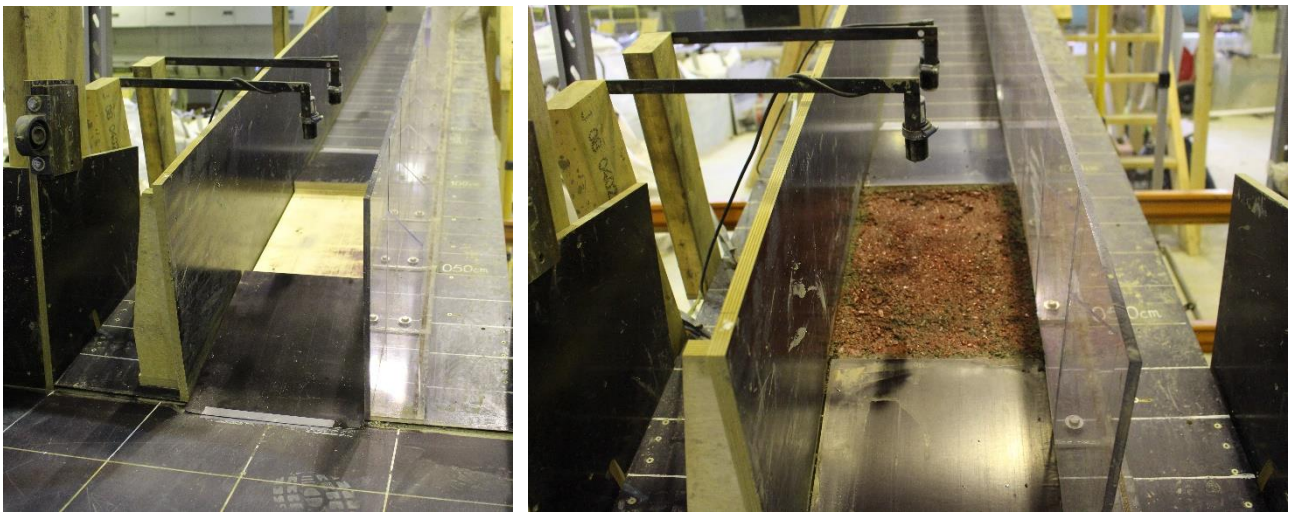

Figure 62: Entrainment space. Left: empty. Right: filled with material and covered with red spray

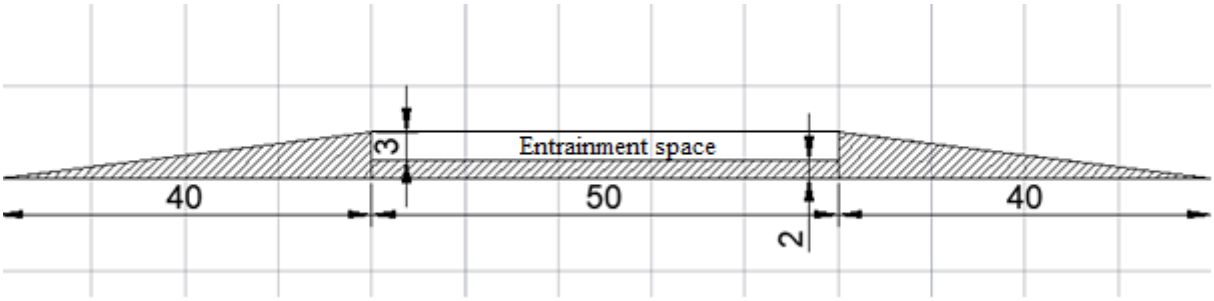

Figure 63: Obstacle, all dimensions are in centimetres

By pure observation and due to the limited sensors used to observe entrainment, it did not look like any of the material was eroded from the space as the material only slides over the masses in the entrainment space. It is well illustrated in figure 64 where one can see a darker and a lighter mass, the latter being the debris flow. The red markings on the wall in the centre of the picture are remains from when it was sprayed, see figure 64. The boundary is pointed out by the red arrow.

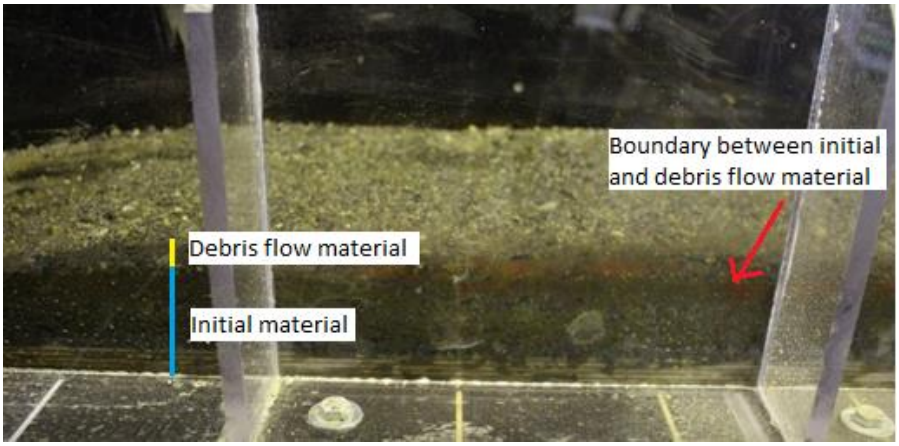

Figure 64: Two layers of material

Flow height at sensor 1 is showing its peak due to the head, see Appendix B.11. Peak flow height in sensor 3 is higher than in sensor 2 due to the flow, see middle left of figure 66 where a deep flow height is about to enter sensor 3. Equal height elsewhere as material only passes and deposits.

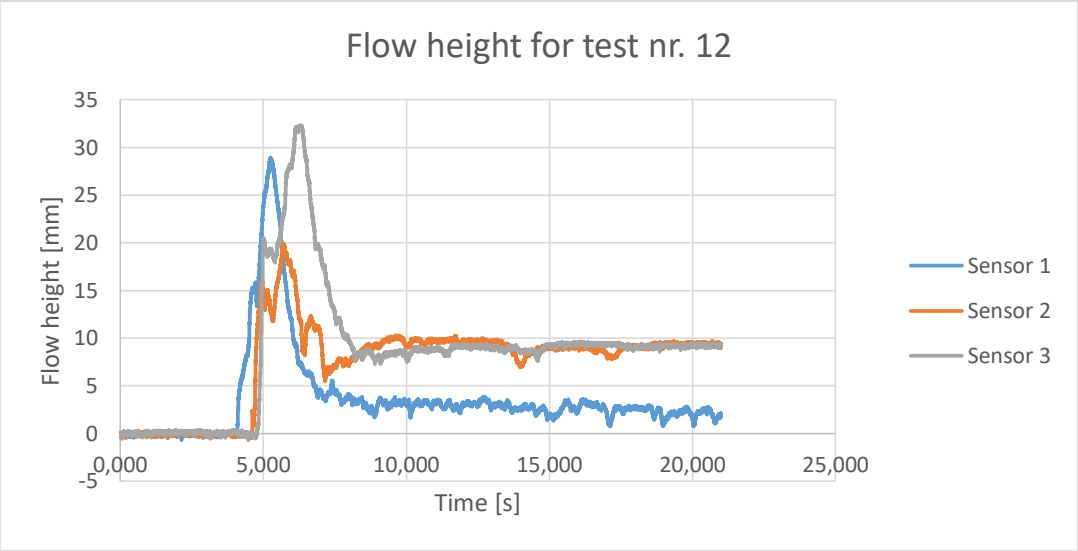

Figure 65: Flow height for test nr. 12

The lack of erosion may be due to several factors, as for example the water content in the material in the entrainment space. This was only 16 % in order for it to stay in its space due to gravity. The inclination of the slope was also low, and should be increased in further research. A more liquid debris flow which was released would have eroded the material more as we experienced in a test the day before, as we released water alone and experienced that almost all the material in the entrainment area was incorporated into the debris flow. This test was not recorded, as we only wanted to observe the erosion done by water. It is not known what solid concentration one need to erode the material in the entrainment space. The spray is not assumed to have any effect.

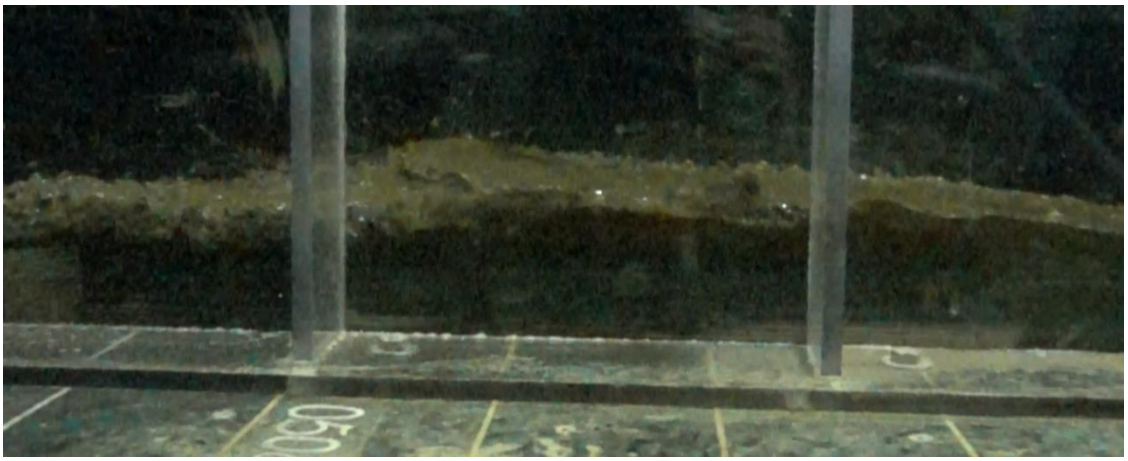

Figure 66: Flow during test nr. 12

High velocity in the start of the test is observed, and is assumed to be due to an inaccurate filling of the cylinder. More water than intentionally is assumed to be present, resulting in a higher water content than before, which gives a higher velocity. The velocity plot is showing a drop at x=-1,25 m, see figure 67, as the material climbs the obstacle and enters the entrainment zone, where measurements shows large jumps and drops, before it drops and flattens out due to the friction from the underlying material. The jump close to x=-0,2 m is because of the inclined downslope of the obstacle.

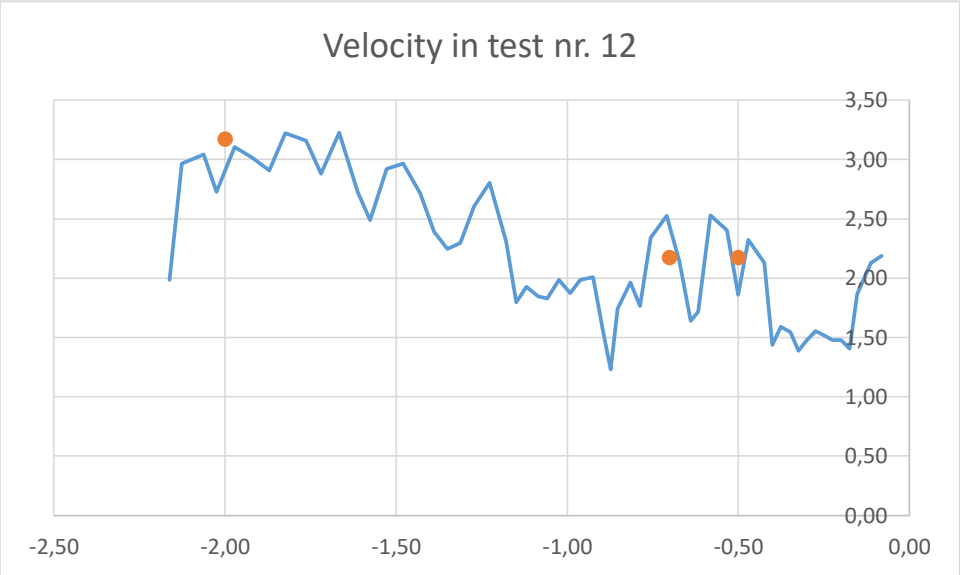

Figure 67: Velocity plot for entrainment test

9. BIBLIOGRAPHY

Au-Yeung, C. H. S. (2015) Flume Investigation of Run-up Mechanisms of Granular and Water Surge Flows Impacting a Rigid Barrier. Master's Thesis. The Hong Kong University of Science and Technology.

Calligaris, C. & Zini, L. (2012) Debris Flow Phenomena: A Short Overview? Dar, I.A. (ed.) Earth Sciences. INTECH.

Choi, C.F., Ng, C. W. W., Song, D., Kwan, J. S. H., Shiu, H. Y. K., Ho, K. K. S. & Koo, R. C. H. (2014). Flume investigation of landslide debris-resisting baffles, Canadian Geotechnical Journal, 2014, 51 (5): 540-553, 10. Available at: https://www.nrcresearchpress.com/doi/10.1139/cgj-2013-0115#.XMlqqOgzZPY (accessed 01.05.19).

Christiansen, L. F. (2013) Flomskred. Specialization Project. Norwegian University of Science and Technology.

Crowe, C. T., Elger, D. F., Williams, B. C & Robersen, J. A., (2009) Engineering Fluid Mechanics. 9th edition, John Wiley & Sons, Inc, Available at: http://www.academia.edu/31141835/Fluid_Mechanics_Crowe_and_Elger_9th_Text_Book.PDF (accessed 07.02.19).

Cui, P., Zeng, C. & Lei, Y. (2015) Experimental analysis on the impact force of viscous debris flow, Earth Surface Landforms and Processes, 40, page 1644-1655. Available at: https://onlinelibrary.wiley.com/doi/pdf/10.1002/esp.3744 (accessed 29.01.19).

Hákonardóttir, K. M., Hogg, A. J., Batey, J. & Wood, A.W. (2003). Flying avalanches. Geophysical Research Letters. 30, No. 23, 2191. Available at:

https://pdfs.semanticscholar.org/bd73/38c8a6c82c2920472937846d32bae6181753.pdf (accessed 02.05.19).

Hausfather, Z. (2018) Explainer: What climate models tell us about future rainfall, CarbonBrief, 19.01.2018. Available at: https://www.carbonbrief.org/explainer-what-climate-models-tell-us-about-future-rainfall (accessed 29.01.19).

He, S., Lui, W. & Li, X. (2016) Prediction of impact force of debris flow based on distribution and size of particles, Environmental Earth Sciences, 75, page 298. Available at: https://link.springer.com/article/10.1007/s12665-015-5180-2#citeas (accessed 29.01.19).

Hiller, P. & Jenssen, L. (2009). Modellforsøk med flomskred mot bruer - Virkning av bruåpning og ledevoller. Teknologirapport. Norges teknisk-naturvitskapelige universitet, Institutt for vann- og miljøteknikk.

Huang, H., Yang, K. & Lai, S. (2007). Impact Force of Debris Flow on Filter Dam. *Geophysical Research Abstracts. European Geosciences Union-General Assembly*. Vienna, Austria, 03218.

Hübl, J., Suda, J., Proske, D., Kaitna, R. & Scheidl, C. (2009) Debris Flow Impact Estimation. International Symposium on Water Management and Hydraulic Engineering. Ohrid/Macedonia, 1-5 September 2009. Paper A56, p. 137-148. Available at: https://www.researchgate.net/publication/258550978_Debris_Flow_Impact_Estimation_steep_slopes (accessed 23.05.19).

Huebl, J. & Fiebiger, G. (2005). Debris-flow mitigation measures. I: Jakob, M. & Hungr, O. (red.) Debris-flow hazards and related phenomena, s. XLII, 739 s., pl. : ill. Berlin: Springer published in association with Praxis PUbl. Available at: https://www.researchgate.net/publication/225262144_Debris-flow_mitigation_measures (accessed 30.01.19).

Hungr, O, Leroueil, S. & Picarelli, L. (2014) The Varnes Classification of landslide types, an update. Landslides. Volume 11, issue 2. Springer, page 167-194. Available at: https://link.springer.com/article/10.1007%2Fs10346-013-0436-y (accessed 28.01.19).

Hungr, O., Morgan, G. & Kellerhals, R. (1984). Quantitative analysis of debris torrent hazards

for design of remedial measures. Canadian Geotechnical Journal, 21 (4): 663-677. Available at: https://www.researchgate.net/publication/237377025_Quantitative_analysis_of_debris_torrent_hazards_for_design_of_remedial_measures (accessed 30.01.19).

Høeg, K., Karlsrud, K. & Lied, K. (2014) Løsmasse - og flomskred. Skred – Skredfare og sikringstiltak. NGI/Universitetsforlaget, pp. 77-93.

Høydal, Ø., A. & Kronholm, K. (2013) Flomskredsikring, utkast til håndbok, Flomskredsikring. NGI.

Iverson, R. M. (1997) The Physics of Debris Flows. Reviews of Geophysics 35 (3): 245–296.

Iverson, R. M., George, D. L. & Logan, M. (2016) Debris flow runup on vertical barriers and adverse slopes, J. Geophys. Res. Earth Surf., 121, pp. 2333–2357. Available at: https://agupubs.onlinelibrary.wiley.com/doi/full/10.1002/2016JF003933 (accessed 28.04.19).

Jóhannesson, T., Gauer, P., Issler, D. & Lied, K. (2009). The design of avalanche protection dams: recent practical and theoretical developments. Brussels, Belgium: European Commission. Available at: https://hal.archives-ouvertes.fr/hal-00575782/PDF/GR2009-PUB00026144.pdf (accessed 02.05.19).

Laache, E. (2015) Effective Debris Flow Countermeasures. Specialization project. Norwegian University of Science and Technology.

Laache, E. (2016) Model Testing of the Drainage Screen Type Debris Flow Breaker. Master's Thesis. Norwegian University of Science and Technology.

Le, T. M. H, Christensen, S. O., Watn, A., Christiansen, L. F., Emdal, A. & Norem, H. (2016) Effects of deflection wall on run-up height of debris flow. Landslides and Engineered Slopes. Experience, Theory and Practice, p. 1237-1244.

Naaim, M., Faug, T., Naaim-Bouvet, F. & Eckert, N. (2010). Return period calculation and passive structure design at the Taconnaz avalanche path, France. Annals of Glaciology, 51, No. 54, 89–97. Naaim-Bouvet. Available at: https://pdfs.semanticscholar.org/da6e/038165ada5fffe1092a8c3aa1bacdcb5c2de.pdf (accessed 02.05.19).

Ng, C. W. W., Choi, C. E., Koo, R. C. H., Goodwin, G. R., Song, D. & Kwan, J. S. H. (2018) Dry granular flow interaction with dual-barrier systems. Géotechnique, 68:5, 386-399. Available at: http://ias.ust.hk/ias/files/pdf/1506410448_b2.pdf (accessed 11.05.19).

Nettleton, I., Martin, S., Hencher, S. & Moore, R. (2005) Debris flow types and mechanisms, Scottish Road Network Landslides Study, 45-67. Available at https://www2.gov.scot/Publications/2005/07/08131738/17492 (accessed 05.02 19).

Norem, H. & Sandersen, F. (2012). Flom- og sørpeskred, Håndbok 284 - Høringsutgave av veileder. 73: Statens Vegvesen. 102 s. Available at: https://www.vegvesen.no/fag/publikasjoner/publikasjoner/Statens+vegvesens+rapporter/_attachment/519072?_ts=140e2d18e58&fast_title=SVV_73_Flom-_og_sorpeskred.pdf (accessed 30.01.19).

Norem, H. (2011). Veger og snøskred - Håndbok om sikring mot snøskred - Høringsutgave. 27: Vegdirektoratet. 94 s. Available at: https://brage.bibsys.no/xmlui/bitstream/handle/11250/2582729/VD%20rapport%2027.pdf?sequence=1&isAllowed=y (accessed 30.01.19).

NVE. (2018) Flood and landslide warning service. Available at http://www.varsom.no/en/flood-and-landslide-warning-service/?date=2018-10-14 (accessed 28.01.19).

NVE. (2013) Jordskred og flomskred. Available at: http://publikasjoner.nve.no/faktaark/2013/faktaark2013_05.pdf (accessed 28.01.19).

NVE. (n.d.) Hvordan varsler NVE flom og jordskredfare? Available at: http://www.varsom.no/flom-og-jordskredvarsling/hvordan-varsler-nve-flom-og-jordskredfare/ (accessed 28.01.19).

Opsahl, K. D. (2018) Impact force from a debris flow on a steel pillar. Specialization project. Norwegian University of Science and Technology.

Pierson, T. (1986) Flow behavior of channelized debris flows Mount St. Helens Washington. *Hillslope Processes*, 269-296.

Rosy, P.N. (2017) *Physical Modeling of Debris Flow by Varying Sediment Transportation*. Master's thesis. Norwegian University of Science and Technology.

Sassa, K., Kaibori, M. & Kitera, N. (1985) Liquefaction and undrained shear of torrent deposits as the cause of debris flows. *Proceedings International Symposium on Erosion, Debris Flows and Disaster Prevention* (pp. 231-236). Toshindo, Tokyo.

Statens Vegvesen (2014). Håndbok V139: Flom- og sørpeskred. Vegdirektoratet, Oslo. Available at: https://www.vegvesen.no/_attachment/740653/binary/1006021 (accessed 26.02.19).

Statens Vegvesen (2005) Håndbok 014 Laboratorieundersøkelser. Available at: https://www.vegvesen.no/s/vegnormaler/hb/014/Kvalitetsikrede%20_filer/Vedlegg/VEDLEGG_1_april_2005.pdf (accessed 26.02.19).

Sæterbø, E., Syvertsen, L. & Tesaker, E. (1998). Vassdragshåndboka. Trondheim: Tapir. Available at: https://www.nb.no/nbsok/nb/89a4337e65b3f0190b501d7e142fcca0?lang=no#75 (accessed 06.02.19).

Takahashi, T. (2014) Debris flow: Mechanics, Prediction and Countermeasures. 2nd edition. London: CRC Press.

Vagnon, F. & Segalini, A. (2016) Debris flow impact estimation on a rigid barrier. Natural Hazards and Earth System Sciences, 16(7), 1691-1697.

VanDine, D. F. (1996) Debris flow control structures for forest engineering. Res. Br., B.C. Min. For., Victoria, B.C., Work. Pap. 08/1996. Available at https://rdck.ca/assets/Services/Emergency~Management/Documents/Debris%20Flow%20Control%20Structures%20for%20Forest%20Engineering.pdf (accessed 30.01.19).

Vicari, H. (2018) Physical and numerical modelling of debris flows. Master's thesis. Norwegian University of Science and Technology.

APPENDICES

Appendix A: Change of velocity in the chute

A.1 Velocity along the chute and start of deposition area in test nr. 1: G4V1C1-r1

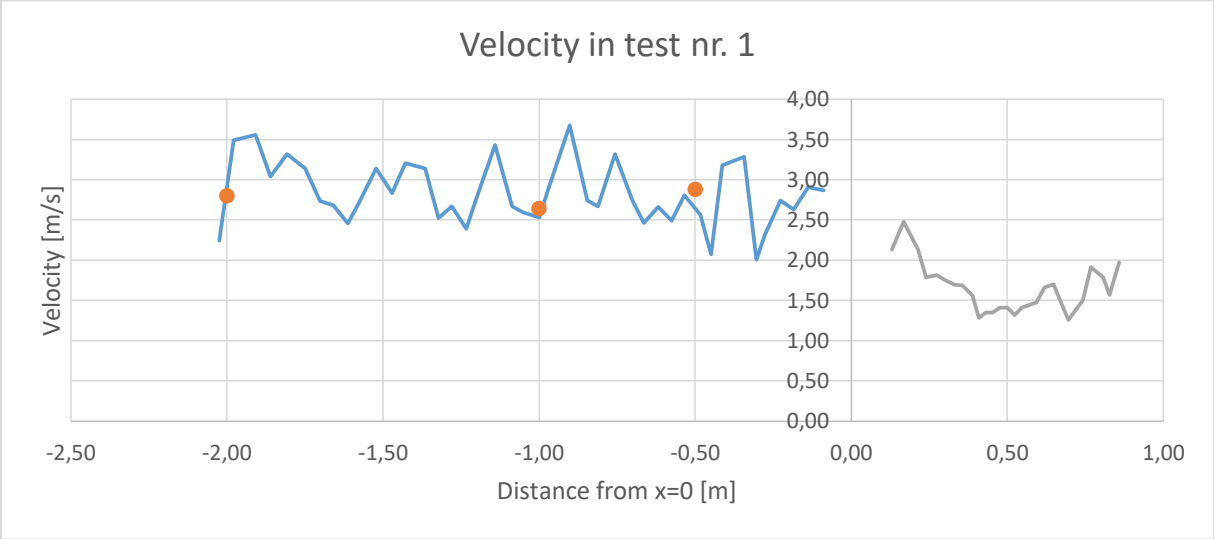

A.2 Velocity along the chute and start of deposition area in test nr. 2: G4V1C1-r2

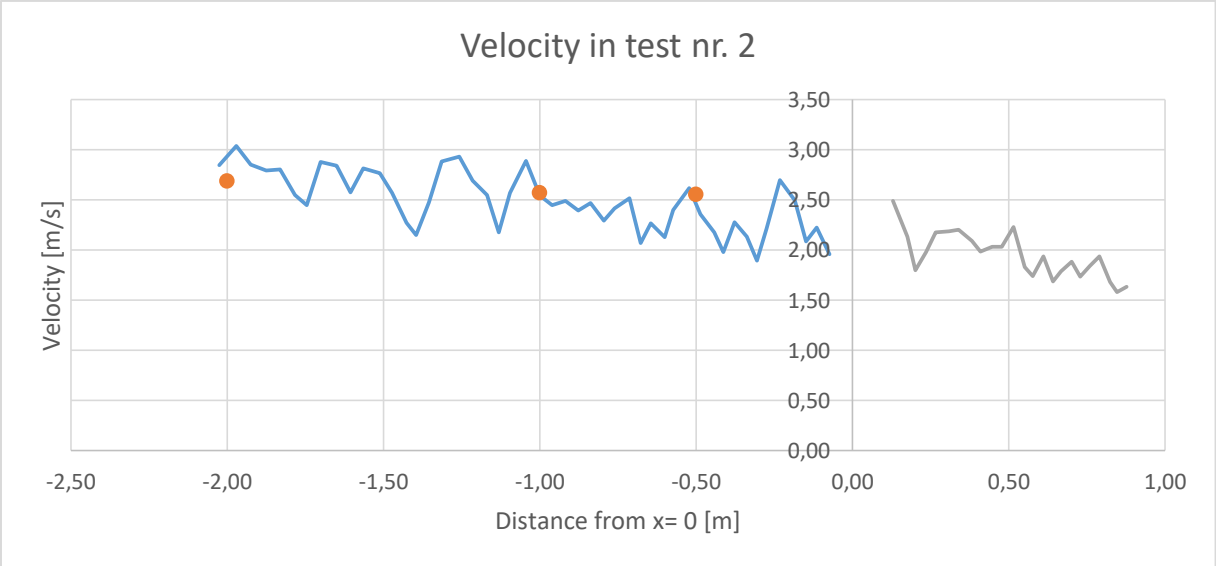

A.3 Velocity along the chute and start of deposition area in test nr. 3 G4V1C1-r3

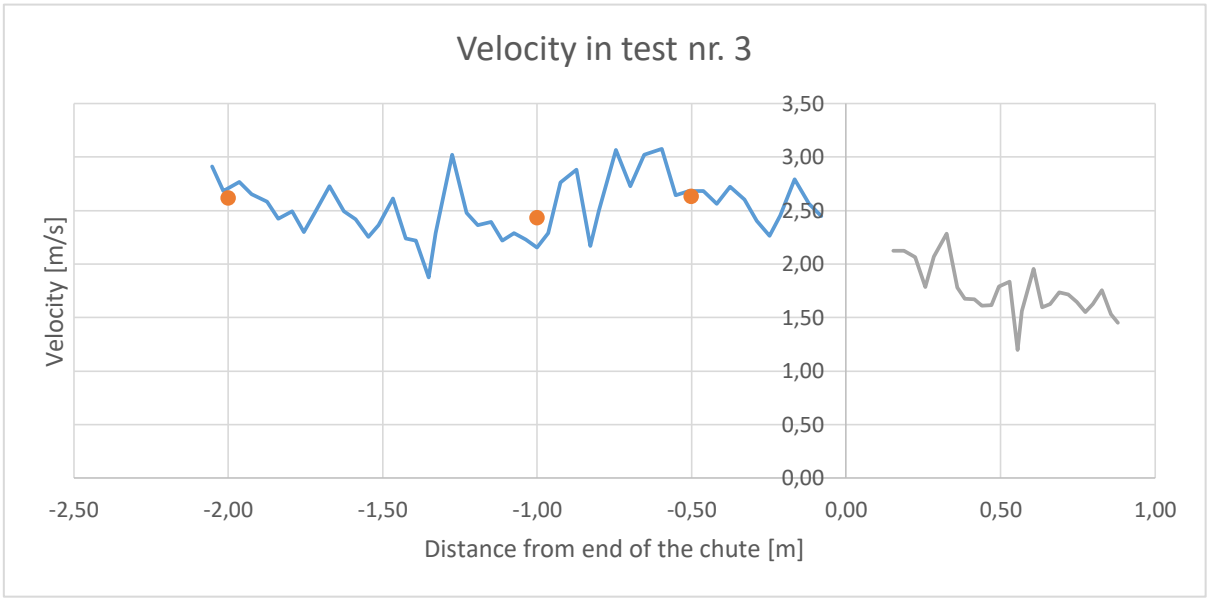

A.4 Velocity along the chute and start of deposition area in test nr. 4 G4V1C1-r1-w90

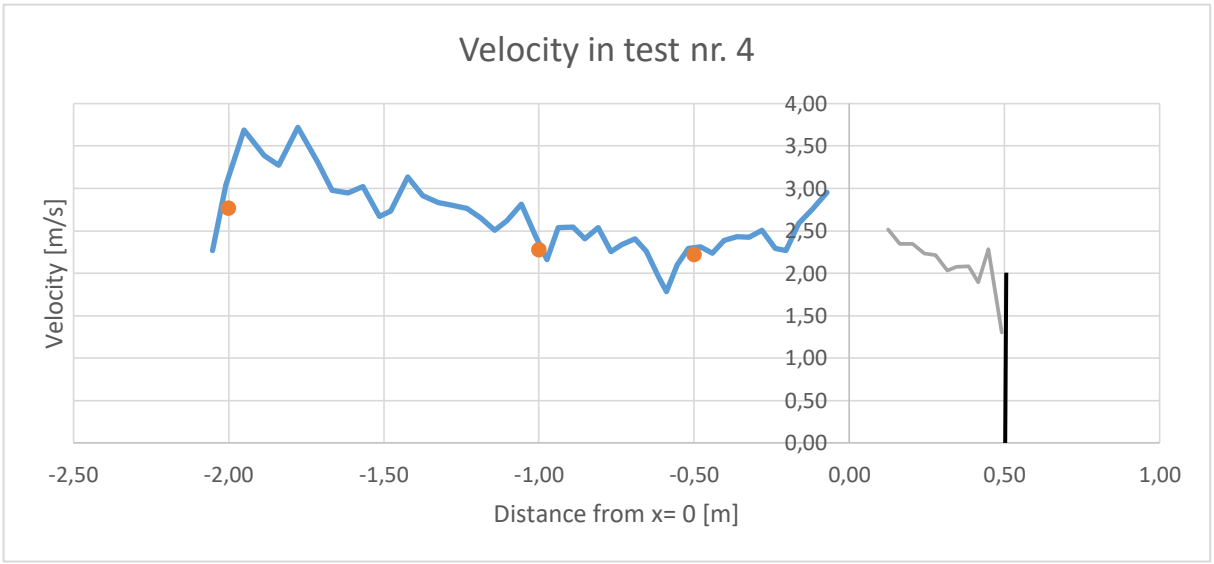

A.5 Velocity along the chute and start of deposition area in test nr. 5 G4V1C1-r2-w90

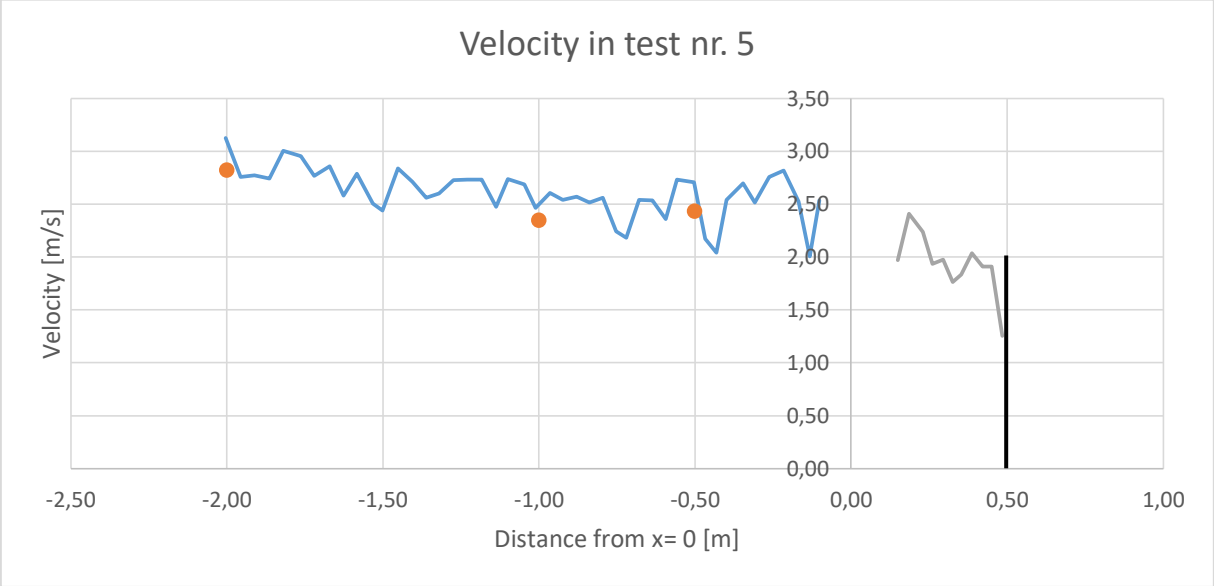

A.6 Velocity along the chute and start of deposition area in test nr. 6 G4V1C1-r1-w45

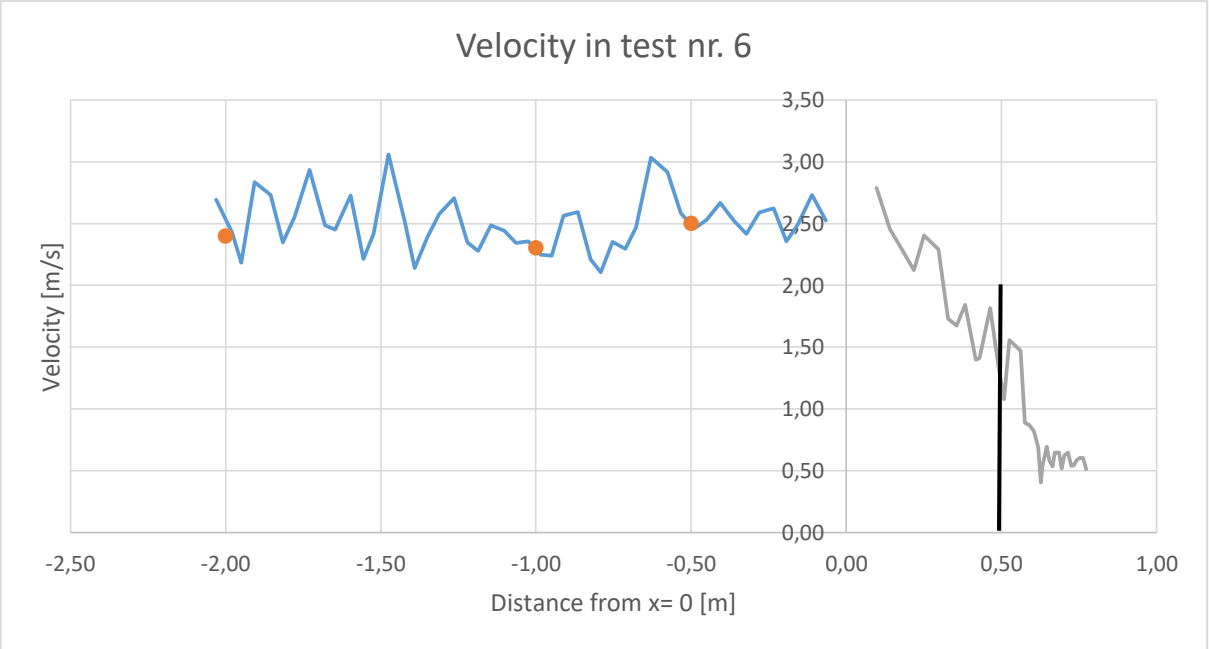

Collision between front and deflection wall happens at x=0,49 m

A.7 Velocity along the chute and start of deposition area in test nr. 7 G4V1C1-r2-w45

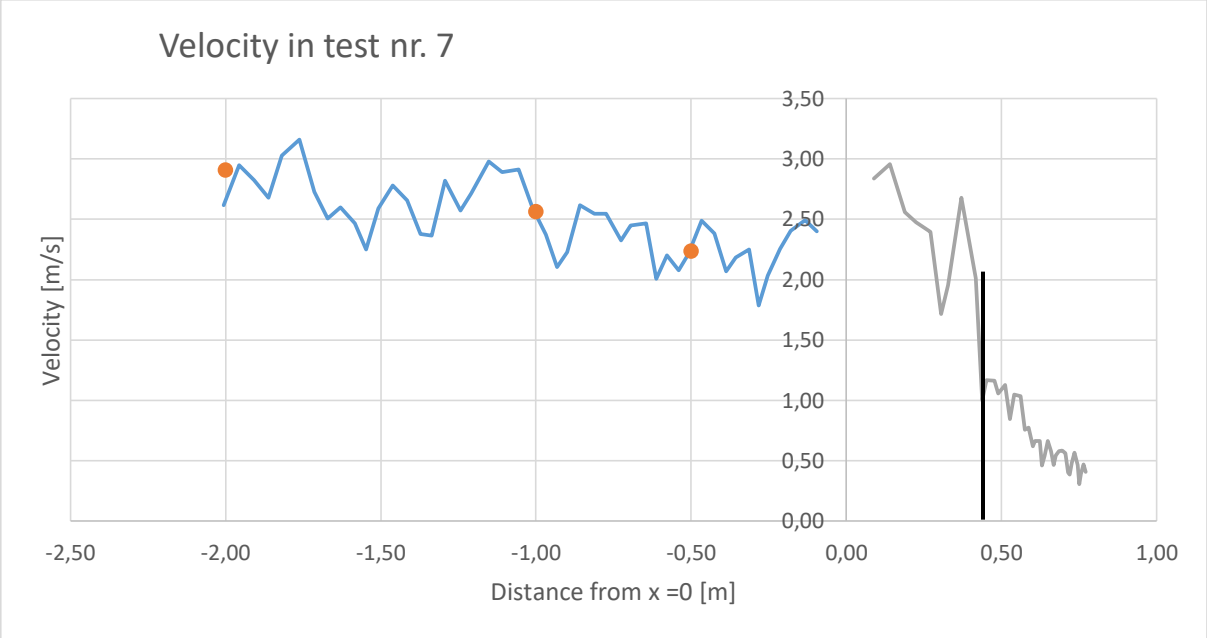

Collision between front and deflection wall happens at x=0,44 m

A.8 Velocity along the chute and start of deposition area in test nr. 8 G4V1C3-r1-w90

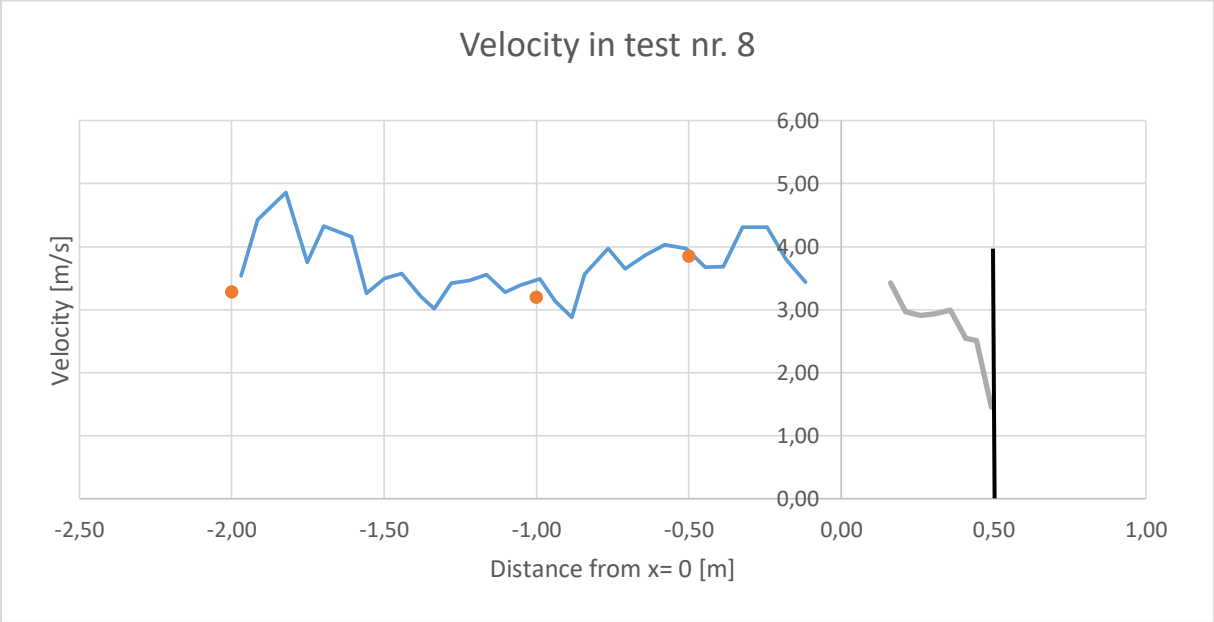

A.9 Velocity along the chute and start of deposition area in test nr. 9 G4V1C3-r1-w90

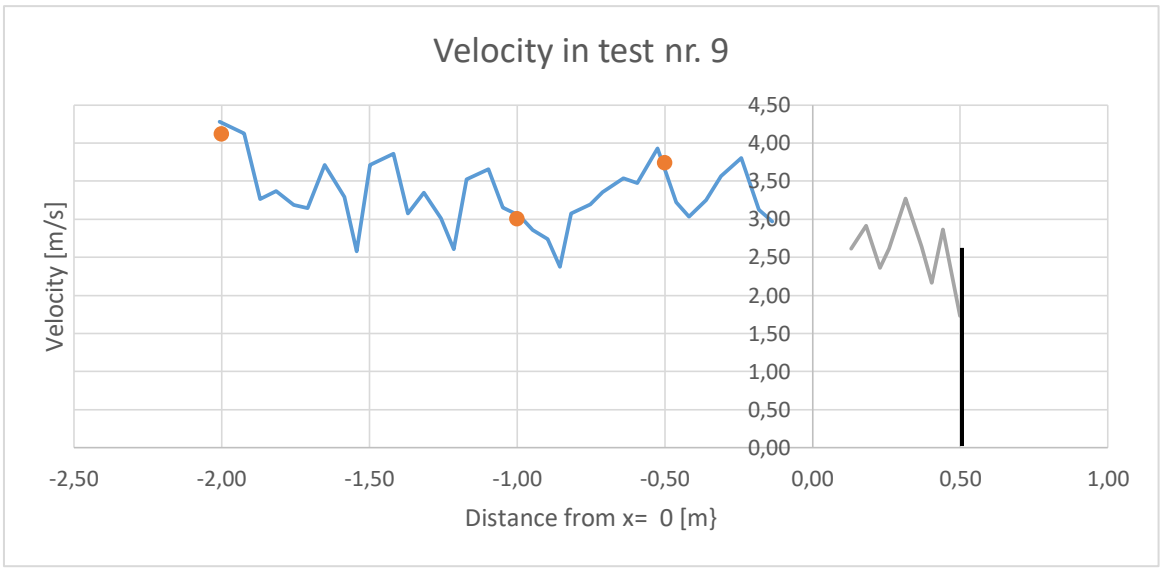

A.10 Velocity along the chute and start of deposition area in test nr. 10 G4V1C3-r1-w90

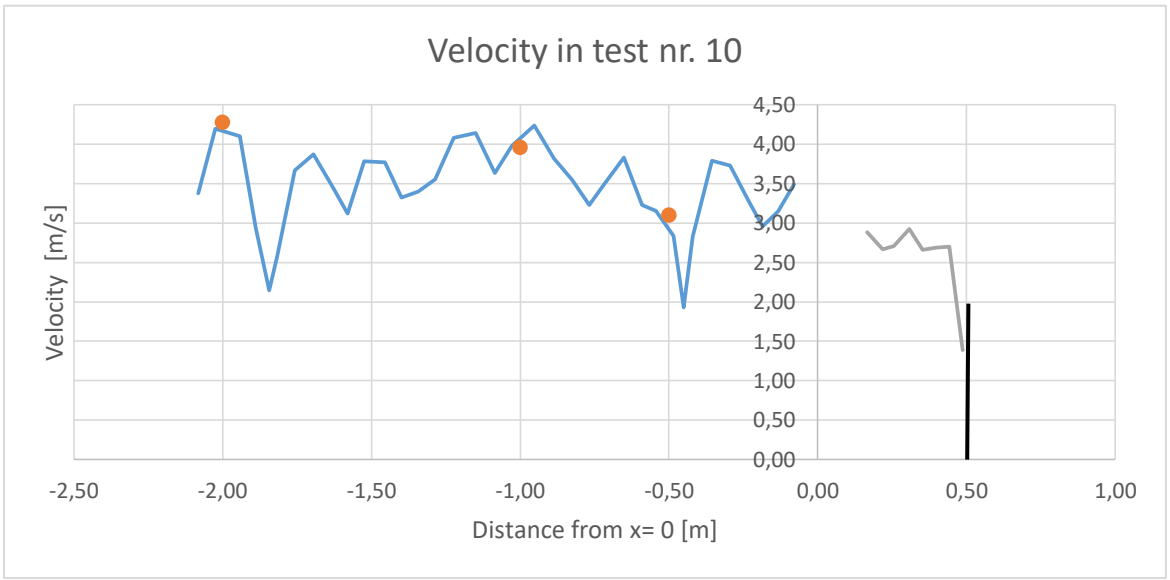

A.11 Velocity along the chute and start of deposition area in test nr. 11 G4V1C1-r3-w90

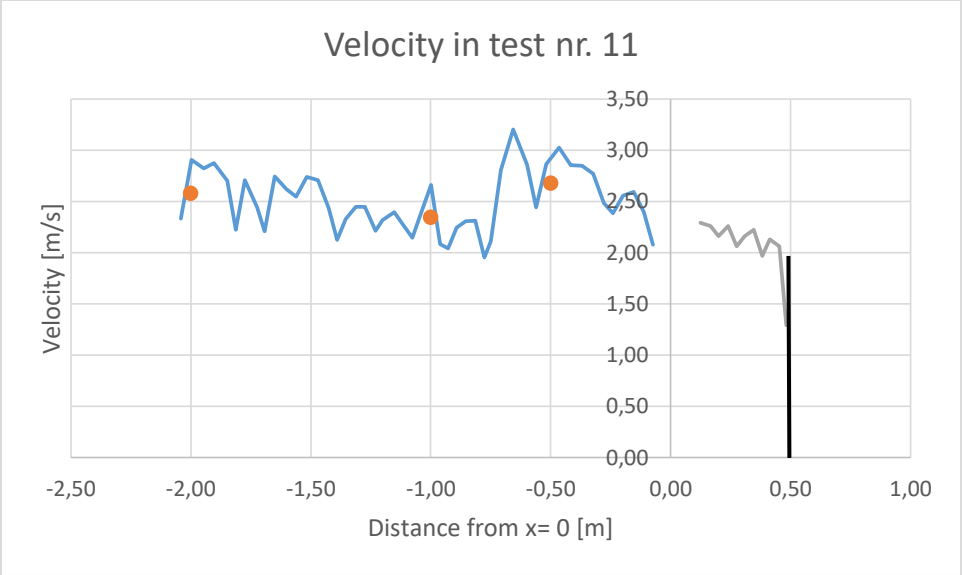

A.12 Velocity along the chute and start of deposition area in test nr. 11 G4V1C1-r3-w90

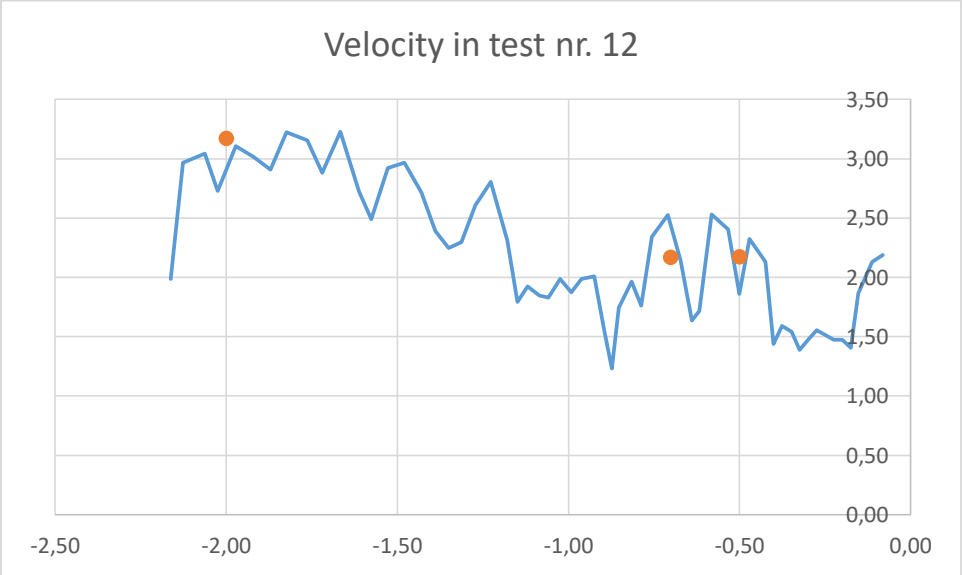

Appendix B: Flow height and run-up height

B.1 Measured flow height in test nr. 2: G4V1C1-r2

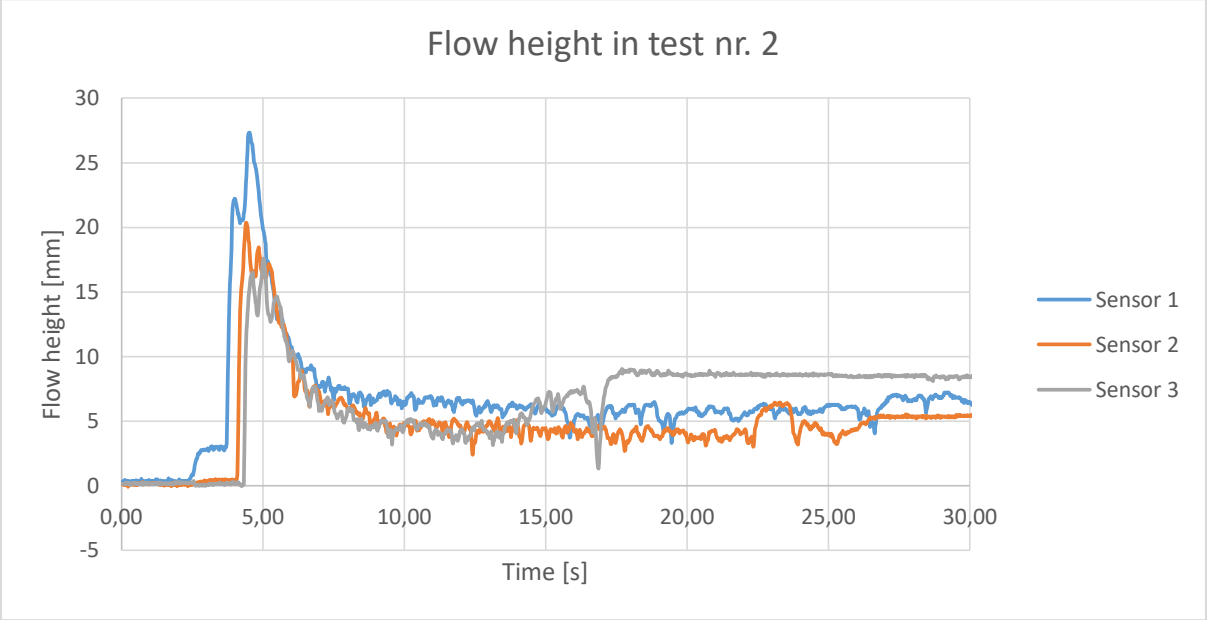

B.2 Measured flow height in test nr. 3: G4V1C1-r3

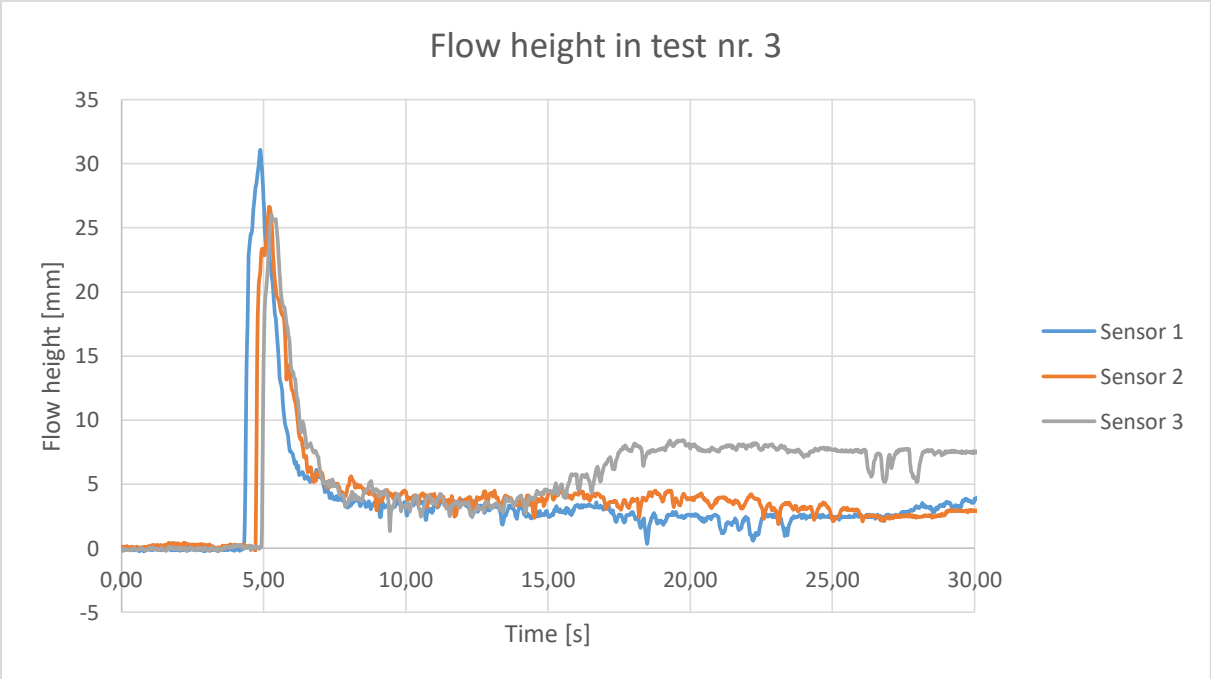

B.3 Measured flow height in test nr. 4: G4V1C1-r1-w90

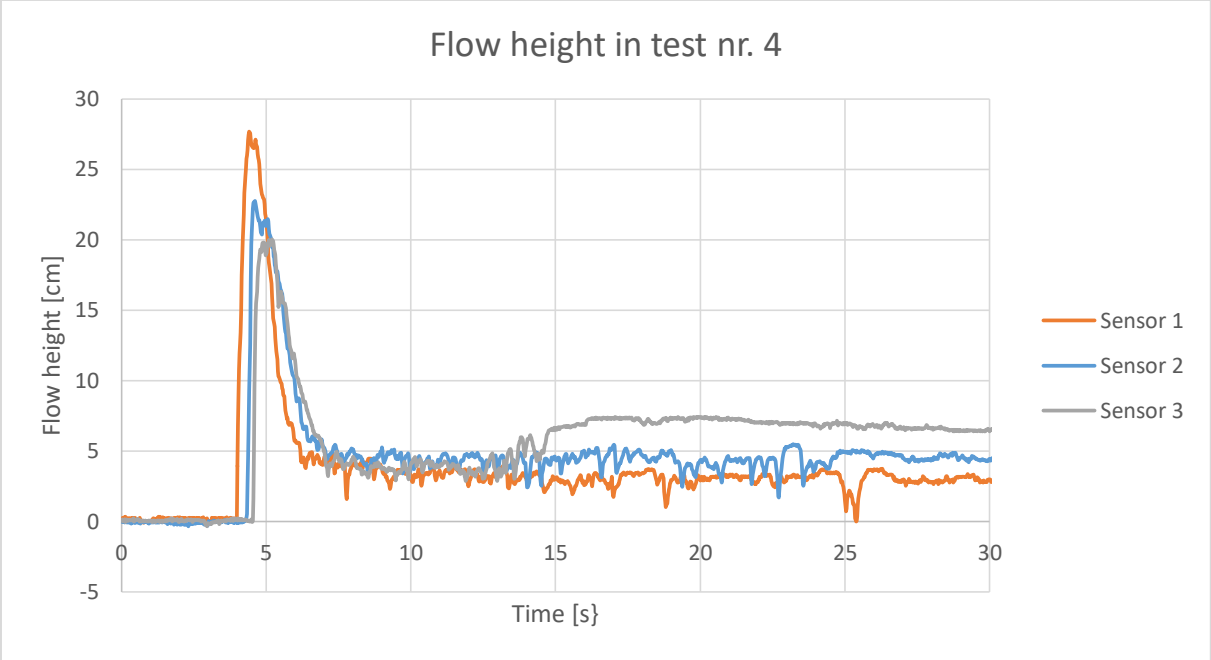

B.4 Measured flow height in test nr. 5: G4V1C1-r2-w90

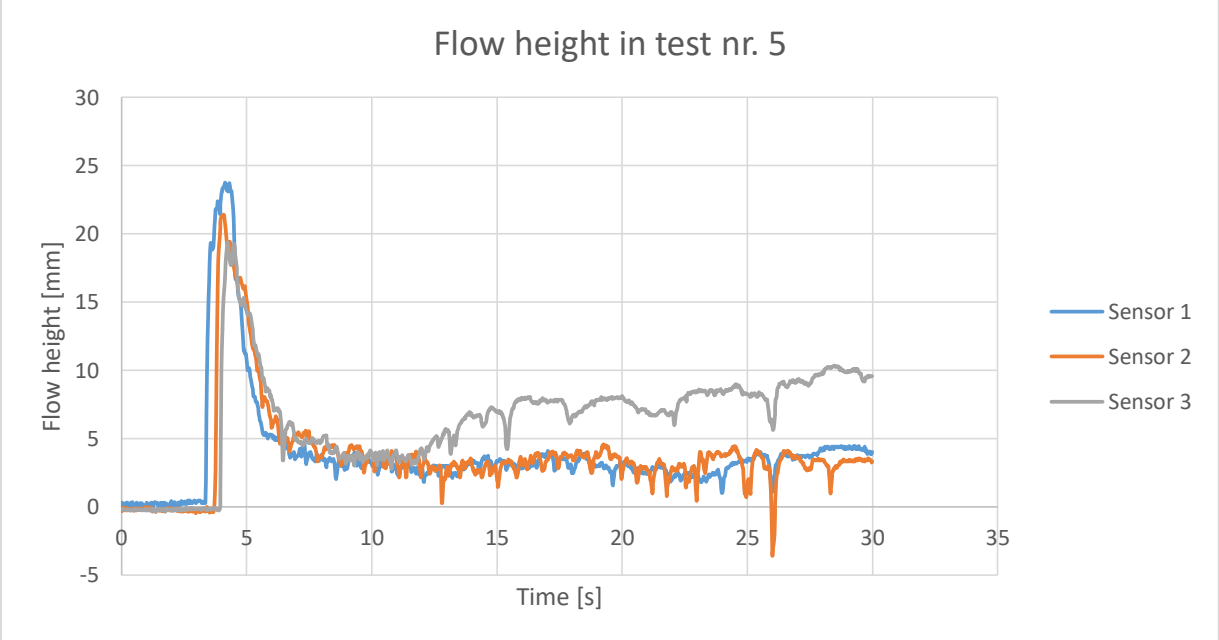

B.5 Measured flow height in test nr. 6: G4V1C1-r1-w45

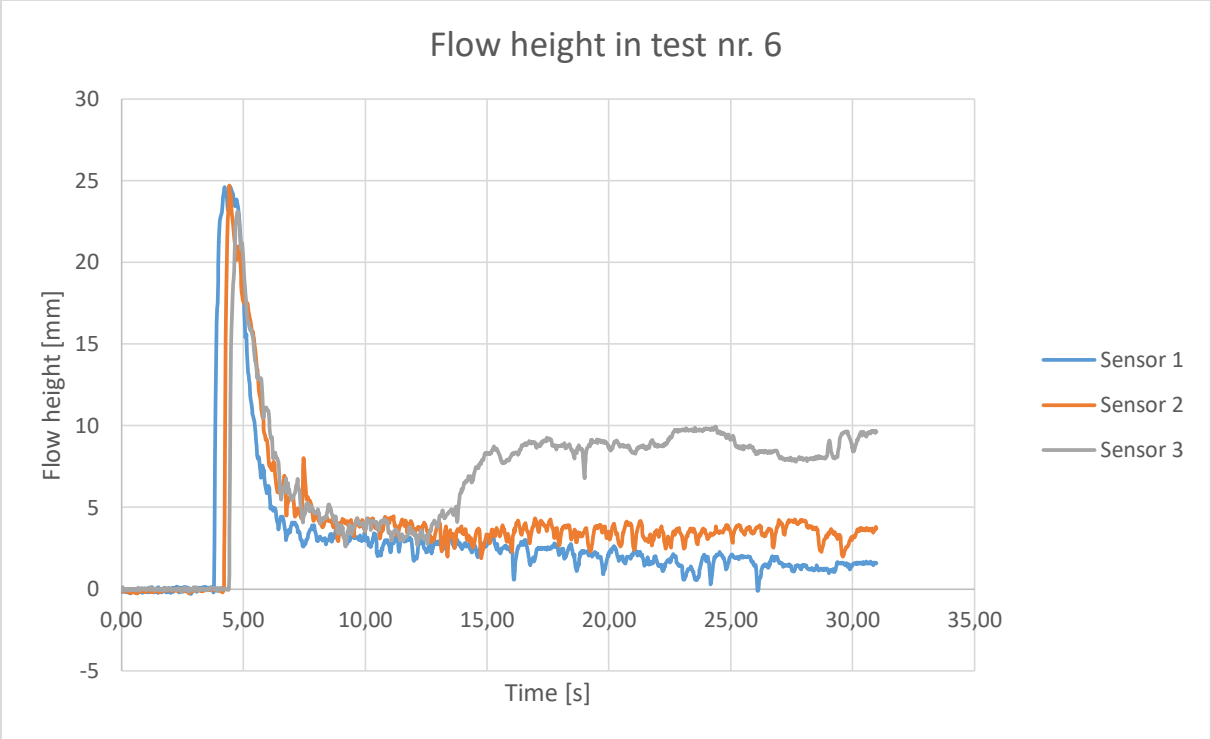

B.6 Measured flow height in test nr. 7: G4V1C1-r2-w45

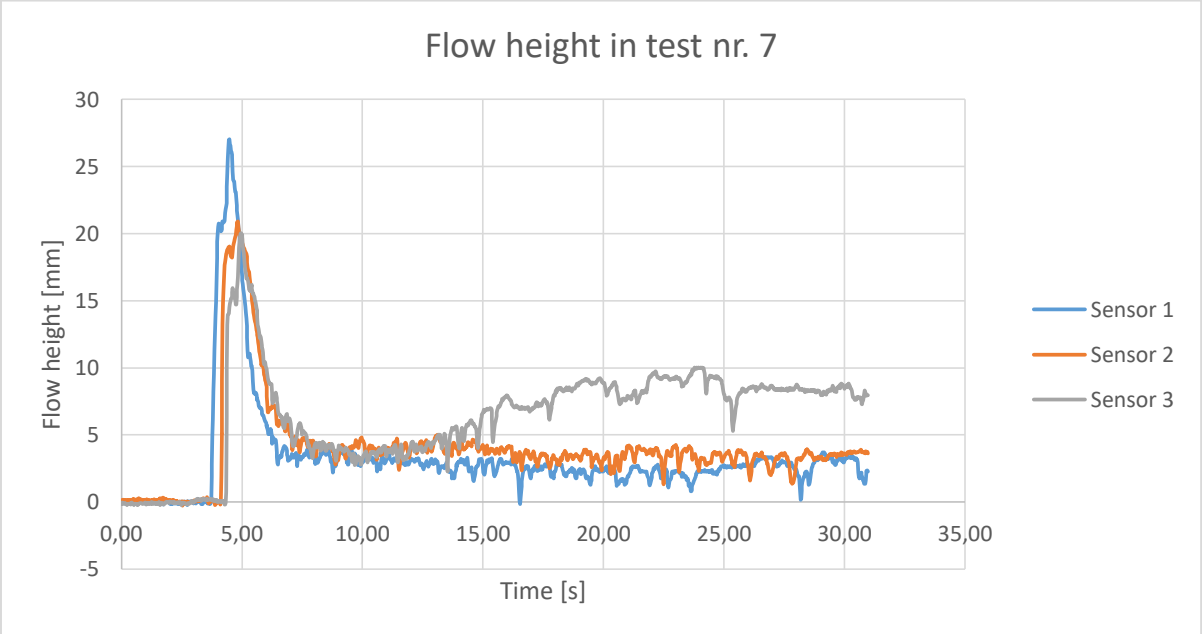

B.7 Measured flow height in test nr. 8: G4V1C3-r1-w90

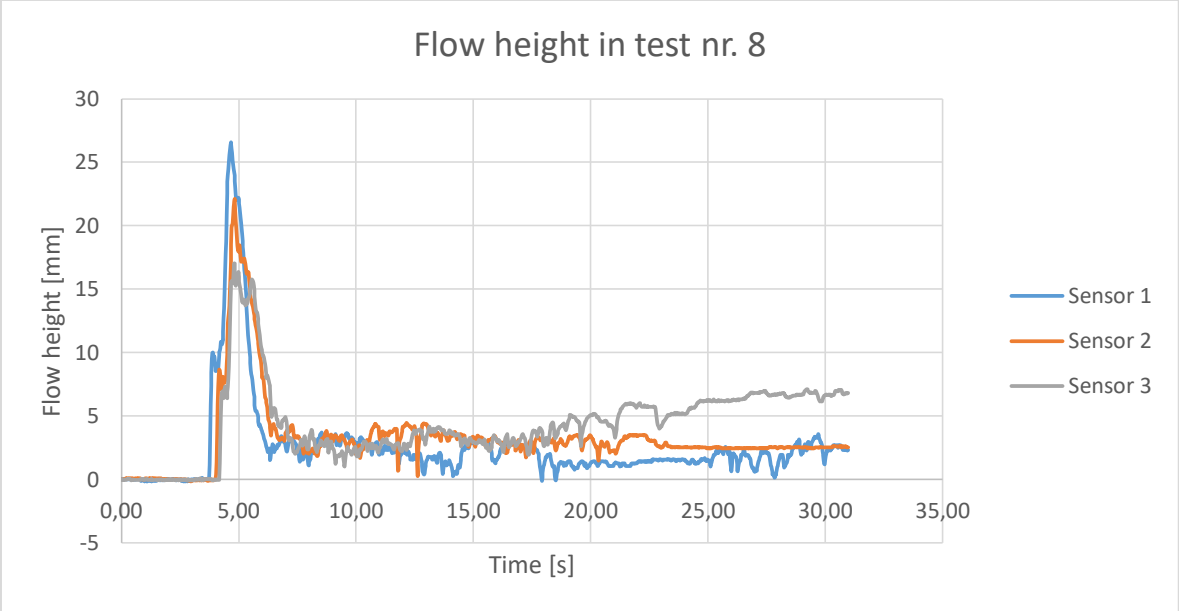

B.8 Measured flow height in test nr. 9: G4V1C3-r2-w90

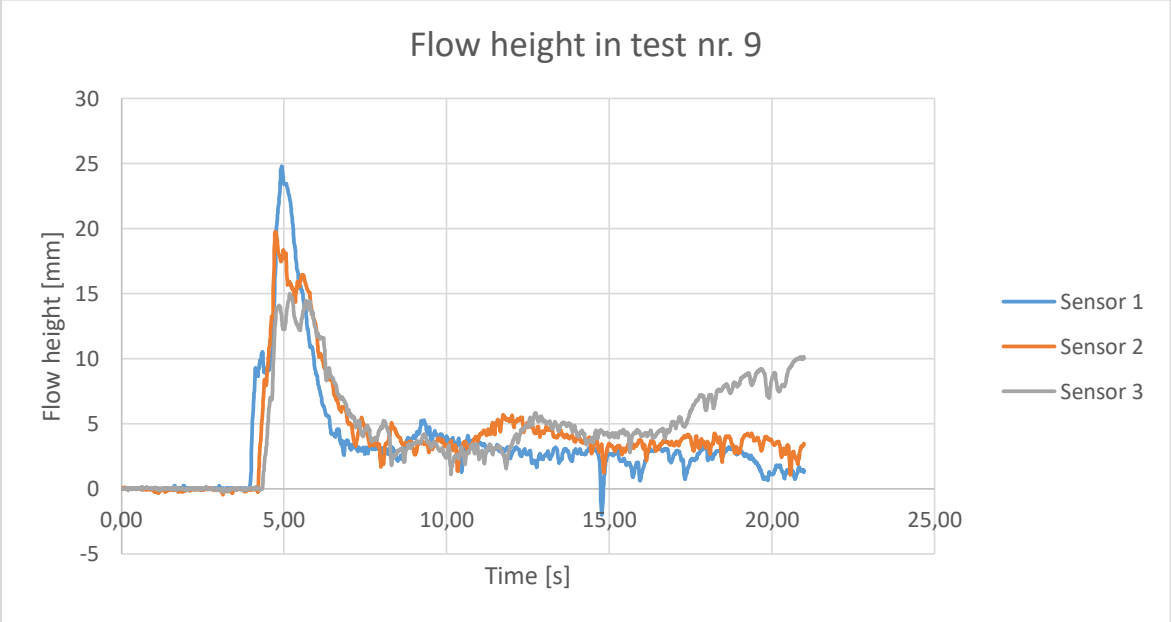

B.9 Measured flow height in test nr. 10: G4V1C3-r3-w90

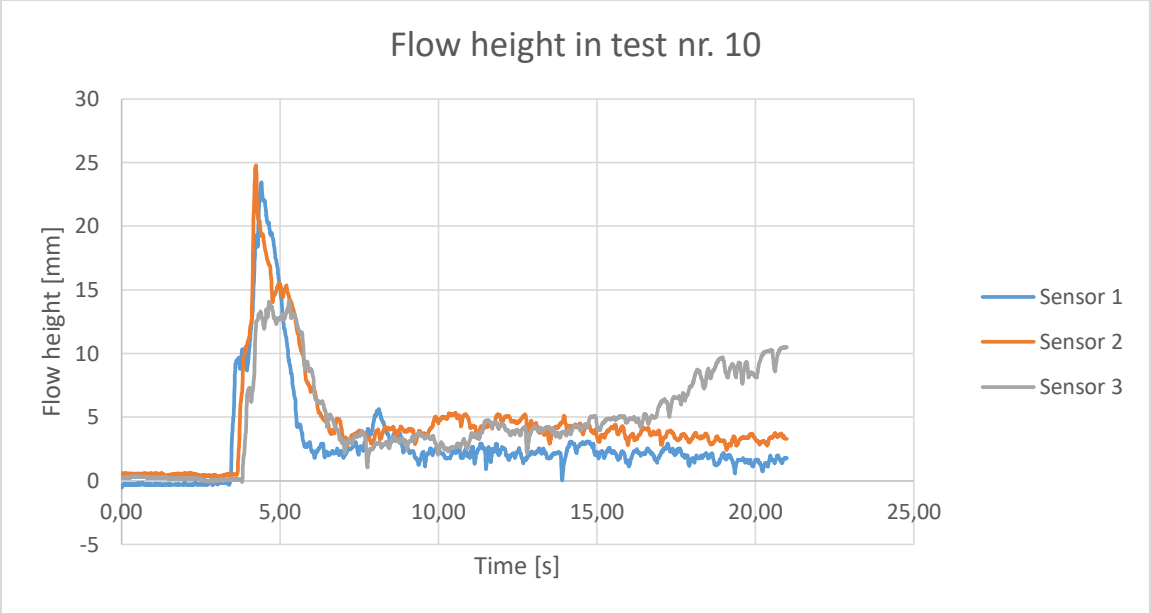

B.10 Measured flow height in test nr. 11: G4V1C1-r3-w90

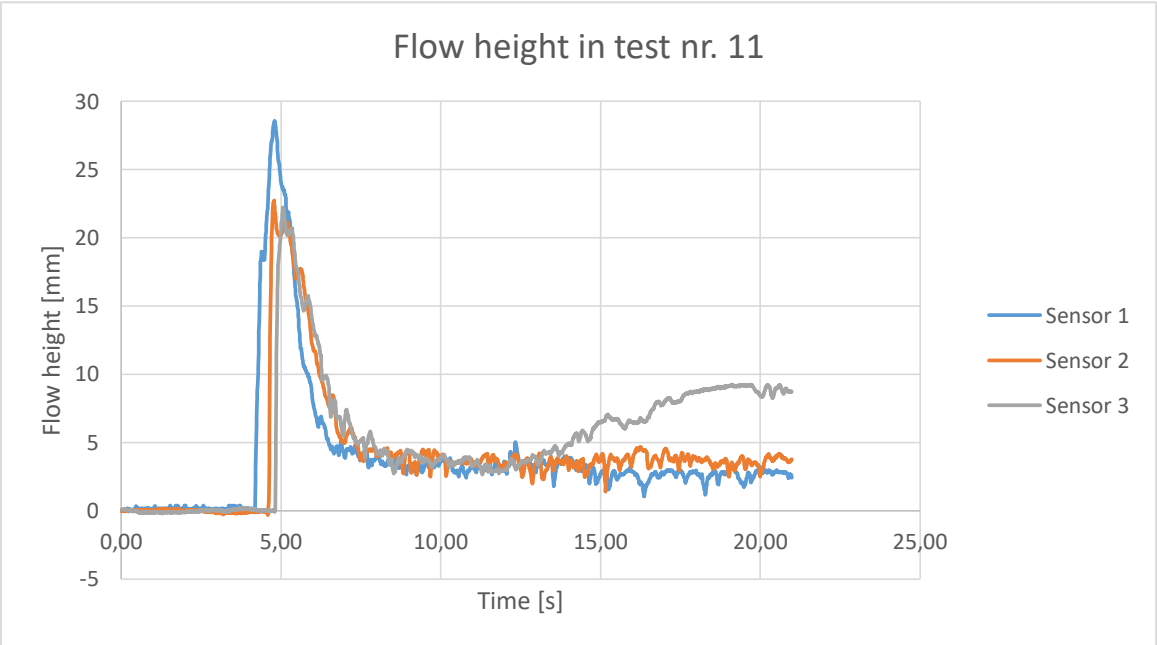

B.11 Measured flow height in test nr. 12: G4V2C2-r1

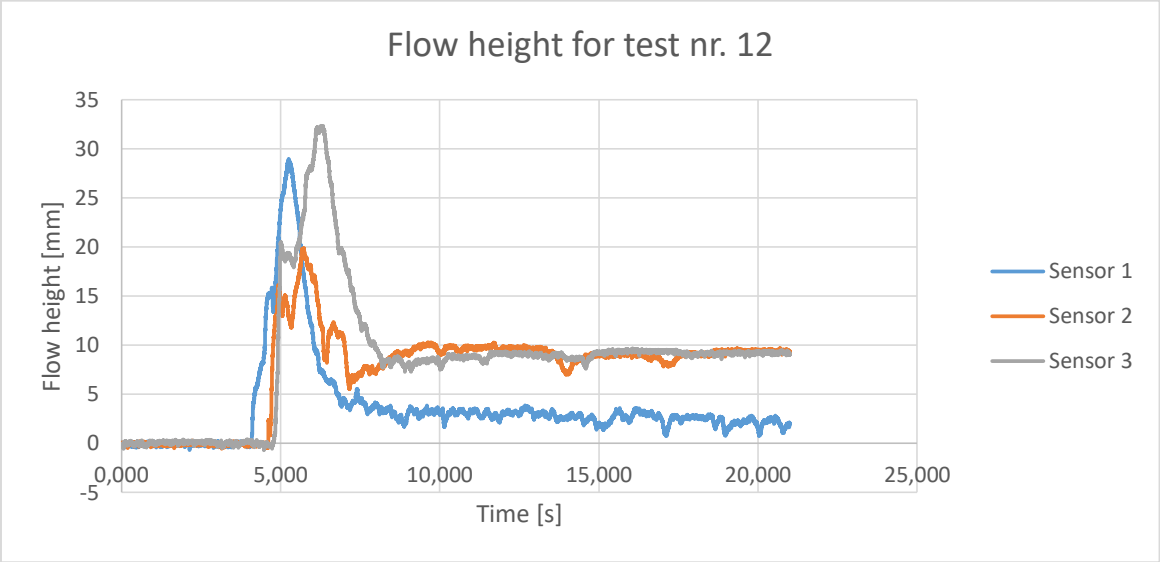

Appendix C: Force measurements

C.1 Measured force in test nr. 4: G4V1C1-r1-w90

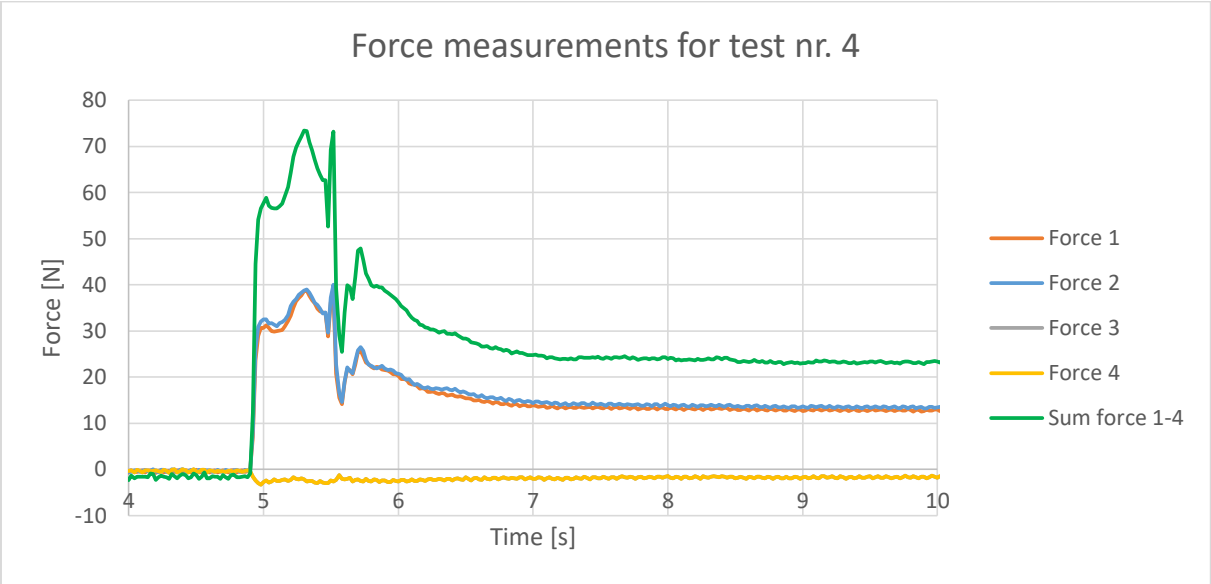

C.2 Measured force in test nr. 5: G4V1C1-r2-w90

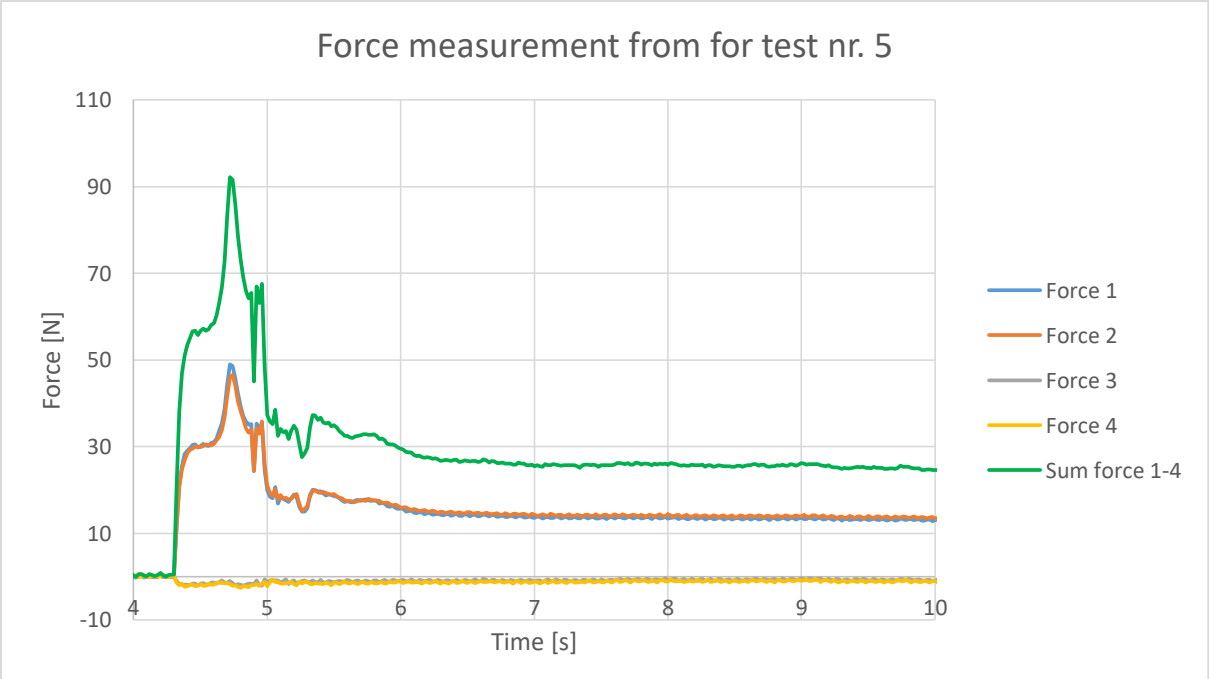

C.3 Measured force in test nr. 6: G4V1C1-r1-w45

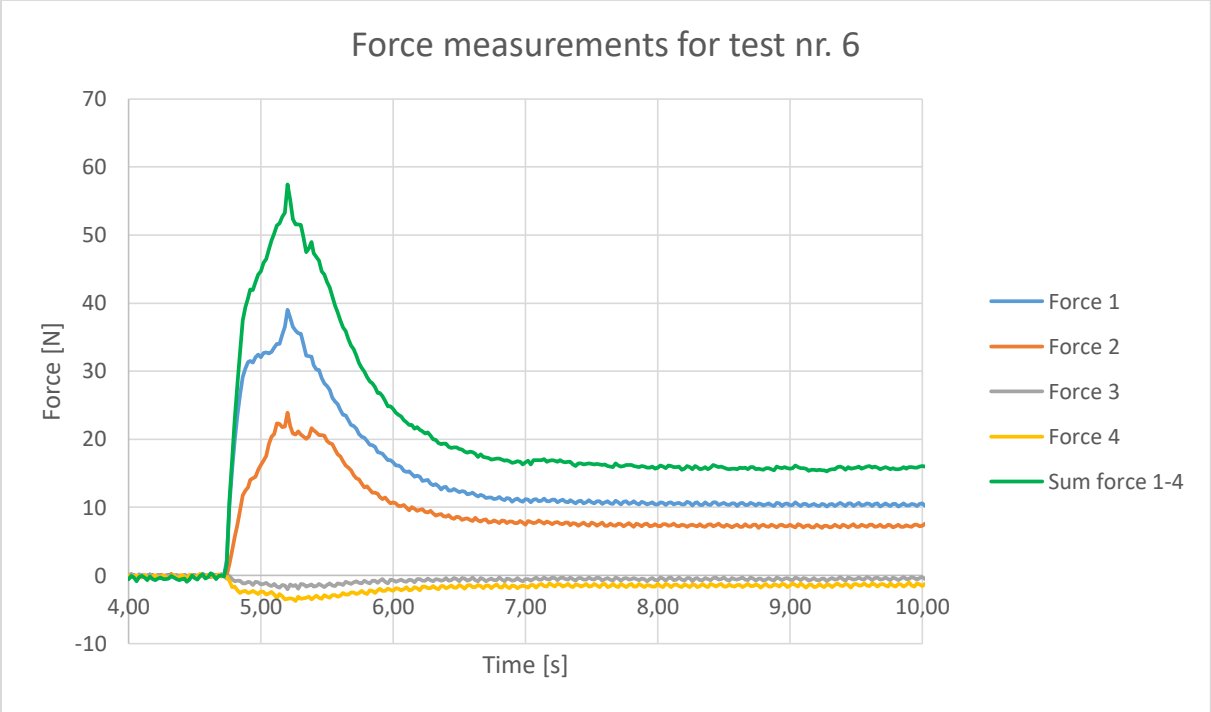

C.4 Measured force in test nr. 7: G4V1C1-r2-w45

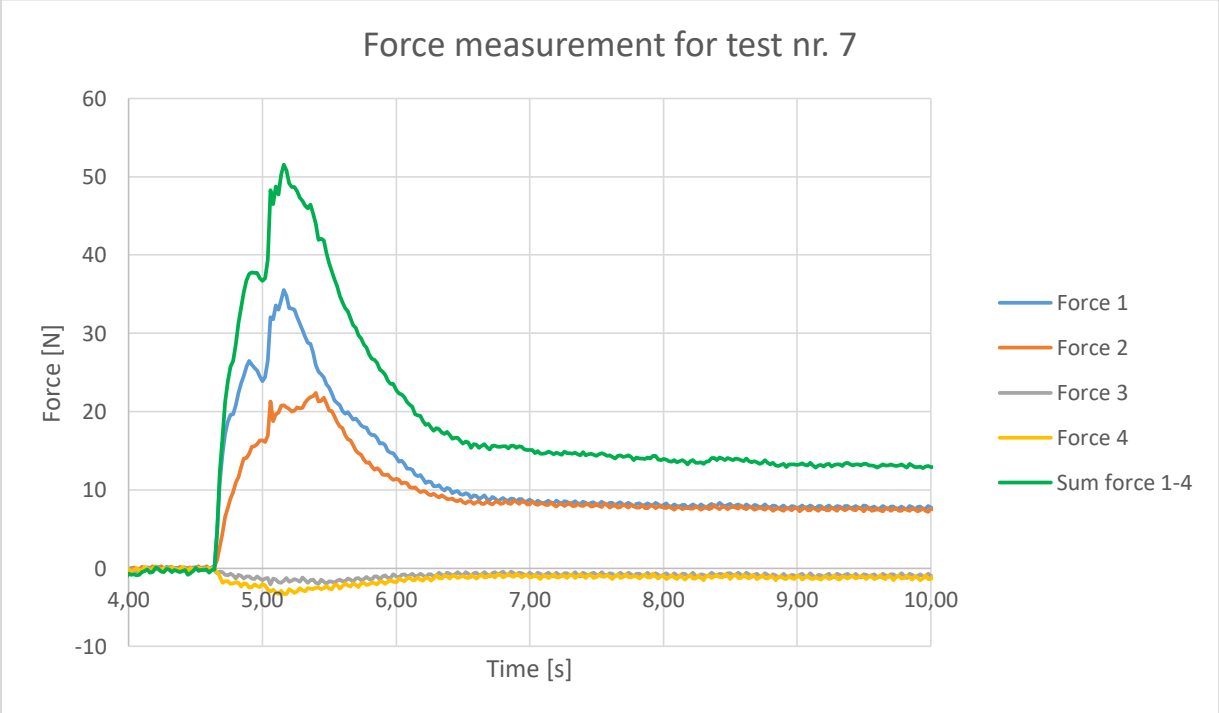

C.5 Measured force in test nr. 8: G4V1C3-r1-w90

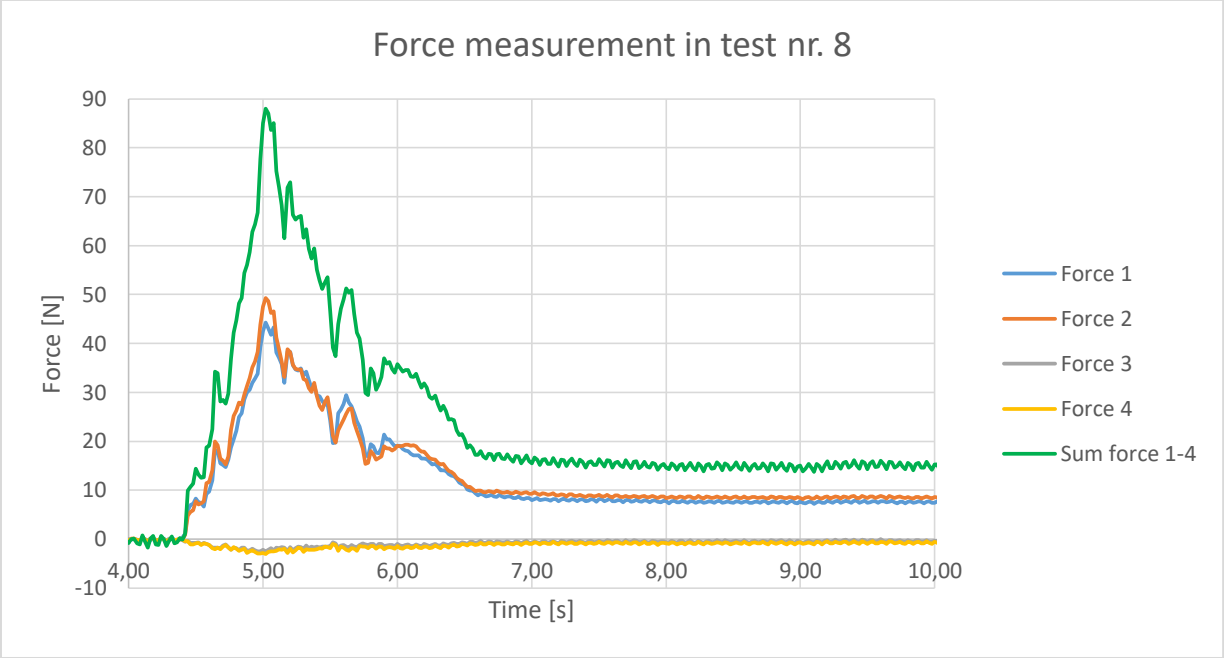

C.6 Measured force in test nr. 9: G4V1C3-r2-w90

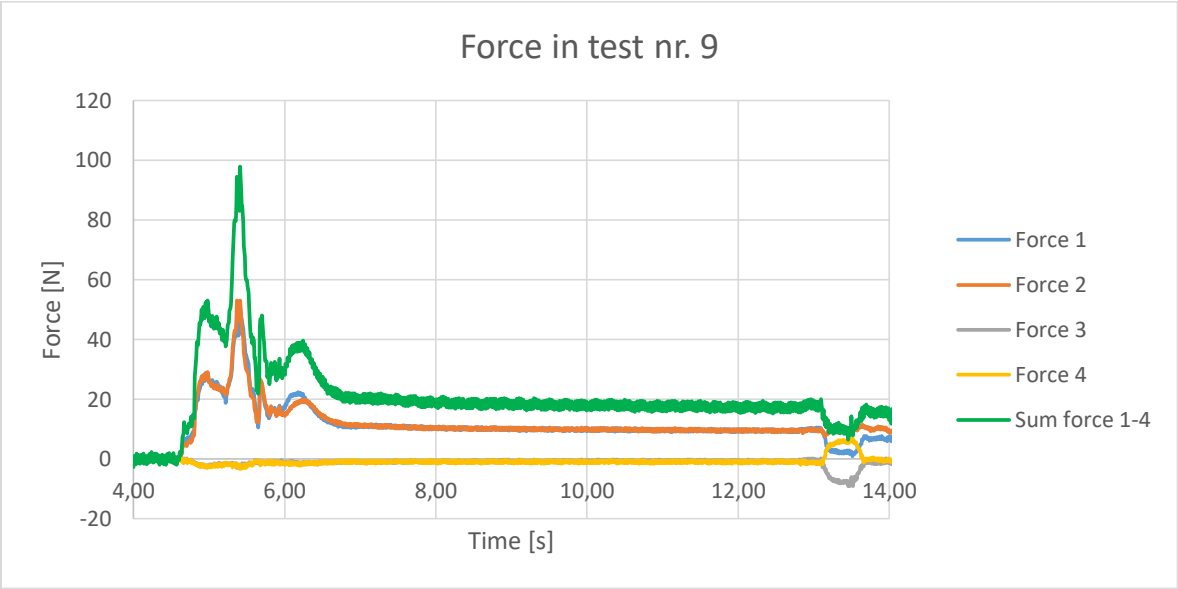

C.7 Measured force in test nr. 10: G4V1C3-r3-w90

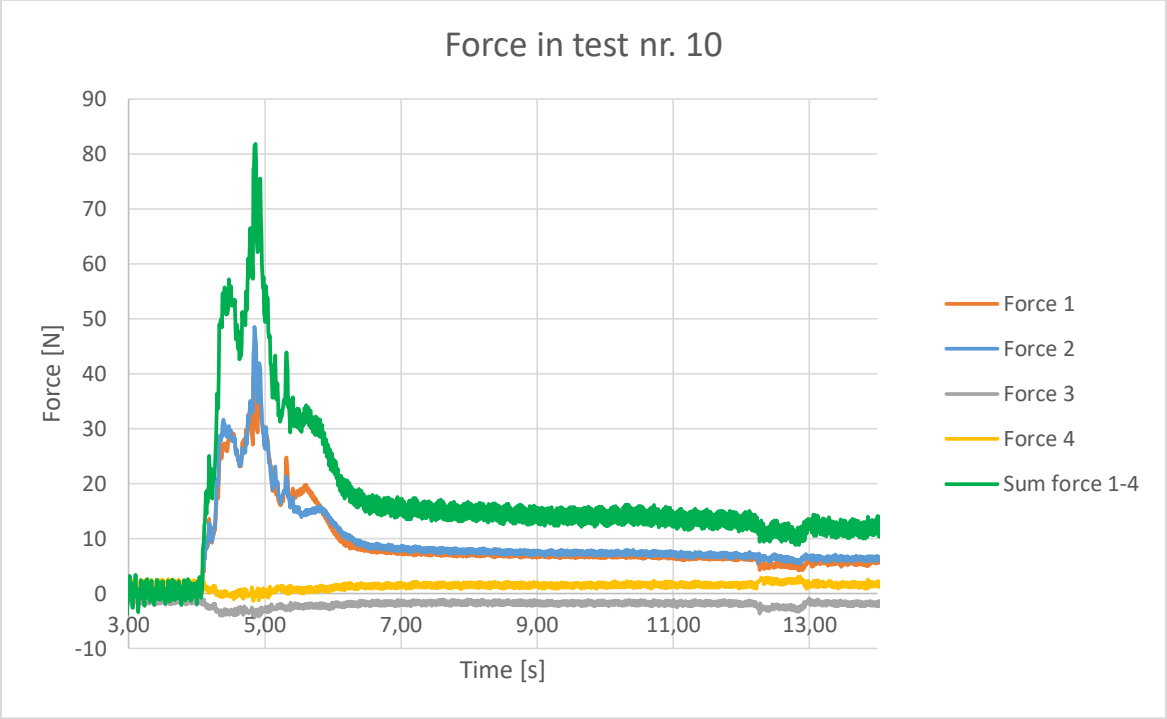

C.8 Measured force in test nr. 11: G4V1C1-r3-w90

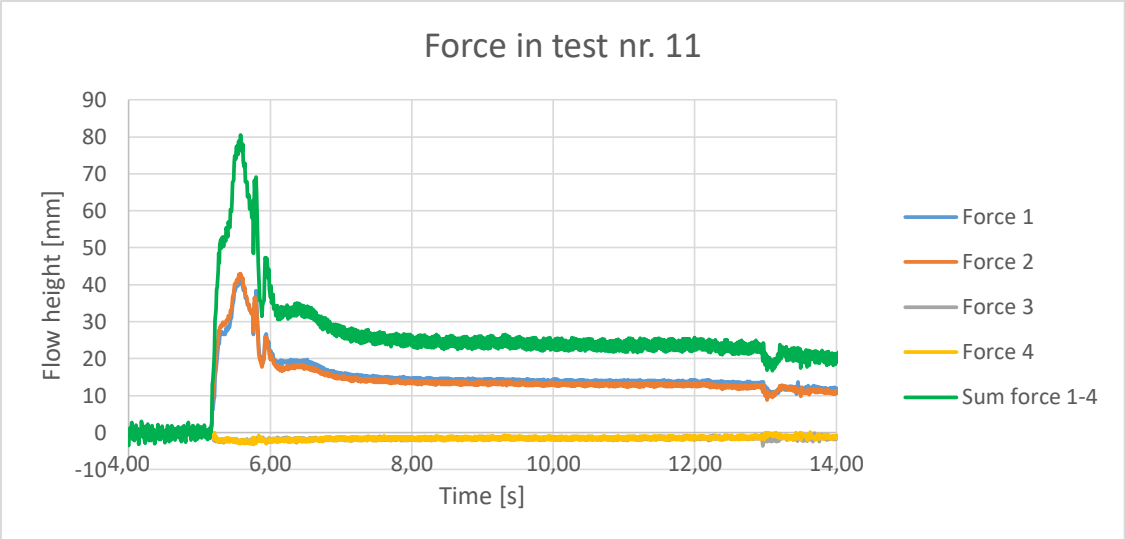

Appendix D: Deposition pattern and run-out length

D.1 Table of run-out lengths

Table 11: Run-out lengths

Test nr.	Name of the test	Deflection angle	Concentration [%]	Run-out length, left	Run-out length, right
		[°]	*[%]*	*[cm]*	*[cm]*
1	G4V1C1-R1	0	60	220	-
2	G4V1C1-R2	0	60	209	-
3	G4V1C1-R3	0	60	215	-
4	G4V1C1-R1-W90	90	60	54	54
5	G4V1C1-R2-W90	90	60	56,5	55,5
6	G4V1C1-R1-W45	45	60	139	-
7	G4V1C1-R2-W45	45	60	123	-
11	G4V1C1-R3-W90	90	60	55	51
8	G4V1C3-R1-W90	90	50	64	64,5
9	G4V1C3-R2-W90	90	50	65,5	66,5
10	G4V1C3-R3-W90	90	50	63,5	67,5

D.2 Deposition patterns

D.2.1 Deposition pattern of G4V1C1-r1

D.2.2 Deposition pattern of G4V1C1-r2

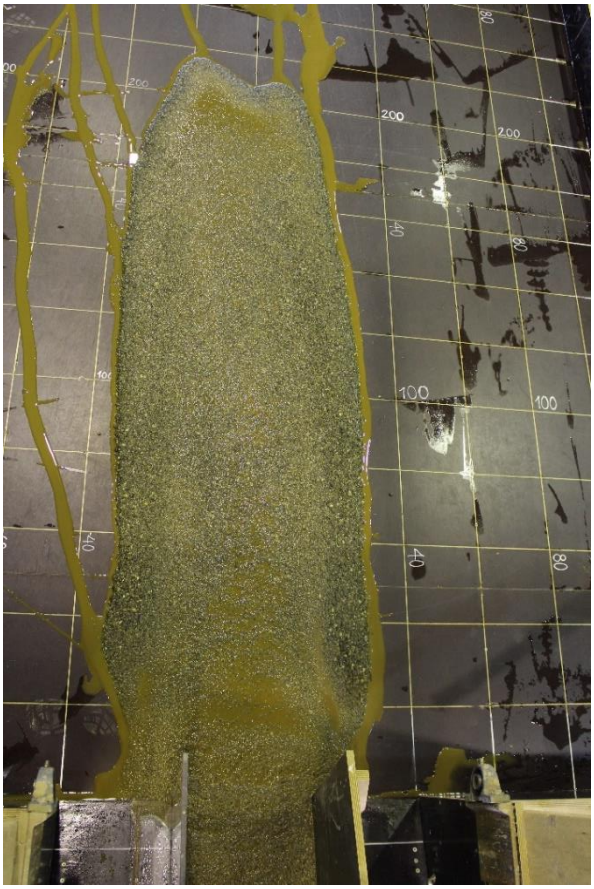

D.2.3 Deposition pattern of G4V1C1-r3

D.2.4 Deposition pattern of G4V1C1-r1-w90

D.2.5 Deposition pattern of G4V1C1-r2-w90

D.2.6 Deposition pattern of G4V1C1-r1-w45

D.2.7 Deposition pattern of G4V1C1-r2-w45

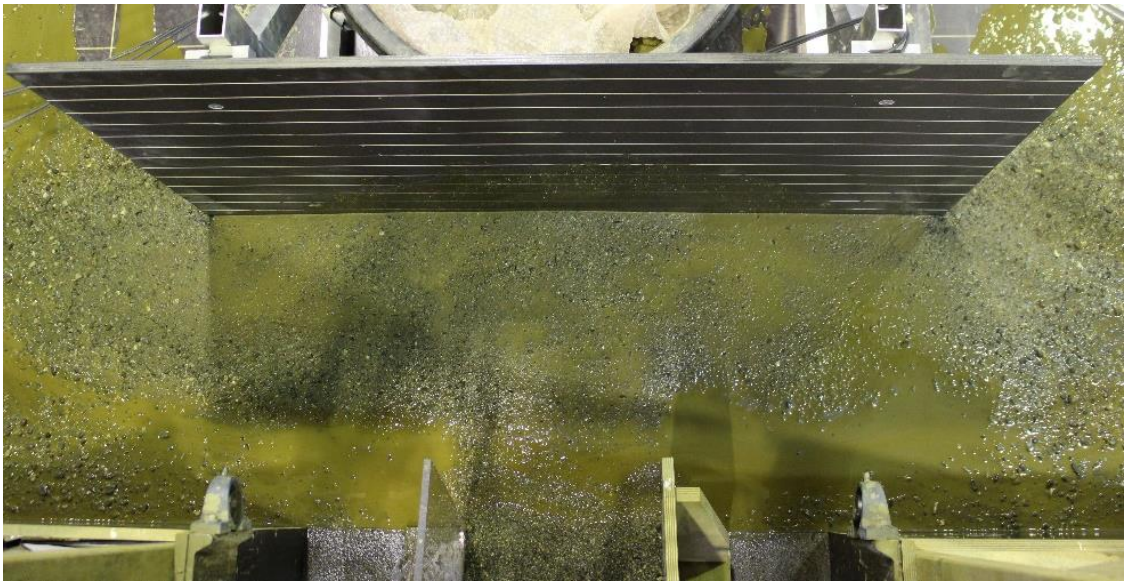

D.2.8 Deposition pattern of G4V1C3-r1-w90

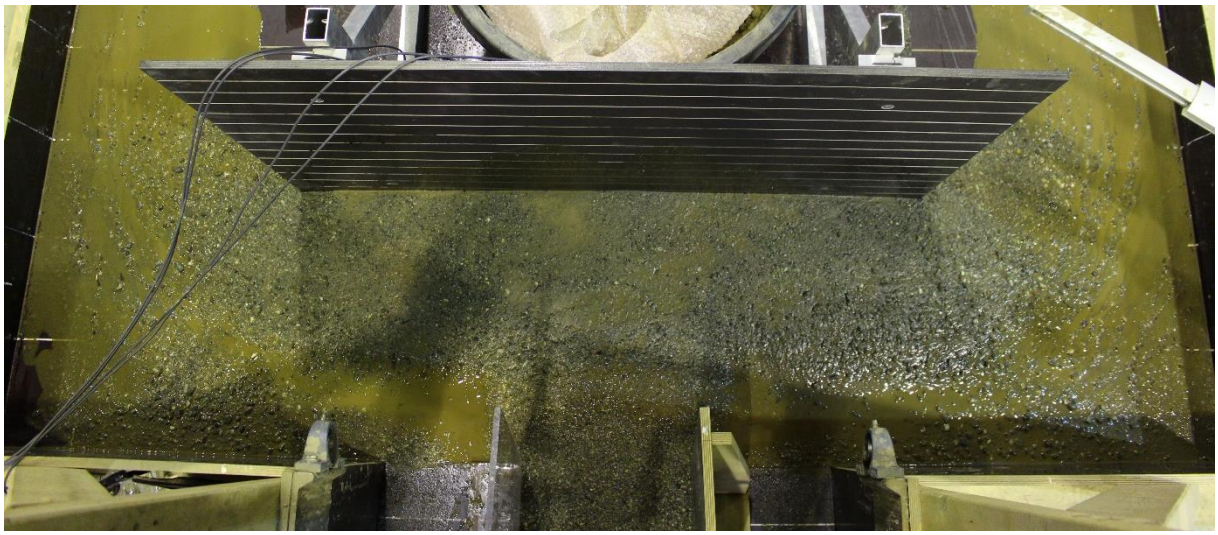

D.2.9 Deposition pattern of G4V1C3-r2-w90

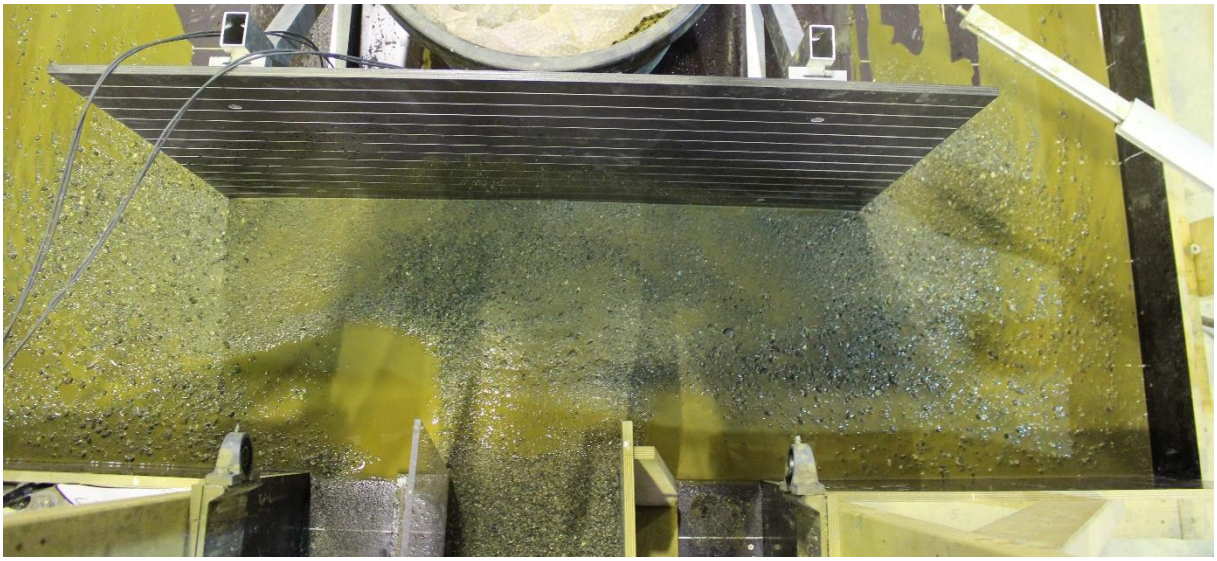

D.2.10 Deposition pattern of G4V1C3-r3-w90

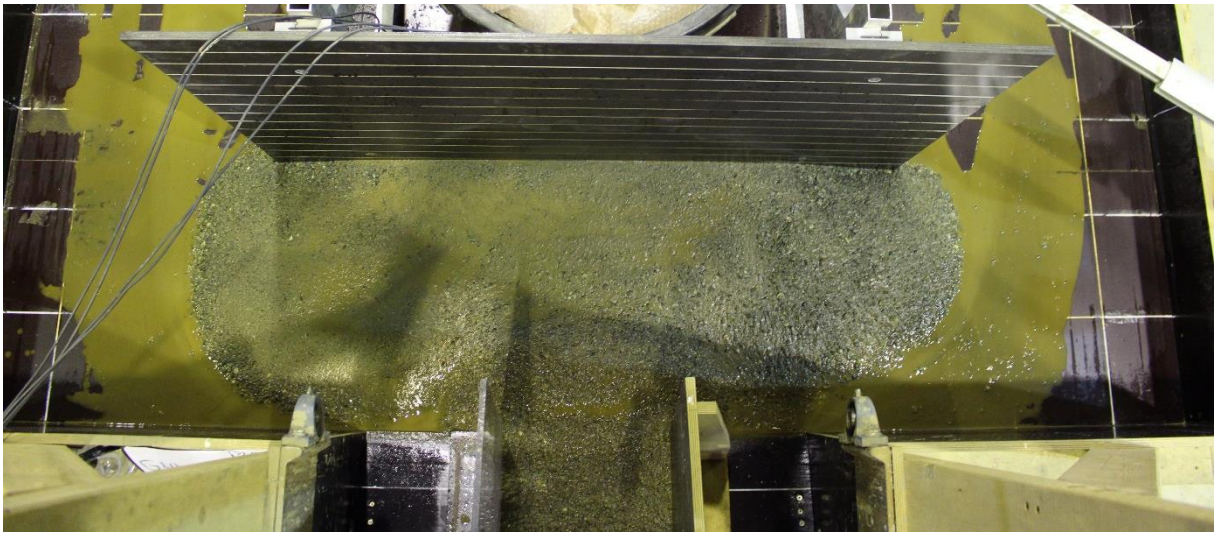

D.2.11 Deposition pattern of G4V1C1-r3-w90